1996

On surface versus atmospheric forcing in regional climate simulations

Zaitao Pan
Iowa State University

INFORMATION TO USERS

This manuscript has been reproduced from the microfilm master. UMI films the text directly from the original or copy submitted. Thus, some thesis and dissertation copies are in typewriter face, while others may be from any type of computer printer.

The quality of this reproduction is dependent upon the quality of the copy submitted. Broken or indistinct print, colored or poor quality illustrations and photographs, print bleedthrough, substandard margins, and improper alignment can adversely affect reproduction.

In the unlikely event that the author did not send UMI a complete manuscript and there are missing pages, these will be noted. Also, if unauthorized copyright material had to be removed, a note will indicate the deletion.

Oversize materials (e.g., maps, drawings, charts) are reproduced by sectioning the original, beginning at the upper left-hand corner and continuing from left to right in equal sections with small overlaps. Each original is also photographed in one exposure and is included in reduced form at the back of the book.

Photographs included in the original manuscript have been reproduced xerographically in this copy. Higher quality 6" x 9" black and white photographic prints are available for any photographs or illustrations appearing in this copy for an additional charge. Contact UMI directly to order.

UMI

A Bell & Howell Information Company
300 North Zeeb Road, Ann Arbor MI 48106-1346 USA
313/761-4700 800/521-0600

On surface versus atmospheric forcing in regional climate simulations

by

Zaitao Pan

A dissertation submitted to the graduate faculty

in partial fulfillment of the requirements for the degree of

DOCTOR OF PHILOSOPHY

Major: Water Resources

Major Professor: Eugene S. Takle

Iowa State University

Ames, Iowa

1996

Graduate College
Iowa State University

This is to certify that the Doctoral dissertation of

Zaitao Pan

has met the dissertation requirements of Iowa State University

Signature was redacted for privacy.

Major Professor

Signature was redacted for privacy.

For the Major Program

Signature was redacted for privacy.

For the Graduate College

TABLE OF CONTENTS

GENERAL INTRODUCTION

1 Overview

Regional climate has been an attractive research area for a longer period than global climate. Public awareness of global changes, such as global warming and environmental deterioration, has brought interest in projecting the global changes onto local or regional climate from scientific community, policy makers, and the general public. Studies of regional climate can be grouped into three broad categories (Giorgi and Mearns 1991, Robinson and Finkelstein 1991): empirical approach, empirical-modeling approach, and modeling approach. Regional climate studies first started from a purely empirical approach, which extracts regional climate information from analysis of recent instrumental observations and by analogy to paleoclimate. By analyzing recent observations, one can develop statistical relationships between regional climate variables, such as precipitation and temperature, and global climate (Vinnikov and Kovyneva 1983). By analogy to paleoclimate, say to the most recent warm phase (~600 years before present), the future climate subject to current global warming can be projected (Flohn and Fantechi 1984). Like all other empirical methods, this approach suffers from not accounting for the future changes in physical forcing and also crucially depends on the sample size.

The empirical-modeling approach is to translate general circulation model (GCM) information of coarse resolution into regional climate variables by using empirically derived relationships between the two. One typical method in this approach is to superimpose the modeled climate changes (the differences between the perturbed and control GCM simulations) onto current observations to form a future climate (Smith and Tirpak 1989). Another popular type of study is the so-called MOS (model output statistics) adopted from short-term weather

forecasts, which produces forecasts of local weather from GCM output by using statistical models (Klein 1982). Even though the large-scale forcing is explicitly incorporated in GCMs, the forcing on the regional scale or mesoscale is still empirically represented in this approach. This statistically based treatment to the mesoscale forcing and its interaction with large-scale forcing may fail if the mesoscale forcing changes in the future.

The modeling approach can explicitly represent both large-scale and mesoscale forcing in physical terms by linking GCMs to regional climate models (RCMs). With rapid advances in computer power and constant refinement in numerical techniques, especially the nesting technique, this approach becomes a major tool in regional climate studies today (Cress et al. 1995, McGregor and Walsh 1994, 1995, Podzun et al. 1995). Projections drawn from this approach are more likely to be realized, compared to the other approaches. A limitation to this approach is that models are often tuned, to certain degree, based on the current climate. The additional limitation of computer speed has constrained the longest simulations to date with RCMs to be the order of years. Another disadvantage with this approach is that the results are often model-dependent because of the wider diversity in parameterization schemes in different models.

2 Current Status of Regional Climate Simulations

General circulation models are the main tool for climate studies. It is unlikely that GCMs will resolve mesoscale features globally in near future even with current projection of computer speed (Robinson and Finkelstein 1991). The current approach in regional climate simulation, which can be thought of localization of GCMs over the local domain of interest, is to nest or embed a limited area model into GCMs (Giorgi et al. 1993a, 1993b, Schär et al. 1996). Good regional climate simulations require three reliable components: GCMs, RCMs, and the coupling between these two models. Most parameterization schemes in GCMs were developed for global scales and may not be suitable for increased resolution (Boer and Lazare 1988). Alternatively, RCMs run in climate mode require more accurate numerics and physical parameterization schemes to minimize the accumulation of errors during the course of long integrations. A

number of problems could occur, ranging from possible drift or separation between these two models to numerical instability, if the accumulated errors are large. For example, atmospheric radiation, a small term for short-term simulations, is a major forcing for long-term RCM simulations and thus must be computed more accurately.

The coupling issue deals with information transfer between the models. There are two types of coupling: pure boundary nudging and long-wave component nudging. In the first, large-scale information enters regional models only through lateral boundary conditions (Davies and Turner 1977, Anthes et al. 1987). This pure boundary forcing is inherent in existing models and thus is easy to apply. A number of regional climate simulations that used this technique produced reasonably good results (*e.g.*, Giorgi et al. 1993a, 1993b, Jones et al. 1995, Machenhauer 1995). The pure boundary forcing in fact has been the classical way of running regional climate models during past a few years. However, a separation can occur between the two models if the regional model is constrained by GCMs at the boundary alone, especially when the simulation domain is large and the forcing boundary zone is narrow. An alternative and relatively new technique to avoid the separation called spectral nudging (Kida et al. 1991, Paegle et al. 1996) has emerged. In this method, long-wave components of atmospheric forcing are nudged to GCMs not only within the boundary zones but also over the interior domain of RCMs. Preliminary results showed that this spectral nudging approach was promising, but being new and only crudely implemented with various artifacts. For example, Paegle et al. (1996) periodically nudged the RCM to GCM solutions for three longest waves. Kida et al. (1991), on the other hand, simply combined short-wave components of the RCM with long-wave components of the GCM. So far there are no reasonable ways to separate the wave spectra between the long and short waves relative to RCM domain sizes or to combine these two pieces of information.

Most present regional climate simulations, if not all, are performed under one-way nesting in which the information can only flow from GCMs to RCMs but not from RCMs to GCMs. Two-way nesting represents better the interaction but requires simultaneous runs of a GCM and RCM with feedbacks between two totally different models. Typically GCMs are spectral

models while RCMs are grid-point models, and alias of information, discontinuity of wave propagation, and other numerical difficulties make the two-way nesting extremely difficult (Zhang et al. 1986).

3 Unresolved Conflicts and Remaining Problems

Regional climate studies project global changes onto regional or local climate. It is generally agreed that: (1) the global climate change will be enhanced at high latitudes and during the winter season; (2) the regional response of global change can be positive or negative because of high nonlinearity of the atmospheric dynamics; (3) precipitation exhibits more complex response patterns than other variables such as temperature due to its stronger dependence on local conditions.

Regional climate simulation involves both large-scale atmospheric and local surface forcing, but disputes still exist on the relative importance of local versus remote forcing. For example, Betts et al. (1994) demonstrated that transpiration had a very important positive contribution to the Midwest flood of 1993 whereas Giorgi et al. (1996) and Paegle et al. (1996) found that soil moisture, a local forcing, had a negative impact on the flood. Clarification of these discrepancies is essential not only to meteorologists but also to hydrologists and agricultural researchers.

Regional climate simulation is a boundary-value problem over limited domains. Since it is a relatively new research area, very few sensitivity studies are available to clarify relative importance of boundary configuration, degree of large-scale constraint, frequency of boundary condition assimilation, etc. These fundamental sensitivity tests are needed before the technique can be widely adopted.

4 Dissertation Organization

This dissertation is organized following the "paper format". The first and last parts provide general introduction and conclusions, respectively, in the context of entire dissertation. The middle three parts are composed of three manuscripts on regional climate simulations, two

of which will be submitted to scientific journals for publication. Each paper (manuscript) is self-contained and has a complete paper structure, which means that it has its own abstract, introduction, conclusion and references. Since the papers are independent, all numbering to the figures, tables, and equations apply to the individual papers only, including the general introduction and conclusions. The dissertation includes also an appendix describing model equations in some detail at the end.

5 Overview of Individual Papers

5.1 Influences of Model Parameterization Schemes on the Response of Rainfall to Soil Moisture in the Central U.S.

Soil moisture is an important forcing for the atmosphere over continents and many studies have been carried out to quantify its impacts on precipitation processes by using different model schemes. Unfortunately the quantified results are often model scheme dependent. In the present study, the sensitivities of soil-moisture impacts on summer rainfall in the central U.S. to different commonly used cumulus parameterization and surface flux schemes are examined under different atmospheric and soil-moisture conditions. Results show that a transient increase in soil moisture enhanced total rainfall over the simulation domain. The increase in soil moisture enhanced local rainfall when the lower atmosphere was thermally unstable and relatively dry, but it decreased the rainfall when the atmosphere was humid and lacked sufficient thermal forcing to initiate deep convection. Soil-moisture impacts were noticeably stronger for the Kuo scheme. The greater sensitivity to soil moisture exhibited by the Kuo scheme than either the Grell or explicit schemes implies that it exaggerated the role of soil moisture. The difference was related to how each scheme partitioned rainfall between convective and stable forms, and possibly to each scheme's closure assumptions.

5.2 Long Simulation of Regional Climate as Collections of Short Segments

We investigated in the second paper the necessity and feasibility of subdividing long integrations through nine experiments by which we examined the effects of reinitialization frequency

and the relative importance of the surface forcing to atmospheric forcing. It was found that as integrations continued without reinitialization, locations of specific meteorological features drifted downstream because of the positive model bias on wind speeds, implying the necessity of periodically reinitializing the model. Results also indicate that the simulated domain-averaged variables, including rainfall, were not sensitive to model reinitialization since they are largely constrained by boundary conditions, suggesting the possibility of dividing long regional climate simulations into a set of shorter simulations that could be run in parallel.

5.3 Simulation of Potential Impacts of Human Habitation on U.S. Summer Climate under Various Climate Regimes

Landuse modification by human activities, such as deforestation, urbanization, and agricultural practice, has been long believed to influence climate. In the last paper, we evaluated numerically the potential impacts of human habitation and associated landuse changes on the summer climate in the continental U.S. The month-long simulation suggested that the current landuse increased domain total rainfall by 0.8 % over the natural landuse during a normal year. The flood year simulations showed a decrease in domain total rainfall with current and future landuse and this slight decrease resulted from a small increase in the western U.S. and large decrease in the east-central U.S. which was associated with the reduced evapotranspiration caused by the weakened southerly flow and cooler surface air. Simulated domain-average rainfall in a drought year indicated little sensitivity to different landuse scenarios since the increased evapotranspiration had less chance to translate into rainfall.

References

Anthes, R. A., E.-Y. Hsie, and Y.-H. Kuo, 1987: Description of the Penn State/NCAR Mesoscale Model Version 4 (MM4). *NCAR Tech. Note*, NCAR/TN-282+STR, 66 pp.

Betts, A. K., J. H. Ball, A. C. M. Beljaars, M. J. Miller, and P. Viterbo, 1994: Coupling between land and surface boundary layer parameterizations and rainfall on local and regional scales: Lessons from the wet summer of 1993. *Preprints, Fifth Symp. on Global Change*, Amer. Meteor. Soc., 65 pp.

Boer, G., and M. Lazare, 1988: Some results concerning the effects of horizontal resolution and gravity-wave drag on simulated climate. *J. Climate*, **1**, 789-806.

Cress, A., D. Majewski, D. R. Podzun, and V. Renner, 1995: Simulation of European climate with a limited area model. Part I: Observed boundary conditions. *Beitr. Phys. Atmos.*, **68**, 161-177.

Davies, H. C., and R. E. Turner, 1977: Updating prediction models by dynamic relaxation: An examination of the technique. *Quart. J. Roy. Meteor. Soc.*, **103**, 225-245.

Flohn, H., and R. Fantechi (Eds.), 1984: The climate of Europe: Past, present and future. D. Reidel, Norwell, Mass, 356 pp.

Giorgi, F., and L. O. Mearns, 1991: Approaches to the simulation of regional climate: A review. *Rev. of Geophysics*, **29**, 191-216.

Giorgi, F., M. R. Marinucci, G. T. Bates, and G. De Canio, 1993a: Development of a second-generation regional climate model (RegCM2). Part I: Boundary-layer and radiative transfer. *Mon. Wea. Rev.*, **121**, 2794-2813.

Giorgi, F., M. R. Marinucci, G. T. Bates, and G. De Canio, 1993b: Development of a second-generation regional climate model (RegCM2). Part II: Convective processes and assimilation of boundary conditions. *Mon. Wea. Rev.*, **121**, 2814-2832.

Giorgi, L. Mearns, C. Shields, and L. Mayer, 1996: A regional model study of the importance of local versus remote controls of the 1988 drought and the 1993 flood over the central United States. *J. Climate*, **9**, 1150-1162.

Jones, R. G., J. M. Murphy, and M. Noguer, 1995: Simulation of climate change over Europe using a nested regional-climate model. I: Assessment of control climate, including sensitivity to location of boundaries. *Qurt. J. Roy. Meteor. Soc.*, **121**, 1413-1450.

Kida, H., T. Koide, H. Sasaki, and M. Chiba, 1991: A new approach for coupling a limited area model to a GCM for regional climate simulations. *J. Meteor. Soc. Japan*, **69**, 723-728.

Klein, W. H., 1982: Statistical weather forecasting on different time scales. *Bull. Amer. Meteor. Soc.*, **63**, 170-177.

Machenhauer, M., 1995: The regionalization project: A synthesis of the final report. EEC Environment Program Contract No. EV5V-CT92-0126.

McGregor, J. L., and K. Walsh, 1994: Climate change simulations of Tasmanian precipitation using multiple nesting. *J. Geophys. Res.*, **99**, 20889-20905.

Paegle, J., K. C. Mo, and J. N. Paegle, 1996: Dependence of simulated precipitation on surface evaporation during the 1993 United States summer floods. *Mon. Wea. Rev.* **124**, 345-361.

Podzun, R., C. D. Majewski, and V. Renner, 1995: Simulation of European climate with a limited area model. Part I: A GCM boundary conditions. *Beitr. Phys. Atmos.*, **68**, 178-225.

Robinson, P. J., and Finkelstein, 1991: The development of impact-oriented climate scenarios. *Bull. Amer. Meteor. Soc.*, **72**, 481-490.

Schär, C., C. Frei, D. Lüthi, and H. C. Davies, 1996: Surrogate climate-change scenarios for regional climate models. *Geophys. Res. Letters*, **23**, 669-672.

Smith, J. B., and D. A. Tirpak (Eds.), 1989: The potential effects of global climate changes on the United States. Vol. 1, Chap. 4.

Vinnikov, K. Ya. and N. P. Kovyneva, 1983: The distribution of climatic changes in global warming (in Russian), *Meteor. Gidrol*, **5**, 10-19.

Zhang, D.-L., H. R. Chang, N. L. Seaman, T. T. Warner, and J. M. Fritsch, 1986: A two-way interactive nesting procedure with variable terrain resolution. *Mon. Wea. Rev.*, **114**, 1330-1339.

INFLUENCES OF MODEL PARAMETERIZATION SCHEMES ON THE RESPONSE OF RAINFALL TO SOIL MOISTURE IN THE CENTRAL U.S.

A paper published in the *Monthly Weather Review*[1]

Zaitao Pan, Eugene Takle, Moti Segal, and Richard Turner

Abstract

The sensitivities of soil-moisture impacts on summer rainfall in the central United States to different commonly used cumulus parameterization and surface flux schemes are examined using the PSU-NCAR MM5 under different atmospheric and soil-moisture conditions. The cumulus convection schemes used are the Kuo and Grell parameterization schemes, while the surface-moisture flux schemes used are the aerodynamic formulation and the Simple Biosphere (SiB) model. Results show that a transient increase in soil moisture enhanced total rainfall over the simulation domain. The increase in soil moisture enhanced local rainfall when the lower atmosphere was thermally unstable and relatively dry, but it decreased the rainfall when the atmosphere was humid and lacked sufficient thermal forcing to initiate deep convection. Soil-moisture impacts were noticeably stronger for the Kuo scheme, which simulated lighter peak rainfall, than those for the Grell scheme, which simulated heavier peak rainfall. The greater sensitivity to soil moisture exhibited by the Kuo scheme than either the Grell or explicit schemes implies that it exaggerated the role of soil moisture. This difference was related to how each scheme partitioned rainfall between convective and stable forms, and possibly to

[1]Reprinted with permission, 1996(8),1786-1802

each scheme's closure assumptions. Adding details to the surface-moisture flux schemes had a secondary influence on soil-moisture impacts on rainfall within a 24-h period.

1 Introduction

Surface-moisture fluxes over land are an important forcing for the atmosphere over continents on a wide range of spatial and temporal scales. Over the last three decades, climate modelers have examined and quantified soil-moisture effects on precipitation climatology. In a pioneering general circulation model (GCM) simulation by Manabe (1969), the importance of surface hydrological processes to the atmospheric circulation was illustrated. Subsequent GCM simulations (*e.g.*, Mintz 1984, Rowntree and Bolton 1983) showed that soil moisture contributed positively to global rainfall. With increasing interest in regional climate modeling (Giorgi et al. 1993), recent soil-moisture impact modeling studies have tended to concentrate on regional scales for shorter time periods. (*e.g.*, a month or a season). For example, Atlas et al. (1993) simulated the effects of soil moisture on rainfall over the Great Plains during the North American drought of 1988.

Monthly total rainfall on regional or local scales is mainly determined by a few heavy rainfall events, creating inhomogeneous regional soil-moisture patterns that may persist for a few weeks or longer. These isolated heavy-rain events may have different climatic impacts than spatially or temporally averaged patterns. Recent studies (*e.g.*, Benjamin and Carlson 1986, Chang and Wetzel 1991, Lakhtakia and Warner 1987, Lanicci et al. 1987, and Yan and Anthes 1988) evaluated the combined impact of inhomogeneity in surface wetness and dynamic processes on deep convection on short temporal scales. A preliminary evaluation of transient soil-moisture effects on rainfall was carried out by Pan et al. (1995) using coarse model resolutions and relatively simple physical parameterizations of cumulus convection and surface fluxes. Segal et al. (1995) also scaled the dependency of local deep convection on the Bowen ratio over uniform surfaces.

The credibility of modeled soil-moisture impacts on rainfall depends on the correctness of simulated rainfall. Unfortunately, rainfall is one of the most difficult variables to simulate due

to contributions from sub-grid scale (*i.e.*, unresolvable) convection and cloud microphysical processes (Molinari and Dudek 1992). Because of the uncertainties involved in parameterizing these processes, simulated precipitation amounts and patterns can vary widely from scheme to scheme (Zhang et al. 1988, Wang and Seaman 1994). For example, since the Kuo cumulus convection scheme usually underestimates peak rainfall, it will be useful to determine whether the soil-moisture impacts on subsequent rainfall also are underestimated if the Kuo scheme is used. Likewise, the surface flux schemes for evapotranspiration (ET) which regulates the surface moisture flow to the atmosphere should influence soil-moisture impact evaluation. As an example, the most commonly used aerodynamic formulation tends to overestimate evaporation (*e.g.*, Sato et al. 1989). Therefore, it is important to determine to what extent this excess moisture influences future rainfall.

The intercomparison of models as a means of promoting progress in atmospheric modeling has been encouraged by the Working Group on Numerical Experimentation of the World Climate Research Program (WGNE 1992). The present paper evaluates the sensitivities of soil-moisture impacts on rainfall by intercomparing different cumulus parameterization schemes and different surface flux schemes over three separate 24-h periods. A wide range of soil-moisture regimes is examined to resolve the nonlinear relationship of rainfall to soil moisture.

Section 2 briefly describes model schemes used in this study. In section 3, sensitivities of soil-moisture impacts on rainfall to cumulus parameterization schemes and to surface flux schemes are examined for the base case (9 July 1993). Soil-moisture impacts on evapotranspiration are evaluated in section 4 for different surface flux schemes. In section 5, the sensitivity of soil-moisture impacts on rainfall is examined for two additional synoptic cases during the 1993 flood.

2 The Mesoscale Model and Parameterization Schemes

2.1 Mesoscale Model

The fifth generation PSU/NCAR mesoscale model (MM5) (Grell et al. 1993) was used for the present study. The main advantages of MM5 over its previous version MM4, which has

been used widely, are its non-hydrostatic option and more detailed model physics formulations incorporated in the cumulus convection, radiative transfer, and cloud schemes.

The non-hydrostatic option and explicit warm cloud physics (Hsie and Anthes 1984) were employed in this study. This explicit moisture scheme operates together with a cumulus parameterization to form a so-called hybrid scheme for the calculation of precipitation. A one-level nested grid was used in which the outer coarse domain had 28 (E-W) x 25 (N-S) grid points with 90-km resolution and the inner nested domain had 37 (E-W) x 34 (N-S) grid points with 30-km resolution. The outer domain covered most of the central and eastern United States, while the nested domain was centered over the heavy rainfall area for the case (as indicated in Fig. 1). Twenty-three layers in the vertical were used for both domains with about 5-hPa resolution near the ground. Because this study emphasizes the transient response of rainfall to soil-moisture change, the period of all simulations was 24 h starting at 1200 UTC of the previous day.

2.2 Cumulus Parameterization Schemes

The two cumulus parameterization schemes used in this study were the Kuo scheme, denoted KS (Kuo 1974, Anthes 1977), a widely used cumulus parameterization, and the Grell scheme, denoted GS (Grell 1993), modified from the Arakawa-Schubert scheme (Arakawa and Schubert 1974) that has a more sound physical base (Raymond and Emanuel 1993). In KS, which does not explicitly account for downdraft circulation, convective precipitation, P, is expressed as

$$P = M_t(1 - b), \tag{1}$$

where M_t is the vertically integrated moisture convergence in a grid column including ET and b is a moistening factor that is a function of relative humidity (Anthes 1977). The characteristics of KS have been widely tested (*e.g.*, Kuo and Anthes 1984, Wang and Seaman 1994). In GS, which explicitly incorporates a single downdraft plume of clouds, convective precipitation is expressed as

$$P = I_1 m_b (1 - \beta), \tag{2}$$

where I_1 is the total condensate normlized by mass flux in the updraft, m_b is the mass flux at cloud base, and β is the fraction of condensate detrained out of clouds and reevaporated. which is determined by vertical wind shear (Fritsch and Chappell 1980). The performance of GS has been evaluated by Giorgi (1991) and Wang and Seaman (1994). The differences in precipitation physics formulations between these two schemes are quite substantial even though the final expressions for precipitation in Eqs. (1) and (2) seem to be similar.

2.3 Surface Moisture Flux Schemes

The conventional aerodynamic (AD) formulation and the more detailed Simple Biosphere (SiB) model (Sellers et al. 1992, Collatz et al. 1990) were used to intercompare the dependence of rainfall on soil moisture under different surface flux parameterization schemes.

The standard version of MM5 computes ET (surface-moisture flux) using an AD formulation (Blackadar 1976, Zhang and Anthes 1982). The evapotranspiration is given by

$$ET = m\rho_a C_q V_a \left(q_{gs} - q_a\right), \tag{3}$$

where q_{gs} is the saturation mixing ratio with respect to surface soil temperature (T_g), ρ_a, V_a, and q_a are the air density, wind speed, and water vapor mixing ratio at the lowest model level, respectively, and C_q is the surface exchange coefficient for moisture. The soil moisture availability, m, is the ratio of actual ET to potential ET. A value of m=0 denotes completely dry top soil and a value of m=1 represents saturated top soil. (Soil moisture hereafter refers to m, unless otherwise indicated.) ET is a nonlinear function of m (most noticeably for low values of m) because of the exponential dependence of q_{gs} on T_g.

SiB2 (a newer version of SiB) was incorporated into MM5 for this study. In SiB2, ET consists of transpiration from the canopy (E_c) and evapotranspiration from the ground cover (E_g). Soil moisture (representing the average soil moisture in SiB2) affects ET by controlling stomata and soil resistances. (An outline of the ET computation in SiB2 is given in the Appendix.)

3 Sensitivity of Soil-Moisture Impacts on Rainfall to Parameterization Schemes – 9 July 1993 Case

In this section, the distribution of rainfall simulated by using different schemes will be examined under various soil-moisture conditions.

3.1 Synoptic Situation

The midwestern United States experienced its worst flood on record in the summer of 1993 (Gerald and Janowiak 1995). This long lasting and wide-spread flood (termed the Great Flood) resulted from a series of heavy rainfall events during June and July (Rodenhuis et al. 1994, Mo et al. 1995). Three days (17 June, 5 July, and 9 July) with peak daily rainfall exceeding 100 mm were simulated.

The 9 July case was the heaviest rainfall event, and thus it serves as the focal (base) case for detailed analysis. A peak rainfall of 150 mm was observed in central Iowa over the 24-h period ending at 1200 UTC 9 July. An unseasonably high amplitude upper-air pattern characterized by a strong ridge over the Gulf of Alaska and a deep trough over the western United States existed during this period. East of the trough, i.e., over the central United States, there was a strong baroclinic zone and an upper level jet with a strong southerly component.

At the surface a quasi-stationary front was positioned through Iowa, extending from western Kansas to central Michigan. A high pressure system anchored over the southeastern United States in conjunction with an area of low pressure over western Kansas and Colorado produced broad southerly surface flow that advected warm moist air into the central United States (Fig. 2). A low-level jet (LLJ) was also present above the region of southerly surface winds and this enhanced the moisture transport into the region and it provided a source of convective instability. The presence of the jet stream aloft, the LLJ, and outflow boundary remnants from storms of the previous night provided extremely favorable conditions for the heavy rainfall event that occurred (Augustine and Caracena 1994).

3.2 Sensitivity of Simulated Rainfall to Cumulus Parameterization Schemes

3.2.1 Rainfall Fields

Soil-moisture availability (m) for the base case was estimated from the weekly Crop Moisture Index and Palmer Drought Index (issued by the NWS) for the second week of July 1993 (Fig. 1). Persistent flooding produced an extremely wet surface with maximum m values above 0.9 over much of the upper Mississippi River basin. On the other hand, low m values existed in the southeast corner of the domain and in the Rocky Mountain region.

Figure 3a shows the simulated 24-h accumulated rainfall field by using GS as the cumulus convection scheme and the AD formulation for the surface fluxes. The model produced a well-organized rainband oriented from east-northeast to west-southwest across Iowa, matching the position of the stationary front through the region. An elongated primary heavy rainfall center (denoted PC, primary center) was simulated in east-central Iowa. A secondary rainfall center (denoted SC, secondary center) with a peak value of 55 mm was simulated over eastern Nebraska. The shape and orientation of the simulated rainband were in close agreement with the observed pattern (Fig. 3b). The simulated peak rainfall (130 mm) matches well the observed peak (150 mm). However, its location was shifted about 100 km (3 grid lengths) to the east of the observed. The simulated peak rainfall and location for the SC over eastern Nebraska were reasonably close to the observations.

The temporal distribution of simulated rainfall was also in close agreement with the observations. Two rainfall episodes, one late in the morning on 8 July and the other that night, accounted for rainfall at the PC. The second episode produced more rain than the first, but in the simulations the two episodes had similar magnitudes. Such overprediction during the early period (and underprediction during the late period) of a simulation has been reported as a deficiency of rainfall simulations (Cai et al. 1992). This deficiency seems to be attributed to the limitations of the cumulus parameterization schemes. Both observed and simulated rainfall for the SC developed late in the night of 8 July.

Simulations using a wide range of m values provide a systematic evaluation of soil-moisture impacts on rainfall for different cumulus convection schemes. Figure 4 presents the simulated

24-h accumulated rainfall fields for various values of m prescribed uniformly over the domain with GS as the cumulus convection scheme and the AD formulation for the surface flux scheme. The most notable feature is that as m increased, the PC intensified whereas the SC diminished. The rainfall at PC was more sensitive to changes in m when m was small (≤ 0.2), but as m increased, the rainfall fields remained essentially the same. This insensitivity for relatively high values of m is in agreement with one dimensional studies (*e.g.*, Kondo et al. 1990, Mahfouf and Noilhan 1991) implying that ET is most sensitive to soil moisture within a narrow range of low m values. The positive soil-moisture impact on rainfall for the PC is in agreement with the earlier findings of Pan et al. (1995). However, the SC over eastern Nebraska, which was not resolved in that study probably because of the coarse model and data resolutions, had an inverse dependence on m. For relatively dry surfaces (m=0.1), the rainfall amount and areal coverage over the SC were only slightly less than those over the PC. However, when m increased, the rainfall area around the SC shrank and the magnitude decreased gradually, vanishing at m=0.6. Also, as the rainfall associated with the SC diminished, the SC shifted towards the southwest, possibly as a result of the intensification of the nocturnal LLJ (see discussion later).

Figure 5 depicts the 24-h accumulated rainfall fields for different m values when KS was used instead of GS for cumulus convection. The general patterns of rainfall fields, including a northeast-southwest oriented rainband with two centers, were similar to those produced by using GS. The major difference between the two schemes, however, is that GS produced spatially concentrated rainfall whereas KS produced a wide-spread rainfall (for PC). The maximum rainfall at the PC, in the range of all m values, was only 55 mm, in contrast to 159 mm for the GS simulation. The impacts of soil moisture on rainfall were also similar to those for GS: the PC strengthened and the SC weakened with increasing m. However, the dependence of rainfall on m was more pronounced in KS. The PC noticeably strengthened over a large area with increasing m. This is in contrast to the GS results where an increase in peak rainfall, but little increase in areal coverage, was simulated. The PC barely existed in Iowa for $m \leq 0.2$. On the other hand, the SC strengthened considerably for the dry surface.

3.2.2 Rainfall Averages

The simulated average rainfall over the nested domain (total rainfall over the entire nested domain divided by total grid points) was computed for various m values. In the GS simulation, the grid-point average rainfall slightly decreased with m for low values of m (except for m=0.1) but increased slightly for high values of m (Fig. 6a). This nonlinear behavior was due to the opposite responses of the two rainfall centers to m (see later). The grid-point average rainfall over the domain was almost constant ($\sim$ 8 mm). On the other hand, average rainfall for the KS simulations increased linearly with m from about 7 to 10 mm. For $m \geq 0.3$, KS produced greater total rainfall than GS although the peak value at the PC for the KS simulation was less than one half of that from the GS results.

Figures 6b and 6c depict the average rainfall changes with m for the two rainfall centers (PC and SC) separately for GS and KS respectively. (Rainfall was averaged over only those areas where the 24 h amounts exceeded 10 mm.) In GS, the average rainfall of the PC was about 30 mm for the entire range of m values. Rainfall at the SC was also about 30 mm for values of m less than 0.3, but for larger values of m rainfall diminished rapidly. For KS, the average rainfall for the PC linearly increased from 20 to 30 mm whereas average rainfall for the SC decreased from 50 to 20 mm over the same range of m values.

3.2.3 The Elaboration on Different Responses of Kuo and Grell Schemes to Soil Moisture

The reasons for the cumulus-scheme-sensitive response of rainfall to soil moisture are discussed in this sub-section. However, it should be realized that isolating the processes responsible for the differences is difficult because of the highly non-linear interactions involved.

One basis for the different responses relates to each scheme's closure assumptions. Convective adjustment of the environment in KS is constrained by a conservation of water substance requirement: convection is assumed to consume moisture at the rate (more accurately, at some fractional rate) at which it is supplied by the large scale environment (Raymond and Emanuel 1993). Moisture convergence and ET contribute to this environmental supply, so for KS, moist

processes directly influence convection, its adjustment of the environment, and the resultant precipitation. Convective adjustment in GS, on the other hand, is constrained by a conservation of available moist static energy: convection is assumed to consume the available moist static energy (i.e., available moist enthalpy) at the rate at which the large scale environment supplies it. Since variations in soil moisture do not alter significantly the surface moist enthalpy flux into the atmosphere (although it controls the partitioning between sensible and latent heat fluxes) the response of convection, and thus the convective rainfall, to soil moisture should be weaker for GS.

The further potential for differences in the response to soil moisture due to differences in the closure assumptions is illustrated by how each scheme treats excess moisture due to convergence. For KS, a fraction of the excess moisture will be instantly (i.e., within a single time step (90 s)) rained out, while the remainder will be vertically redistributed in the atmospheric column. For GS, excess moisture is not necessarily rained out instantly because precipitation is only influenced by such excessive moisture indirectly through the cloud work function (Arakawa and Schubert 1974). Therefore, convective rainfall in KS responds more directly and more rapidly to the excess moisture than GS.

Another possible explanation for the greater sensitivity of rainfall to m in KS relates to differences in how each scheme partitions total rainfall between sub-grid (convective) and resolvable scale (stratiform) forms. For this case in KS, precipitation was mostly sub-grid scale whereas in GS it was mostly resolvable. It is generally accepted that convective precipitation is more strongly dependent on surface forcing (e.g., Benjamin and Carlson 1986), and thus it is expected that KS would be more sensitive to surface forcing for this case.

To explore the effects of rainfall partitioning between sub-grid and resolvable scales, further simulations were conducted in which precipitation was treated as being totally resolvable. The use of only a fully explicit cloud scheme (EX) can be partly justified considering that the rainfall system was quite large in this case, although the model horizontal resolution of 30 km is relatively coarse (Rosenthal 1978). The results from these fully explicit cloud simulations were very similar to those produced by GS except that they produced about 0.8 mm more

rainfall averaged over the domain (Fig. 6a). This result supports the argument that the reduced sensitivity of rainfall to m in GS is because it partitions more precipitation into the resolvable form.

Given the reduced sensitivity of simulated rainfall to m when the fully explicit cloud scheme was used and the more rapid and direct response of KS to excess moisture, it is suggested that rainfall exhibits an *exaggerated* sensitivity to soil moisture for the KS simulations. This exaggerated sensitivity is responsible for the major differences in the soil-moisture impacts on the simulated rainfall between the cumulus parameterizations.

3.2.4 Effects of Local Conditions

Two possible causes are offered to explain the inverse response of rainfall to m at the SC. The first is related to the difference in the temperature and humidity stratification between the PC and SC. Figure 7 shows the soundings at these two rainfall centers at the initial time (1200 UTC 8 July, Fig. 7a, b) and 18 h into the integration (0600 UTC 9 July, Fig. 7c, d), when rainfall at the SC was near peak intensity. (Note the KS and AD schemes were used and m was set to 0.2 in this simulation.) The main difference was that the atmosphere was more moist and stable at the SC where a deep stable layer extended up to 800 hPa. Thus, the relatively humid and thermally stable atmosphere at the SC had enough moisture to sustain convection, but it lacked sufficient sensible heating to break the inversion. As m increased, the increased ET reduced the sensible heat flux, which, in turn, suppressed the development of the convective boundary layer (CBL). More sensible heating, not moistening, is needed to increase rainfall (Otterman et al. 1990, Fuelberg et al. 1991, Sanders and Blanchard 1993). At the PC, on the other hand, the atmosphere was dry and nearly neutral, and the increased ET fueled convection and enhanced rainfall as convection developed during the day.

The contrasting behaviors at PC and SC suggests that an increase in ET enhances rainfall if a dry and well developed CBL has already been established, but it decreases rainfall if ET suppresses the development of surface based convection. It is worth noting that increased soil moisture also can suppress the development of fair weather boundary layer clouds (Ek and

Mahrt 1994, Segal et al. 1995).

The second cause for the decreased rainfall with increasing m at the SC may be linked to the nocturnal LLJ. Nocturnal southwesterly flow at $\sim$ 700 m AGL, around which the LLJ typically reaches its peak intensity (Mitchell et al. 1995), was stronger to the south of the SC for m=0.2 than for m=0.6 (Fig. 8). Thus for m=0.2, there was increased advection of moisture, from the south, into the region. The simulated intensification of the LLJ with decreasing m is in agreement with the results of McCorcle (1988) and Turner (1993). The intensification is caused by the increased daytime heating of the CBL for the drier surfaces. As a result, the nocturnal wind strengthened and consequently the southerly flow intensified.

3.3 Sensitivity of Simulated Rainfall to Surface Flux Schemes

The aerodynamic formulation, AD, and the SiB scheme were used to evaluate the sensitivity of soil-moisture impacts to surface flux schemes. Overall, rainfall fields simulated using the SiB scheme resembled those produced using the AD scheme for both GS and KS. The change in domain average rainfall with m, when SiB was incorporated into the model as the flux scheme, is depicted in Fig. 9. For $m \leq 0.6$, average rainfall simulated with KS increased linearly with m whereas that simulated with GS remained constant. This is similar to the results obtained with the AD scheme (see Fig. 6a), and it suggests that surface flux schemes had only a secondary influence on soil-moisture effects. One difference, however, is that for simulations in which SiB was used rainfall did not change when $m \geq 0.6$ (even for KS). This could be caused by differences in the spatial distribution of ET (discussed in the next section) as computed by the two flux schemes.

A modified AD formulation, which has been shown to reduce the overestimation of surface-moisture flux (Pan et al. 1994), also was compared with the conventional (MM5) formulation to estimate possible effects of the overestimation on rainfall. Results indicated that the use of the alternative formulation had little influence on soil-moisture effects.

4 Sensitivity of Evapotranspiration to Different Surface Flux Schemes – 9 July, 1993 Case

Figure 10 presents the daily ET field calculated using the AD formulation with the estimated m field as shown in Fig 1. The dependence of ET on m is modulated by clouds, surface temperature, and surface layer humidity. On this day, a minimum ET of $\sim$ 2 mm was simulated over eastern Nebraska and South Dakota due to lower m values (see Fig. 1), and ET values of 4.0-6.5 mm were simulated in the southern part of the domain. The predicted daily ET over Iowa, where the heavy rainfall event occurred, of $\sim$ 3 mm was lower than the climatological value of $\sim$ 4 mm (Shaw, 1981) because of the above average cloudiness.

There are no directly observed values of ET to verify the simulations. However, by multiplying the pan evaporation by a conversion factor of 0.77 (Shaw 1981), crude estimates of actual ET can be obtained. Pan evaporation measurements available from three locations in Iowa on 9 July gave an average ET of $\sim$ 3.5 mm. This indicates that the simple AD formulation produced reasonable ET values over Iowa on this particular day.

Figure 11 shows the average ET in the entire nested domain over the 24-h period for various m values. Uniform values of m were specified over the entire domain for this set of experiments. Both SiB and AD schemes showed that ET increased rapidly with m when m was small and then leveled off as m increased further. The two schemes showed no significant difference when $m \geq 0.3$, but ET was lower for the SiB scheme when $m \leq 0.2$. This was in part because soil moisture approached the wilting point (*i.e.*, a condition where evapotranspiration nearly stops) in the SiB scheme. The AD formulation in this study has no constraints to account for the wilting point. Another reason for the reduced sensitivity of ET to m when $m \leq 0.2$ in this AD formulation is that the surface specific humidity is assumed to be proportional to soil temperature. The AD formulation tends to overestimate ET for high soil temperatures.

The spatial distributions of ET were different between the two schemes even though their domain-averaged ET's were very close. The AD scheme produced high values of ET over the southwest corner and low values over the northern part of the domain because of the two previously described effects (*i.e.*, wilting point and temperature).

The differences in ET in the range of m=0.2-0.8 were only $\sim$ 1 mm over the PC area (not shown). The maximum differences in simulated rainfall over the PC, however, changed by 8 mm (Fig. 6c). The rainfall enhancement was therefore $\sim$ 8 times as large as the enhancement of local ET. In other words, the increased rainfall at one grid cell at the rainfall center was equal to the total increased ET contributed from 8 neighboring grid cells. The total rainfall over the whole domain (nested only) for KS increased by 4.0 mm (Fig. 9) whereas the total ET increased only by 1.2 mm (Fig. 11) as m increased from 0.2 to 0.8. This result suggests that over a domain of $\sim 10^6$ km^2, the rainfall increased 3-4 times more than the ET had.

5 Further Simulations — 5 July and 17 June 1993 Cases

The base simulations for 9 July suggested that the soil-moisture impacts on rainfall were more strongly dependent on cumulus schemes than on surface-moisture flux schemes. Furthermore, simulated rainfall in KS was noticeably more sensitive to m than in GS. To further test these findings, two additional events were examined.

The upper-air synoptic pattern for the 5 July case was very similar to that for 9 July. At 1200 UTC 4 July a deep surface low-pressure area was centered in northwestern South Dakota (Fig. 12a). A squall line almost parallel with the cold front extended from southeast South Dakota to the Oklahoma panhandle. A narrow band of heavy rain with two maxima (Fig. 12b) was produced along the squall line. In this case, both GS and KS basically produced the rainband structure, especially for m=0.6 (Fig. 13), however, KS was more sensitive to m. The average rainfall at the PC increased by about a factor of three as m increased from 0.2 to 0.6 for KS. On the other hand, for GS, rainfall increased by only 30 %, although the absolute increase was larger than in KS.

Rainfall averaged over the nested domain increased linearly with m for KS whereas for GS (and EX) it increased rapidly for $m \leq$0.3 and leveled off for larger m (Fig. 14a). Rainfall at the PC for GS increased with m first and then leveled off (Fig. 14b), whereas for KS rainfall at the PC increased almost linearly with m (Fig. 14c). The slight drop in rainfall at PC for GS at large m values was due to the expansion of rain areas without total rainfall increase. The

overall sensitivity of rainfall to m for the two rainfall centers (PC and SC) for both cumulus convection schemes was very similar to that of the 9 July case.

The second event, 17 June, was selected to further evaluate model sensitivities. The upper-air flow pattern around 17 June was characterized by a strong zonal flow that provided a "duct" for an intense cyclone propagating into the Midwest from the western Pacific (Gerald and Janowiak, 1995). The surface low pressure associated with the cyclone was located in central Nebraska at 12 UTC 16 June (Fig. 15a). The system produced heavy rainfall (Fig. 15b) as it moved eastward during the next 24 h. The rainfall fields simulated using GS and KS for m=0.2 and 0.6 are presented in Fig. 16. The rainband for GS was affected slightly by the change in m. In contrast, the rainband for KS was hardly recognizable when m=0.2, whereas a well-organized rainband was produced with m=0.6. The domain-averaged rainfall in this event was noticeably more sensitive to m for KS than for either GS or EX (Fig. 17).

6 Summary and Conclusions

The present study evaluates influences of cumulus parameterization and surface flux schemes on summer rainfall response to transient soil-moisture changes over the central United States. Simulations of 24-h duration allowed for a large number of realizations (various m values) for each event. The cumulus convection schemes used were the Kuo scheme, Grell scheme, and a fully explicit cloud physics scheme. Sensitivities to surface flux schemes were tested by comparing the results from the aerodynamic formulation to those with the Simple Biosphere Model.

Increased soil moisture was found to enhance domain total rainfall but to enhance or suppress local rainfall, depending on local thermal and moisture conditions of the atmosphere. For two events (5 and 9 July 1993), each having two separate rainfall centers, the primary centers located in eastern Iowa strengthened as m increased whereas the secondary rainfall centers located in eastern Nebraska weakened. It was found that increased evapotranspiration (ET) from a wet surface reduced local rainfall when the lower atmosphere was humid and lacked sufficient thermal forcing to initiate deep convection. On the other hand, when the lower atmosphere

was thermally unstable but relatively dry, an increase in soil moisture increased local rainfall. It may therefore be speculated that during the early stage of convective development when the convective boundary layer is still shallow, increased ET may suppress convection and thus precipitation. On the other hand, after a deep unstable layer has been already established, increased ET may fuel convection by adding more moisture and thus enhance precipitation. In other words, sensible heating is more important in initiating convection and ET is more important in amplifying convection (precipitation). More studies are needed to confirm this conjecture.

The nocturnal low level jet, a major mechanism influencing heavy rainfall in this region, is an additional complicating factor in determining precise soil-moisture impacts on rainfall for the cases simulated in this study. The nocturnal low level jet weakened with increasing m. This reduced the transport of moisture into the region, and contributed to the decrease in rainfall at the secondary center for high m values.

Soil-moisture impacts were noticeably stronger for the Kuo scheme, which produced lighter peak rainfall, than those for the Grell scheme, which simulated heavier peak rainfall. The impacts were roughly linear with soil-moisture availability m for the Kuo scheme, whereas for the Grell scheme they were nonlinear and varied among cases. The difference in rainfall response to m between the two schemes was attributed, in part, to how each scheme partitioned total rainfall between the sub-grid and resolvable scales. The different responses could also be attributed to differences in the parameterization formulations, such as closure assumptions. For example, a fraction of any ET contributing to excess moisture is directly rained out in the Kuo scheme because moisture is assumed to be consumed by convection at the rate at which it is supplied. However, this is not the case for the Grell scheme because the available moist static energy, not moisture, is conserved.

The fully explicit cloud physics simulations (without a cumulus parameterization scheme) showed a significantly weaker response of rainfall to m than the Kuo scheme, which produced rainfall mostly in sub-grid convective form. This suggests that a cumulus convection parameterization scheme like the Kuo scheme can exaggerate the soil-moisture impacts on rainfall.

Since most previous soil-moisture impact simulations used only one cumulus parameterization scheme (the Kuo scheme has been most frequently used), the impacts could have been exaggerated.

The simple but widely used aerodynamic formulation and the more physically sound Simple Biosphere scheme produced similar rainfall responses to m, suggesting that details of the surface flux scheme have only a secondary effect on transient soil-moisture impacts compared with those of cumulus convection schemes.

Acknowledgment

This is a journal paper No. J-16466 of the Iowa Agriculture and Home Economics Experiment Station, Ames, Iowa (Project No. 3153). Partial support was provided by NASA grant NAG 5-2491 and NSF grant ATM-9319455. Data and computer support used in this study were partly provided by the Science Computing Division of the National Center for Atmospheric Research sponsored by the NSF. The authors wish to thank Dr. Sue Chen for valuable consulting on the MM5 code and Dr. James Collatz for providing the SiB2 code and some input parameters. We would like also to thank Drs. John Brown and Ray Arritt for helpful discussions and Richard Carlson for providing climatological data.

Appendix. Outline of Evapotranspiration Computation in SiB Model

The SiB2 model (Sellers et al. 1992, Collatz et al. 1990) is the improved version of the original SiB model. It uses a semi-analytical form of integrated canopy resistance that is proportional to photosynthesis rate. The stomatal conductivity is given by

$$g_s = M\frac{A_n}{C_s}h_s P_s + b \qquad (A1)$$

where M and b are constants, C_s is the CO_2 concentration, h_s is an adjustment factor for relative humidity of air at the surface, P_s is the surface pressure, and A_n is the photosynthesis rate.

The canopy is divided into an upper story, which represents tall trees and plants, and lower story representing sub-canopy grass. The soil is represented by a thin top layer, middle root layer, and deep layer below. The moisture flux from the surface consists of evapotranspiration from canopy (E_c) and ground cover (E_g) (Sellers et al 1986):

$$E_c = [e(T_c) - e_a]\frac{\rho c_p}{\gamma L_v}\left[\frac{W_c}{\overline{r_b}} + \frac{1 - W_c}{\overline{r_b} + \overline{r_c}}\right], \tag{A2a}$$

$$E_g = [e(T_g) - e_a]\frac{\rho_a c_p}{\gamma L_v}\left[\sigma_g\left(\frac{W_g}{r_d} + \frac{1 - W_g}{r_d + r_g}\right) + \frac{(1 - \sigma_g)\, h_s}{r_{surf} + r_d}\right] \tag{A2b}$$

where T_c is the canopy temperature, $e(T_c)$ and $e(T_g)$ are the saturation vapor pressure at T_c and T_g respectively, e_a is the ambient water vapor pressure, W_c and W_g are the wetted fractions of canopy and ground cover, respectively (W_c and W_g are assumed to zero in this study), σ_g is the ground fraction covered by vegetation (herein assumed to be 0.79), $\overline{r_b}$ and $\overline{r_c}$ are the bulk boundary layer and canopy resistance, respectively, r_d is the aerodynamic resistance between ground and air at canopy source height, r_g is the bulk stomatal resistance of ground cover, r_{surf} is the bare soil surface resistance, γ is the psychrometric constant, L_v is the latent heat of condensation, and c_p is the specific heat at constant pressure.

In SiB2, the predicted soil water content η is defined as the ratio of actual to saturation volumetric water content of soil. The soil-moisture availability (m) also can be approximated as this ratio (Deardorff 1972, Manabe 1969). Thus, in our application, it is assumed that η defined in SiB2 and m used in the aerodynamic formula have equivalent effects on evapotranspiration. Considering the ambiguity associated with the definition of m (Davies and Allen 1973), this rough equivalence is justified. To be consistent with uniformly specified soil moisture, the vegetation over the entire domain was assumed as a mixture of crop and grass fields grown on loam soil. This assumption is reasonable since our domain of interest is over the United States Midwest, an intensively cultivated region.

References

Anthes, R. A., 1977: A cumulus parameterization scheme utilizing a one-dimensional cloud model. *Mon. Wea. Rev.*, **105**, 270-286.

Arakawa, A., and W. H. Schubert, 1974: Interaction of a cumulus cloud ensemble with the large scale environment. Part I. *J. Atmos. Sci.*, **31**, 674-701.

Atlas, R., N. Wolfson, and J. Terry, 1993: The effect of SST and soil moisture anomalies on GLA model simulations of the 1988 U. S. summer drought. *J. Climate*, **6**, 2034-2048.

Augustine, J. A., and F. Caracena, 1994: Lower-tropospheric precursors to nocturnal MCS development over the central United States. *Wea. Forecasting*, **9**, 116-135.

Benjamin, S. G., and T. N. Carlson, 1986: Some effects of surface heating and topography on the regional severe storm environment. Part I: Three-dimensional simulations. *Mon. Wea. Rev.*, **114**, 307-329.

Blackadar, A. K., 1976: Modeling the nocturnal boundary layer. *Preprints, Third Symp. on Atmospheric Turbulence, Diffusion and Air Quality*. Raleigh, NC, Amer. Meteor. Soc., 46-49.

Cai, Z. Y., Z. S. Wang, and Z. T. Pan, 1992: A numerical study on forecasting the Henan extraordinary heavy rainfall event in August 1975. *Advances in Atmos. Sci.*, **9**, 53-62.

Chang, J.-T., and P. J. Wetzel, 1991: Effects of spatial variations of soil moisture and vegetation on the evolution of a prestorm environment: A numerical case study. *Mon. Wea. Rev.*, **119**, 1368-1390.

Collatz, J. G, J. A. Berry, G. D. Farquhar, and J. Pierce, 1990: The relationship between the rubisco reaction mechanism and models of photosynthesis. *Plant, Cell and Env.*, **13**. 219-225.

Davies, J. A., and C. D. Allen, 1973: Equilibrium, potential and actual evaporation from cropped surfaces in southern Ontario. *J. Appl. Meteor.*, **12**, 649-657.

Deardorff, J. W., 1972: Parameterization of the planetary boundary layer for use in general circulation models. *Mon. Wea. Rev.*, **100**, 93-106.

Ek, M., and L. Mahrt, 1994: Daytime evolution of relative humidity at the boundary layer top. *Mon. Wea. Rev.*, **122**, 2709-2721.

Fritsch, J. M., and C. F. Chappell, 1980: Numerical prediction of convectively driven mesoscale pressure systems. Part I: Convective parameterization. *J. Atmos. Sci.*, **37**, 1722-1733.

Fuelberg, H. E, R. L, Schudalla, and A. R. Guillory, 1991: Analysis of sudden mesoscale drying at the surface. *Mon. Wea. Rev.*, **119**, 1391-1406.

Gerald, D. B., and J. E. Janowiak, 1995: Atmospheric circulation associated with the Midwest flood of 1993. *Bull. Amer. Meteor. Soc.*, **76**, 681-685.

Giorgi, F., 1991: Sensitivity of simulated summertime precipitation over the western United States to different physics parameterizations. *Mon. Wea. Rev.*, **119**, 2870-2888.

Giorgi, F., M. R. Marinucci, G. T. Bates, and G. De Canio, 1993: Development of a second-generation regional climate model (RegCM2). Part II: Convective processes and assimilation of boundary conditions. *Mon. Wea. Rev.*, **121**, 2814-2832.

Grell, G. A, 1993: Prognostic evaluation of assumptions used by cumulus parameterizations. *Mon. Wea. Rev.*, **121**, 764-787.

Grell, G. A., J. F. Dudhia, and D. Stauffer, 1993: A description of the fifth generation Penn State/NCAR Mesoscale Model (MM5). *NCAR Tech. Note*, NCAR/TN-398+IA, 107pp. [Available from NCAR P.O. Box 3000, Boulder, CO 80307.]

Hsie, E.-T., and R. A. Anthes, 1984: Simulations of frontogenesis in a moist atmosphere using alternative parameterizations of condensation and precipitation. *J. Atmos. Sci.*, **41**, 2701-2716.

Kondo, J., N. Saigusa, and T. Sato, 1990: A parameterization of evaporation from bare soil surfaces. *J. Appl. Meteor.*, **29**, 385-389.

Kuo, S. L., 1974: Further studies of the parameterization of the effect of cumulus convection on large-scale flow. *J. Atmos. Sci.*, **31**, 1232-1240.

Kuo, Y.-H., and R. A. Anthes, 1984: Semiprognostic tests of Kuo-type cumulus parameterization schemes in an extratropical convective system. *Mon. Wea. Rev.*, **112**, 1498-1509.

Lakhtakia, M. N., and T. T. Warner, 1987: A real-data numerical study of the development of precipitation along the edge of an elevated mixing layer. *Mon. Wea. Rev.*, **115**, 156-168.

Lanicci, J. M., T. N. Carlson, and T. T. Warner, 1987: Sensitivity of the Great Plains severe-storm environment to soil-moisture distribution. *Mon. Wea. Rev.*, **115**, 2660-2673.

Mahfouf, J. F., and J. Noilhan, 1991: Comparative study of various formulations of evaporation from bare soil using in situ data. *J. Appl. Meteor.*, **30**, 1354-1365.

Manabe, S., 1969: Climate and the ocean circulation I: The atmospheric circulation and the hydrology of the earth's surface. *Mon. Wea. Rev.*, **97**, 739-774.

McCorcle, M. D., 1988: Simulation of surface-moisture effects on the Great Plains low-level jet. *Mon. Wea. Rev.*, **116**, 1705-1720.

Mintz, Y., 1984: The sensitivity of numerically simulated climates to land-surface boundary conditions. In *The Global Climate*, J. T. Houghton (ed), Cambridge University Press. 79-105.

Mitchell, M. J., R. W. Arritt, and K. Labas, 1995: A climatology of warm season Great Plains low-level jet using wind profiler observations. *Wea. Forecasting*, **10**, 576-591.

Mo, K. C., J. N. Paegle, and J. Paegle, 1995: Physical mechanisms of the 1993 floods. *J. Atmos. Sci.*, **52**, 879-895.

Molinari, J., and M. Dudek, 1992: Parameterization of convective precipitation in mesoscale numerical models: A critical review. *Mon. Wea. Rev.*, **120**, 326-344.

Otterman, J., A. Manes, S. Rubin, P. Alpert, and D. O'C. Starr, 1990: An increase of early rains in southern Israel following land-use change? *Bound.-Layer Meteor.*, **53**, 333-351.

Pan, Z., S. G. Benjamin, J. M. Brown, and T. Smirnova, 1994: Comparative experiments with MAPS on different types of parameterization schemes for surface moisture flux and boundary-layer processes. *Mon. Wea. Rev.*, **122**, 449-470.

Pan, Z., M. Segal, R. Turner, and E. Takle, 1995: Model simulation of impacts of transient surface wetness on summer rainfall in the United States Midwest during drought and flood years. *Mon. Wea. Rev.*, **123**, 1575-1581.

Raymond, D. J., and K. A. Emanuel, 1993: The Kuo cumulus parameterization. in *The Representation of Cumulus Convection in Numerical Models*, Emanuel and Raymond (ed), Amer. Meteor. Soc. 246pp.

Richards, F., and M. D. Hudlow, 1994: Hydrometeorological conditions during the Great Flood of 1993. *Preprints, Symposium on the Great Flood of 1993*, Nashville, TN, Amer. Meteor. Soc., 65pp.

Rodenhuis, D. R., D. Miskus, G. D. Bell, and K. C. Mo, 1994: Meteorological flood - origin, description, and causes of the Great Flood of 1993. *Preprints, Symposium on the Great Flood of 1993*, Nashville, TN, Amer. Meteor. Soc., 65pp.

Rosenthal, S. L., 1978: Numerical simulation of tropical cyclone development with latent heat release by resolvable scales. I: Model description and preliminary results. *J. Atmos. Sci.*, **35**, 258-271.

Rowntree, P. R., and J. R. Bolton, 1983: Simulation of the atmospheric response to soil moisture anomalies over Europe. *Quart. J. Roy. Meteor. Soc.*, **109**, 501-526.

Sanders, F., and D. O. Blanchard, 1993: The origin of a severe thunderstorm in Kansas on 10 May 1985. *Mon. Wea. Rev.*, **121**, 133-149.

Sato, N., P. J. Sellers, D. A. Randall, E. K. Schneider, J. Shukla, T. L. Kinter III, Y.-T. Hou, and E. Albertazzi, 1989: Effects of implementing the simple biosphere model in a general circulation model. *J. Atmos. Sci.*, **46**, 2757-2782.

Segal, M., R. W. Arritt, C. Clark, R. Rabin, and J. M. Brown, 1995: Scaling evaluation of the effect of surface characteristics on potential for deep convection over uniform terrain. *Mon. Wea. Rev.*, **123**, 383-400.

Sellers, P. J., Y. Mintz, Y. C. Sud, and A. Dalcher, 1986: The design of a simple biosphere model (SiB) for use within general circulation models. *J. Atmos. Sci.*, **43**, 505-531.

Sellers, P. J., J. A. Berry, G. J. Collatz, C. B. Field, and F. G. Hall, 1992: Canopy reflectance, photosynthesis, and transpiration. III. A reanalysis using improved leaf models and a new canopy integration scheme. *Remote Sens. Env.*, **42**, 187-216.

Shaw, R. H., 1981: Evaporation climatology of Iowa: *Special Report No 88.* Agriculture and Home Economics Experiment Station, Iowa State University, 20pp. [Available from Iowa State University.]

Turner, R. W., 1993: The impact of climate change on the Great Plains low-level jet. Ph. D. dissertation, Dept. of Agronomy, Iowa State University, Ames, IA 50011 116pp.

Wang, W., and N. Seaman, 1994: A comparative study of cumulus convection schemes in MM5. *Preprints, Tenth Conference on Numerical Weather Prediction.* Portland, OR, Amer. Meteor. Soc. 99-101. [Available from World Meteorological Orgnization, Geneva, Switzerland.]

WGNE, 1992: Report of the Seventh Session of the CAS/JSC Working Group on Numerical Experimentation. WMO.TD-No. 477. 50pp.

Yan, H., and R. A. Anthes, 1988: The effect of variations in surface moisture on mesoscale circulations. *Mon. Wea. Rev.*, **116**, 192-208.

Zhang, D.-L., and R. A. Anthes, 1982: A high resolution model of the planetary boundary layer–sensitivity tests and comparisons with SESAME-79 data. *J. Appl. Meteor.*, **21**, 1594-1609.

Zhang, D.-L., E.-Y. Hsie, and M. W. Moncrieff, 1988: A comparison of explicit and implicit prediction of convective and stratiform precipitating weather systems with a meso-scale numerical model. *Quart. J. Roy. Meteor. Soc.*, **114**, 31-60.

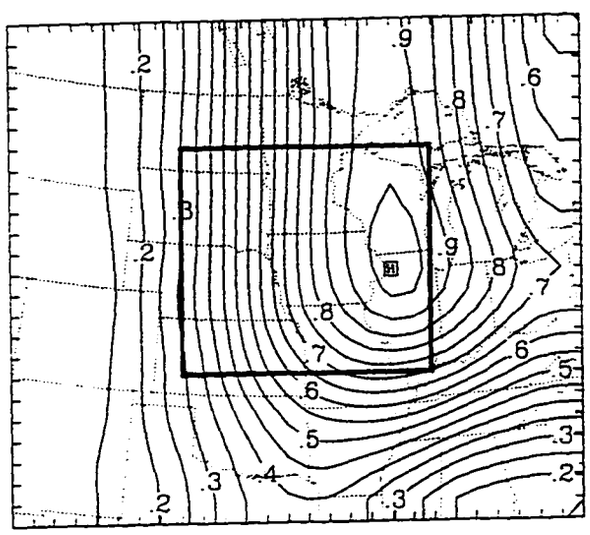

Figure 1 Simulation domains and estimated soil-moisture availability m field for 9 July 1993. The nested domain is indicated by the inner frame.

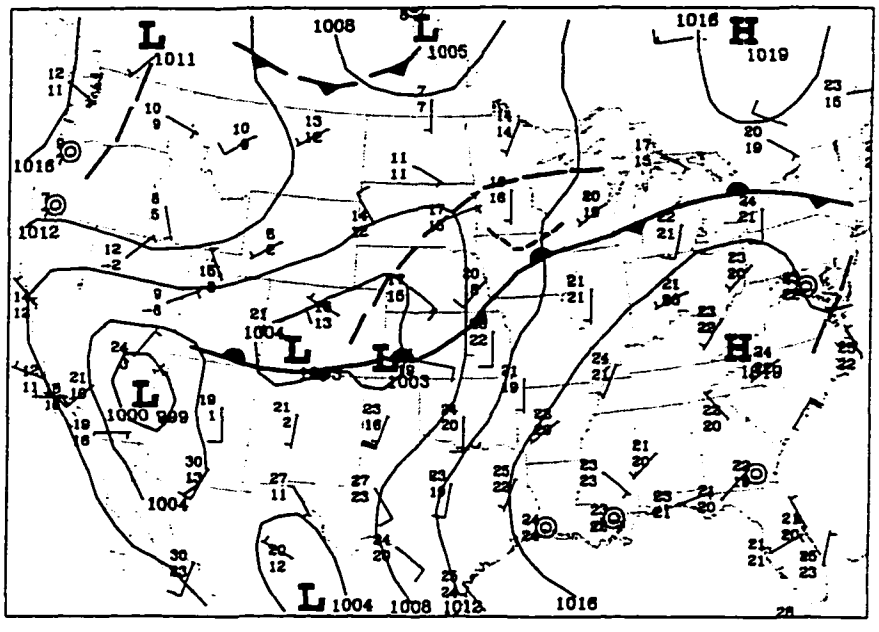

Figure 2 Surface synoptic chart at 1200 UTC 8 July 1993 (adapted from the Daily Weather Maps issued by the Climate Analysis Center of the NMC). The long-dashed lines are troughs and the short-dashed line is an outflow boundary.

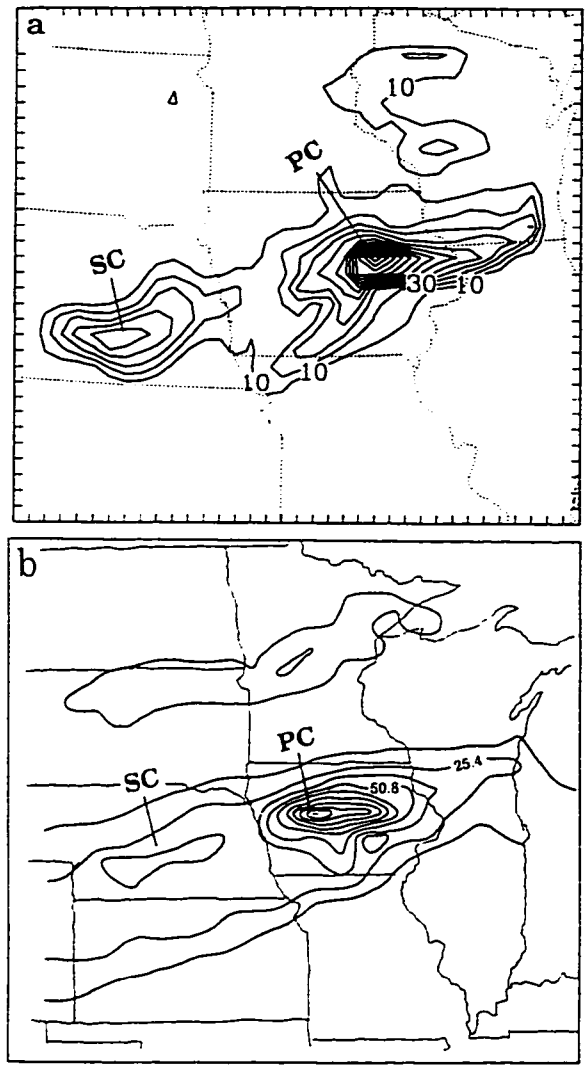

Figure 3 The 24-h accumulated rainfall fields (mm) at 1200 UTC 9 July 1993: (a) simulated (contour interval 10 mm), (b) observed (adapted from Richards and Hudlow (1994); contour interval 12.7 mm (0.5 in)). PC and SC denote the primary and secondary rainfall centers, respectively.

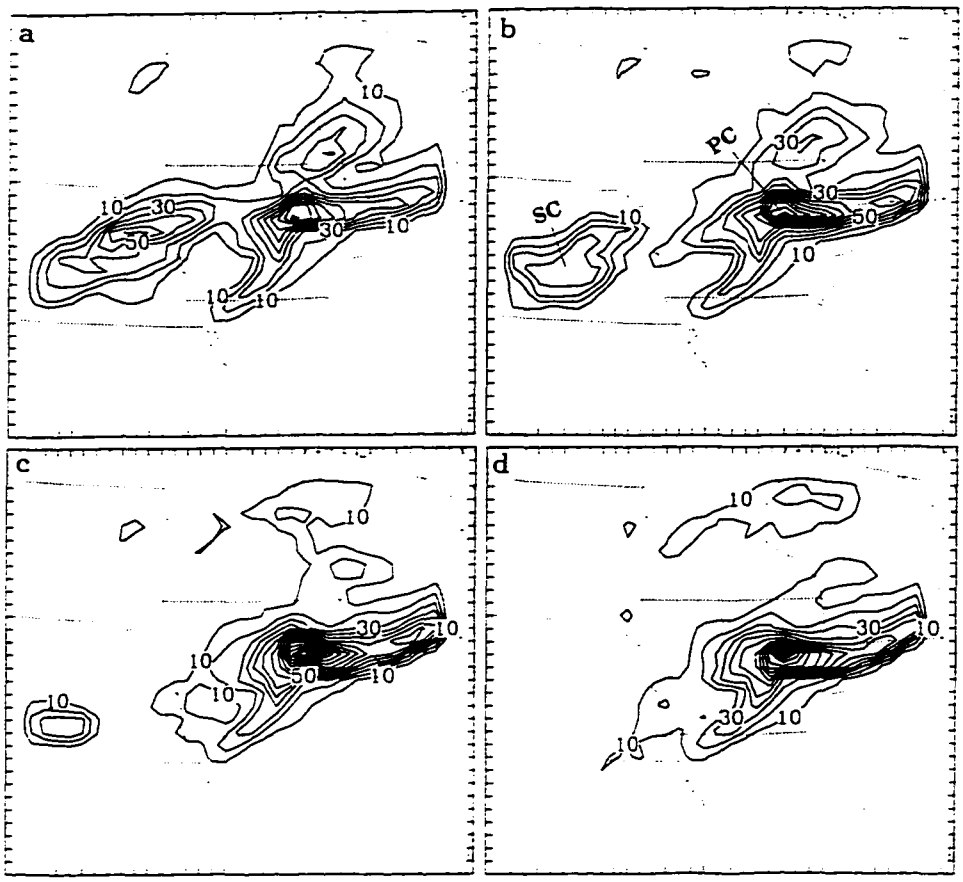

Figure 4 Simulated 24-h accumulated rainfall (mm) at 1200 UTC 9 July 1993 using GS as the cumulus convection scheme and AD as surface flux scheme for different m values: (a) $m = 0.1$, (b) m=0.2, (c) m=0.4, (d) m=0.6. PC and SC denote the primary and secondary rainfall centers, respectively.

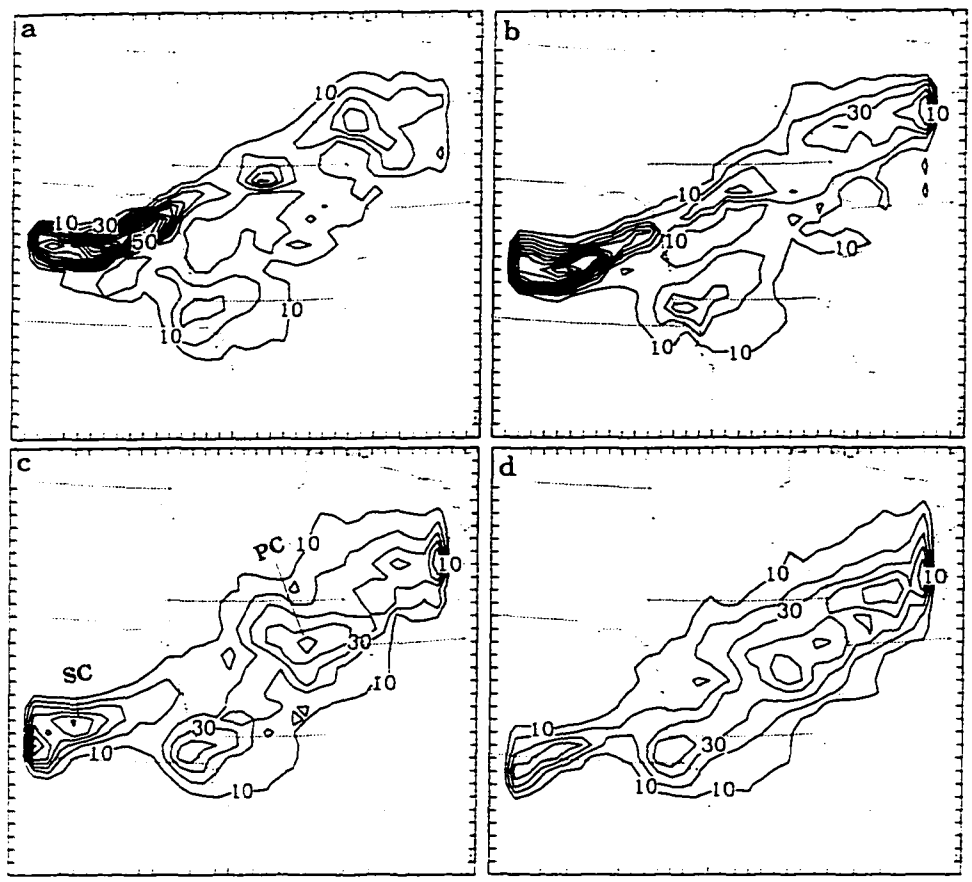

Figure 5 Same as Fig. 4 except for using KS as the cumulus convection scheme.

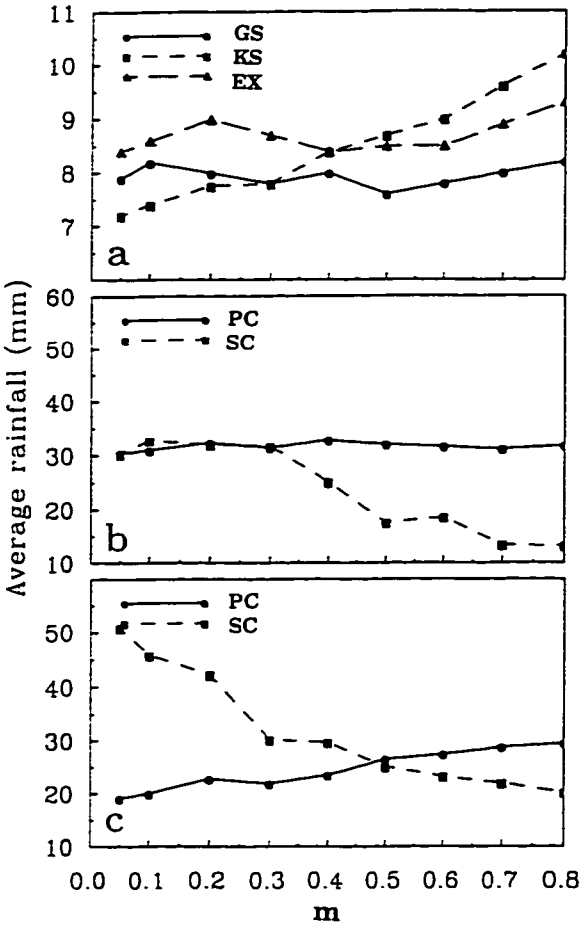

Figure 6 Dependence of average 24-h accumulated rainfall (mm) simulated at 1200 UTC 9 July 1993 on m for different cumulus convection schemes: (a) averaged over the nested domain (EX denotes the fully explicit cloud scheme), (b) averaged over the PC and SC separately using GS, (c) same as (b) except KS was used.

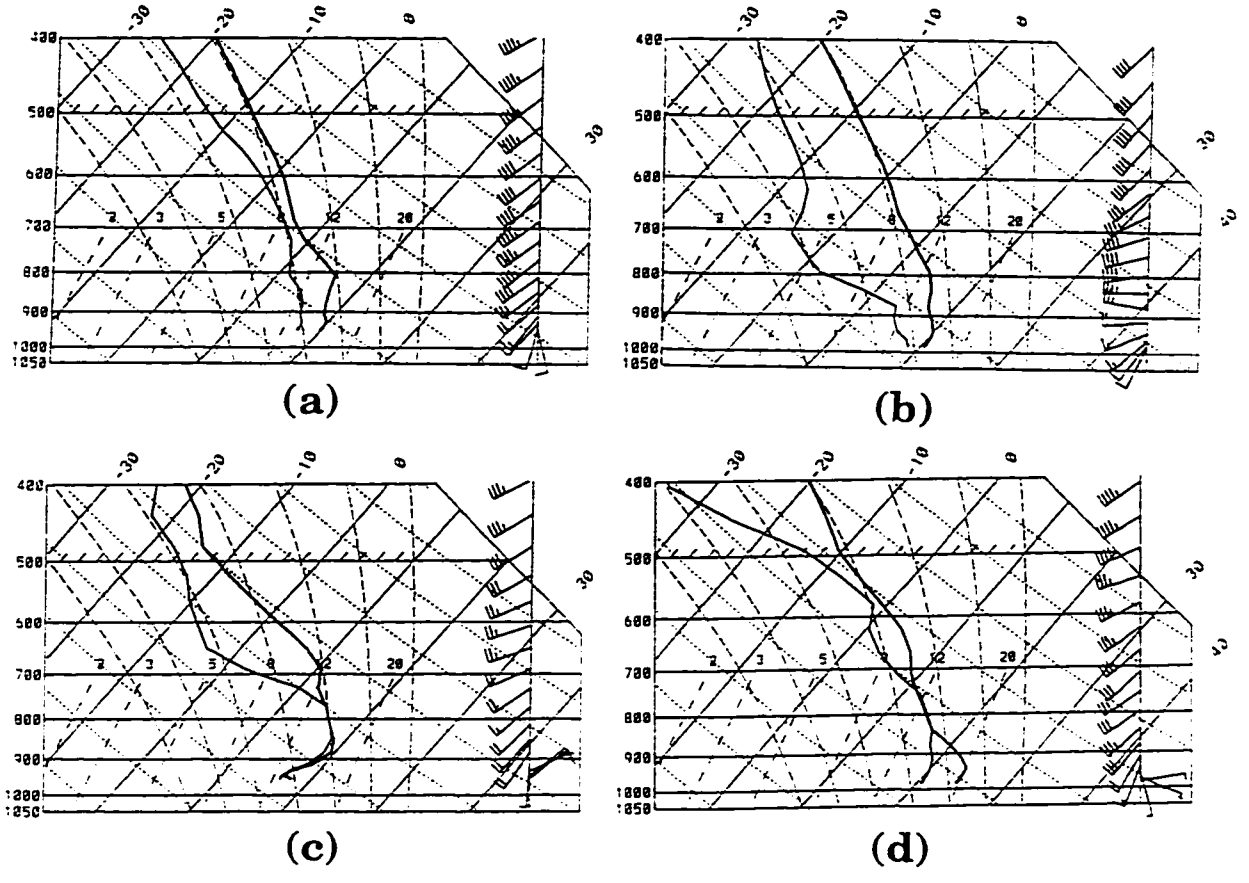

Figure 7 Soundings at the PC (42.0N, 93.0W) and SC (42.3N, 98.0W): (a) and (b) for the SC and PC observed at 1200 UTC 8 July 1993, respectively. (c) and (d) for the SC and PC simulated at 0600 UTC 9 July 1993 with m=0.2, respectively.

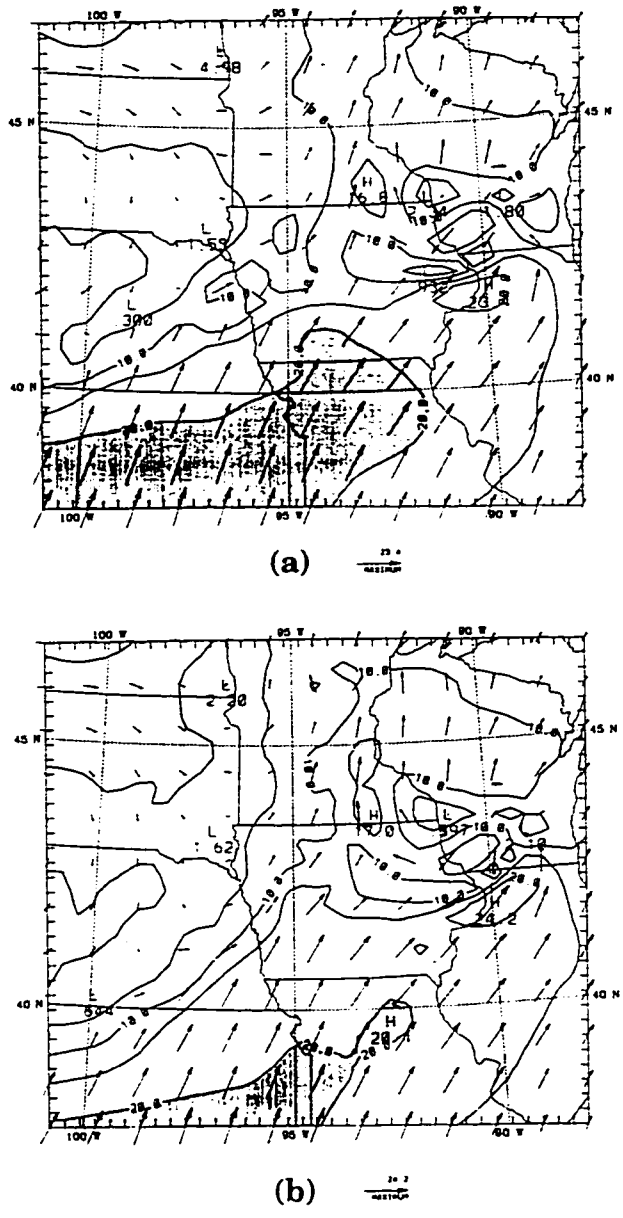

Figure 8 Simulated wind speed (m s^{-1}) and direction at the level $\sigma = 0.91$ (about 700 m AGL) at 0600 UTC 9 July 1993 for (a) m=0.2 and (b) m=0.6. Areas with wind speeds above 20 m s^{-1} are stippled.

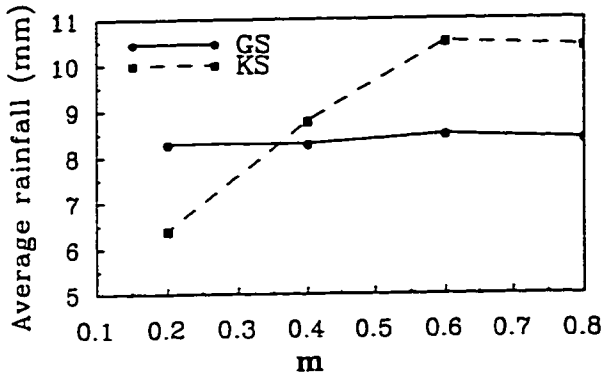

Figure 9 Simulated domain-averaged 24-h accumulated rainfall (mm) at 1200 UTC 9 July 1993 using the SiB as surface flux for different cumulus parameterization schemes and m values.

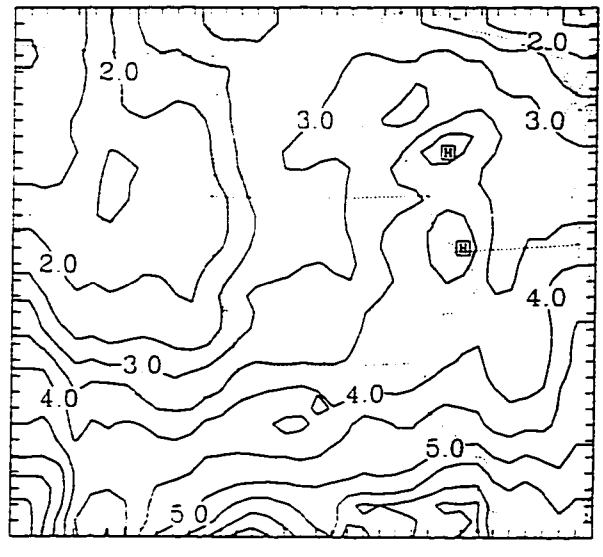

Figure 10 Simulated 24-h ET (mm) distribution at 1200 UTC 9 July 1993 with estimated m field given in Fig. 1 using the AD formulation and GS scheme.

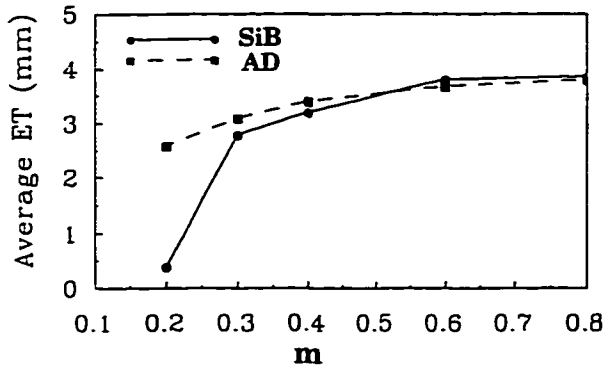

Figure 11 Domain-averaged 24-h ET at 1200 UTC 9 July 1993 for different m values using the SiB and AD schemes.

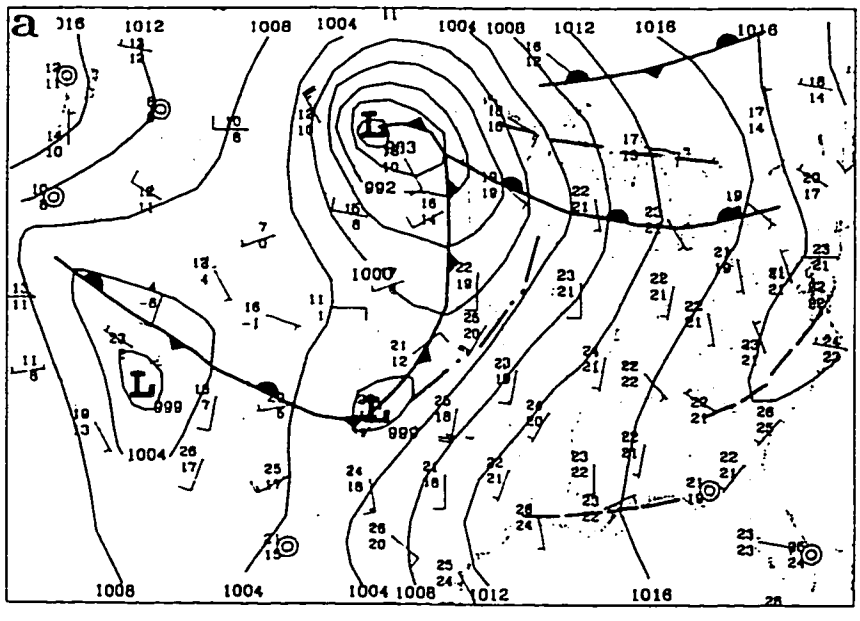

Figure 12 (a) Surface synoptic chart at 1200 UTC 4 July 1993. The dashed lines are troughs and the dash-dotted line is the squall line.

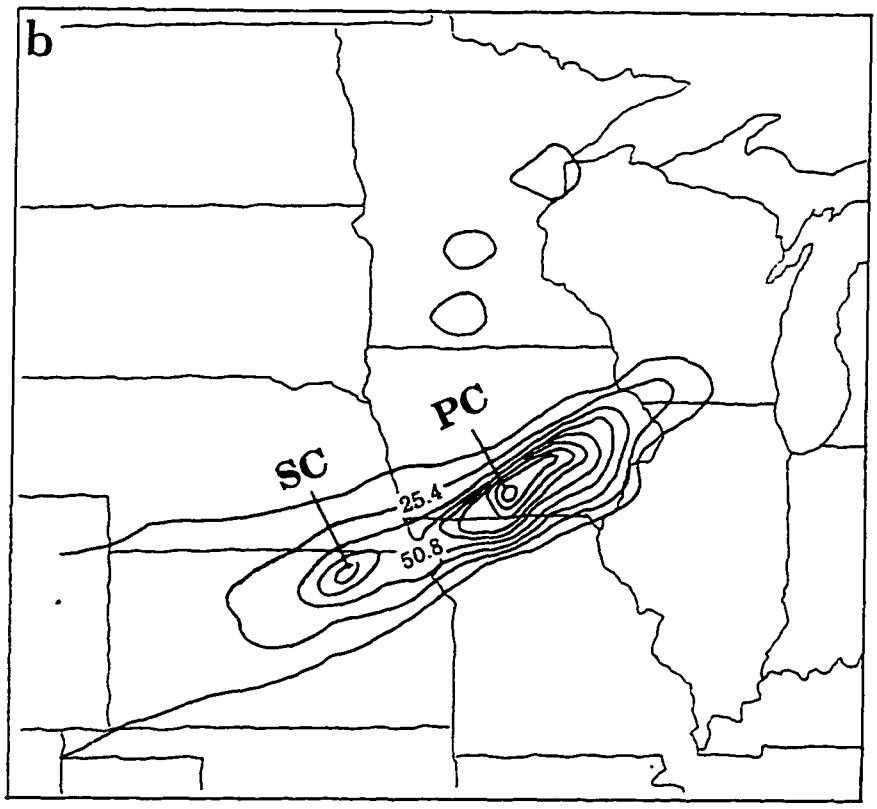

Figure 12 (continued) (b) Same as Fig. 3b except at 1200 UTC 5 July 1993.

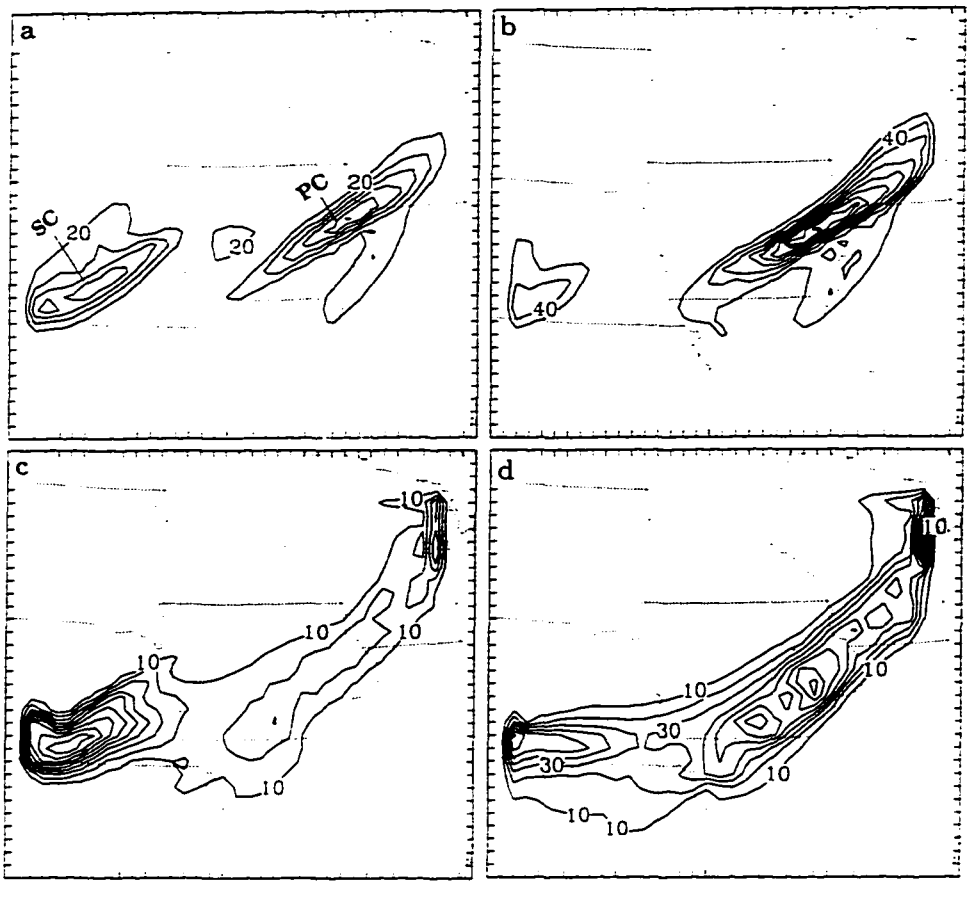

Figure 13 Simulated 24-h accumulated rainfall (mm) at 1200 UTC 5 July 1993 by GS and KS for different m values: (a) and (b) GS for m=0.2 and m=0.6, respectively, (c) and (d) KS for m=0.2 and m=0.6, respectively. PC and SC denote the primary and secondary rainfall centers, respectively.

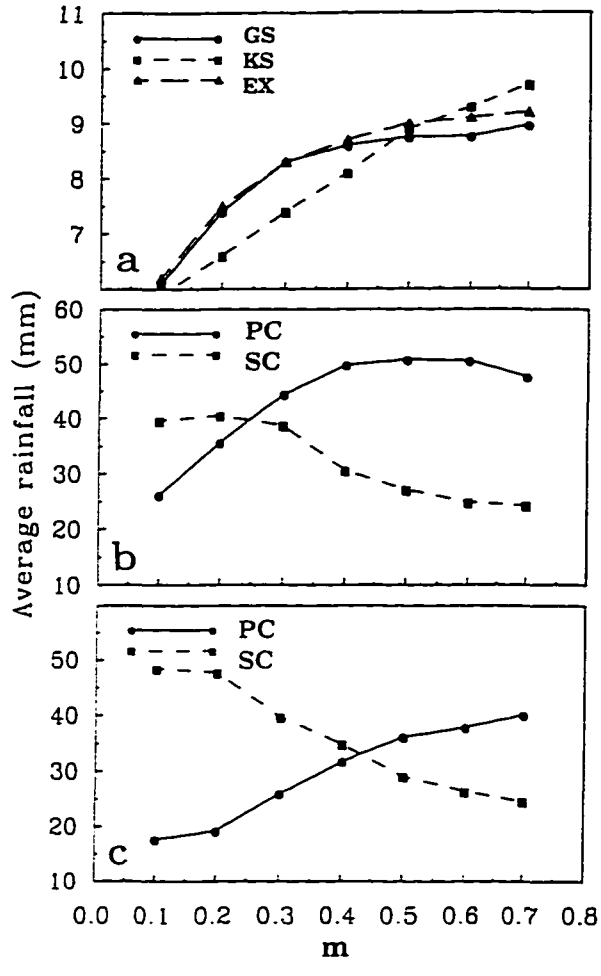

Figure 14 Same as Fig 6 except at 1200 UTC 5 July 1993.

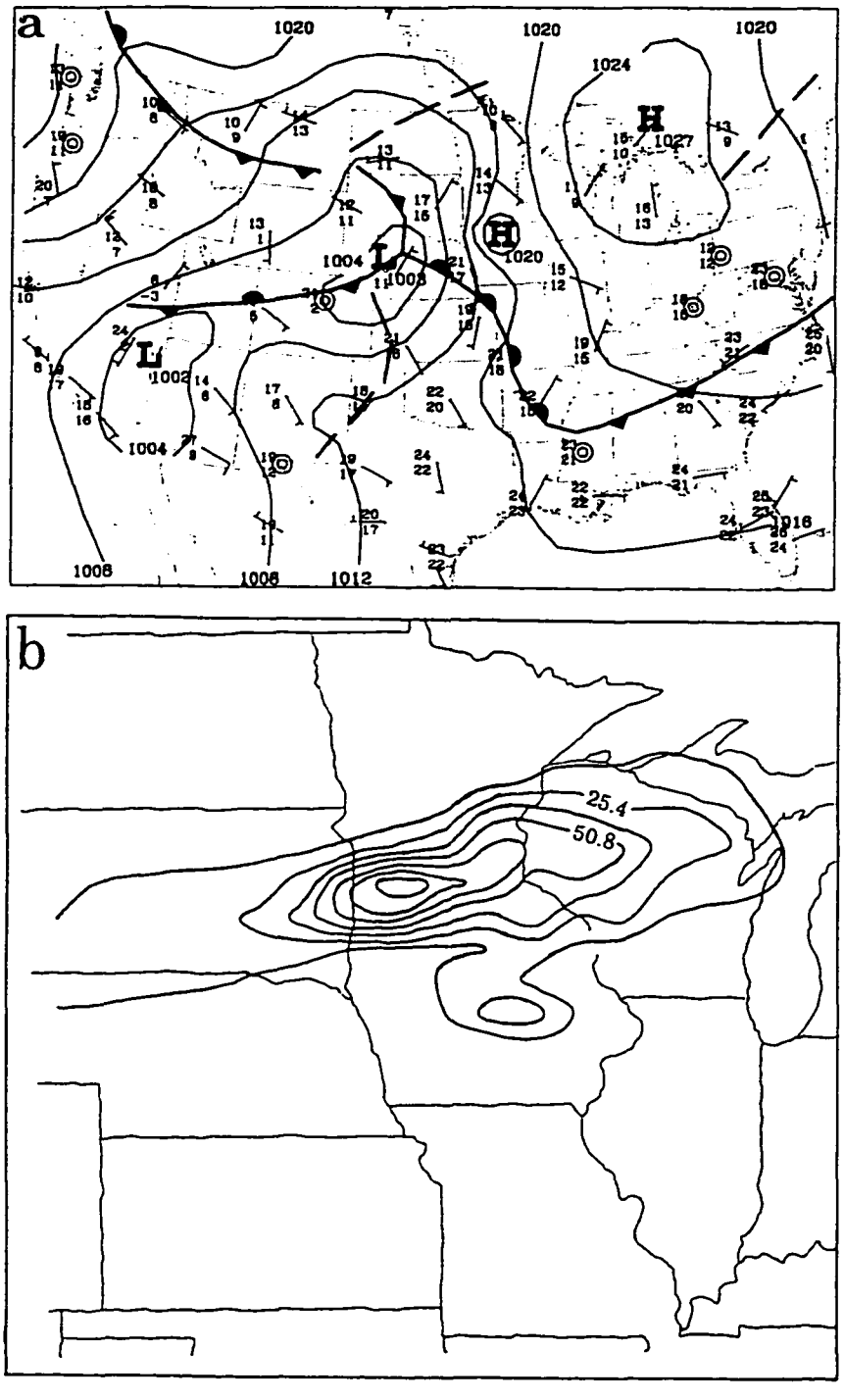

Figure 15 (a) Surface synoptic chart at 1200 UTC 16 June 1993. The dashed lines are troughs. (b) Same as Fig. 3b except at 1200 UTC 16 June 1993.

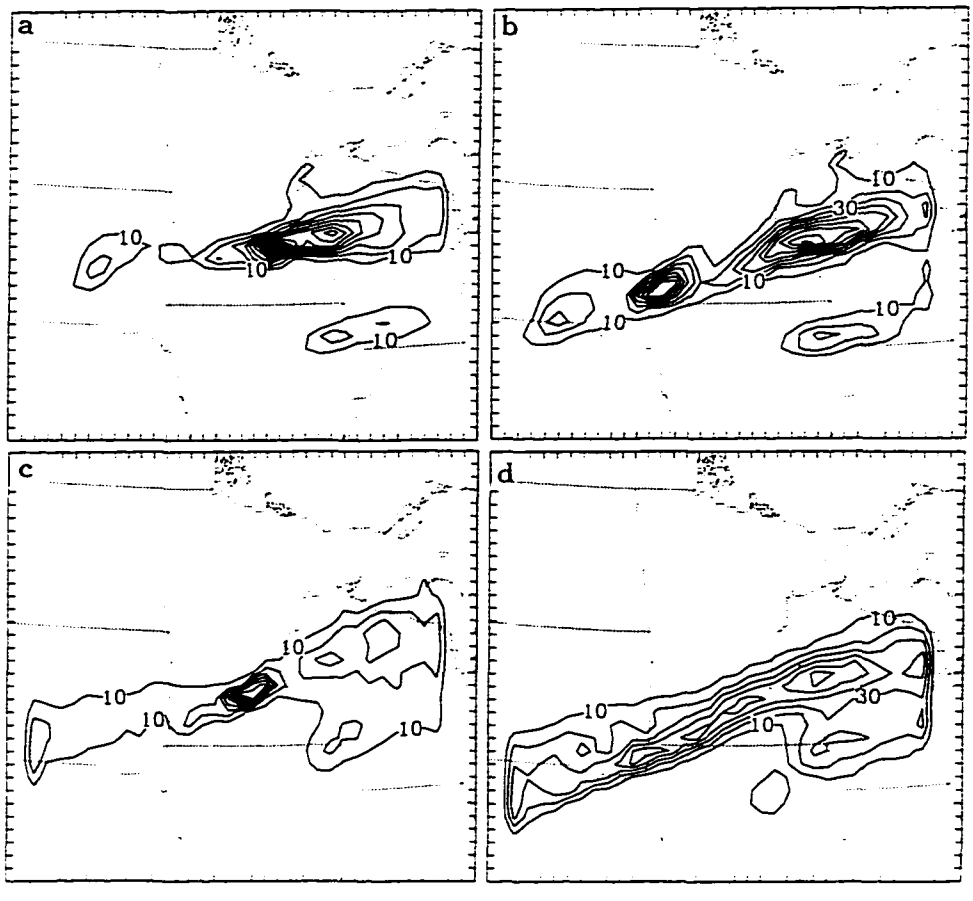

Figure 16 Simulated 24-h accumulated rainfall (mm) at 1200 UTC 17 June 1993 by GS and KS for different m values: (a) and (b) GS for m=0.2 and m=0.6, respectively, (c) and (d) KS for m=0.2 and m=0.6, respectively.

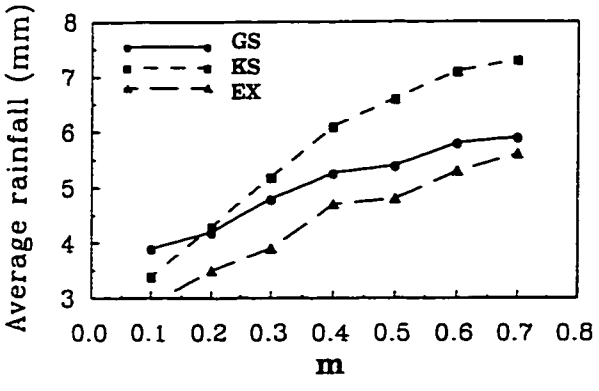

Figure 17 Dependence of simulated domain-averaged 24-h accumulated rainfall (mm) on m at 1200 UTC 17 June 1993 for different cumulus convection schemes (EX denotes the fully explicit cloud scheme).

LONG SIMULATION OF REGIONAL CLIMATE AS COLLECTIONS OF SHORT SEGMENTS

A paper to be submitted to *Journal of Climate*

Zaitao Pan, Eugene Takle, William Gutowski, and Richard Turner

Abstract

Regional climate simulations are long time integrations over an open system where model variables over part of the model domain are updated periodically. Model reinitialization after a certain length of integration can save wall-clock time and avoid possible drift caused by accumulated model errors. We investigate the necessity and feasibility of subdividing long integrations through nine experiments by which we examined the effects of reinitialization frequency and the relative importance of surface forcing and atmospheric forcing. The results show that for integrations that continued without reinitialization, locations of specific meteorological features drifted downstream because of the positive model bias on wind speeds, implying the necessity of periodically reinitializing the model. The results also indicate that the simulated domain-averaged variables, including rainfall, were not sensitive to model reinitialization since they are largely constrained by boundary conditions, suggesting the feasibility of dividing long regicnal climate simulations into a set of shorter simulations that could be run in parallel.

1 Introduction

Simulations of regional climate, like simulations of global climate, require integrations over several model years. High resolution and more detailed parameterizations make the computational cost greater for regional climate simulations than for global simulations. An advantage of such long integrations is the continuous representation of the long-term forcing. One such long-term forcing is soil moisture, which introduces seasonal or even interannual memory. In some sense, the atmospheric forcing by soil moisture over continents is similar to that of sea surface temperature over oceans. In fact, a partial cause for the 1993 Midwest Great Flood can be traced back to the wet soil in the winter of 1992 and spring of 1993 (Rodenhuis et al. 1994, Mo et al. 1995).

A disadvantage of long integrations, however, is that the model atmosphere in regional climate models (RCMs) can drift from forcing general circulation models (GCMs) or observations. The RCMs tend to separate from or decouple with GCMS during the integration, especially when integration domain is large (Kida et al. 1991, Machenhauer 1995, Paegle et al. 1996). Model errors, inaccurate numerics, and errors in physical parameterizations create artifacts that may remain in the domain for a long time. Although the model atmosphere is constrained by the boundary conditions provided by either GCMs or observations, differences between the modeled and observed atmospheres can still persist throughout the integration, especially far from the boundaries. These errors can then affect accumulated variables such as rainfall although they may not noticeably affect the simulated atmospheric states at the end of the simulation. Drift from forcing fields can be avoided if the long-wave components in RCMs are nudged frequently to the forcing GCMs over the whole interior domain (Kida et al. 1991, Paegle et al. 1996) or the slowly-varying variables (*e.g.*, lake and sea surface temperature) are updated along with the boundary conditions (*e.g.*, Giorgi et al. 1996). An alternative strategy is to increase the width of the boundary forcing zone, where the RCM variables are partly provided by GCMs.

The RCMs are open systems where the atmosphere over part of the domain (boundary forcing zones) or some components of the model atmosphere must be updated during the

course of the integration. In this regard, the RCMs are different from GCMs where no part of information in the model has to be updated. A question arises as to how much information from days ago is still left in the model system after a certain period of integration, especially when the interior domain is not large compared to the forcing zone. If very little previous information is left, we can break a long simulation into shorter ones, and thus both cost and wall-clock time could be reduced by performing regional climate simulations on collections of workstations rather than on supercomputers. These independent segments are perfectly scalable to any computers since they all have the same problem size.

Soil moisture is a long-term forcing in climate simulations. It may be argued that frequent restart of the model would interrupt this long memory or alter its spatial distribution through rainfall-soil interaction. The effects or penalty of this interruption need to be determined if frequent restart are to be employed. It is noteworthy that previous studies have found that the soil-moisture forcing within the model domain tended to be small compared to remote large scale forcing (Giorgi et al. 1996, Paegle et al. 1996).

This study aims to answer the following questions: 1) Is it necessary and appropriate to break a long simulation into several short ones, and if so, what are the quantitative effects of the reinitialization on simulations? 2) How important is the surface forcing relative to the atmospheric forcing in RCMs?

2 Experimental Design

In the present study we adopt an approach where the atmospheric fields are considered high-frequency forcing while the surface variables (primarily soil moisture and deep soil temperature) are considered low-frequency forcing. The modeled atmosphere is periodically updated with observations regardless of its wave components (or frequency). This simple updating scheme may be considered as the extreme case of the spectral nudging approaches (Kida et al. 1991, Paegle et al. 1996). The advantage of this straightforward updating method, in addition to its simplicity, is that it incorporates observed information on small scales, which would otherwise be wasted. The ECMWF analyses we use as forcing boundary conditions should be more

reliable than the model predicted atmosphere on both large and small scales.

Nine experiments were designed as summarized in Table 1. Each experiment is labeled as MxND where M is the number of segments in the overall run and N is the length of the segments in days. For example, experiment 3x10D is the collection of three segments of 10 days in length. Integrations in all experiments except for the 1x20D were carried out for 30 days. The first experiment, 1x30D, was integrated for 30 days without any reinitialization and served as the control. In the second experiment, 3x10D, all the model fields including soil moisture were initialized by observations every 10 d to see the effects of restart. The frequency of updating is increased further in experiments that restart the simulations every five days (6x5D), the approximate frequency of synoptic events, and every day (30x1D) to amplify the effects of reinitialization. If the model updates too frequently, spinup problems may be severe; on the other hand, if the integration is too long, the model fields may drift from actual observations. This range of updating frequency allows us to explore the relative effects of spinup and drift.

Table 1 Description of the experiments

Description	name	remarks
No reinitialization	1x30D	climatological M
Reinitialize model every 10 d	3x10D	climatological M
Reinitialize model every 5 d	6x5D	climatological M
Reinitialize model every 1 d	30x1D	climatological M
Same as 3x10D but overlap	3x13D	climatological M
Start at 10th day	1x20D	climatological M
Soil is un-interrupted	3x10DM	climatological M
Saturated soil	1x30DS	M=1 over flood area
Dry soil	1x30DD	M=0.05 everywhere

To minimize the effects of spinup and related adjustment (Yap 1995), in the 5th experiment, 3x13D, the model is still reinitialized every 10 d, but with a 3-d overlap with the previous 10 days. Each segment thus consists of 13 days with a three-day overlap period, which presumably contains the spinup effects and thus is disregarded, and then we compare results with the control experiment to evaluate this restart procedure. The effects of starting point on the integration

are examined in experiment 1x20D which started on the 10th day of the 30-d period without subsequent reinitialization.

Reinitialization effects may be attributed to updating the atmospheric states or to updating surface forcing. Experiment 3x10DM tests the effects of atmospheric and surface forcing separately by resetting the model to the observed state every 10 days. However in this experiment, soil moisture was maintained uninterrupted (same as the control 1x30D), allowing the determination of the relative impacts of the atmospheric and surface forcing updating.

The effects of soil moisture are further examined by two experiments specifying the surface as wet (1x30DS) and dry (1x30DD). In 1x30DS, the soil is set to the saturation level over the flood area along the Mississippi basin. This experiment is similar to that used in Giorgi et al. (1996) where soil over the entire domain was prescribed as saturated. In 1x30DD soil moisture availability is set to 0.05 everywhere as an extreme contrast of soil moisture effects.

3 The Model Used

The regional climate model used in this study (RegCM2) was developed at NCAR based on the Penn State/NCAR MM4 (Giorgi et al. 1993a, 1993b). The model incorporates the CCM2 radiation package (Briegleb 1992) and BATS version 1e (Dickinson et al. 1992) surface package (see Appendix for model equations). The model domain is 46x77x(50 km)^2 centered at (40.5 N, 106.5W) with 14 layers in the vertical. The simple Kuo cumulus parameterization scheme (Kuo 1974, Anthes 1977) is used. The Grell (1993) scheme is probably more accurate but was not chosen because it usually is accompanied by an explicit cloud scheme which is computationally intensive and unnecessary.

Climatological soil moisture availability (M) is used except in 1x30DS and 1x30DD where soil moisture was set to the saturation and dry, respectively. The setting can be roughly justified in 1x30DS because of the long length of the flood period. Additionally this setting is consistent with the observed Palmer Drought Index and Crop Moisture Index (Pan et al. 1995).

The integration covers the period from 0000 UTC 11 June to 0000 UTC 11 July 1993, the

peak period of the Midwest Great Flood (Gerald and Janowiak 1995). During this eventful period. physical and dynamic processes (*e.g.*, surface and precipitation) have prominent roles thereby providing a revealing test of model physics.

The initial and boundary conditions were interpolated from ECMWF T42 analyses. These analyzed fields are consistent and in balance with each other. Thus no further effort was attempted to adjust the initial and boundary conditions although the spatial interpolation to our model resolution may introduce slight imbalance. The model-predicted variables were nudged to the observations within the buffer zone of width 500 km where the tendencies of predicted variables are updated every 6 h (Giorgi 1993b).

4 Effects of Initialization Frequency

4.1 Surface Pressure

Regional climate simulations may require more time steps than global climate simulations and are therefore more vulnerable to accumulation of numerical errors of a given truncation (Δx and Δt) because of the exponential growth of the model errors. Conservation of domain total mass, determined from surface pressure, is one measure of the accumulation of errors. The temporal variation of domain-averaged pressure shown in Fig. 1 exhibits the passage of several synoptic waves, the strongest of which was on the day 23, when the heaviest rainfall occurred over the Midwest. Both the 3x10D and 1x30D experiments produced surprisingly accurate temporal variation and minimum drift of surface pressure compared with the observations. In fact, for the 1x30D integration, the pressure prediction in the last 10 d was even more accurate than the first two 10-d periods. The spatial distribution of surface pressure also was reproduced reasonably well with errors of about +3 hPa centered in the Oklahoma panhandle (Fig. 2). The positive bias may weaken the southerly flow over Texas where the low-level jet occur frequently. A narrow band of about -2 hPa occurred along the California coast. The overall simulation error in pressure is about 0.5 hPa. The good agreement between the observed and forecast surface pressure fields is somewhat expected since the pressure systems that dominate synoptic-scale phenomena are manifestations of large-scale waves. Other experiments (not

shown) simulated similar distributions of surface pressure.

4.2 Spatial Distribution of Rainfall

Rainfall is the end product of numerous atmospheric processes and can be very sensitive to the model configuration and atmospheric state. The spatial distribution of observed 30-d accumulated rainfall in Fig. 3a reveals a heavy-rainfall area with over 200 mm centered on Iowa and covering most neighboring states. An elongated heavy rainfall center was observed near the Nebraska-Missouri border and produced more than 300 mm averaged over the grid box (with a maximum of 530 mm at one station). Daily reinitialization (30x1D) reproduced the heavy rainfall area with similar shape and location, although the amount and extent were larger. The rainfall center observed in northeastern Kansas was shifted northward to central Iowa in the simulation (Fig. 3b). The main rainfall in the 6x5D (Fig. 3c) and 3x10D (Fig. 3d) experiments shifted downstream to eastern Iowa and western Wisconsin. In the 1x30D simulation (Fig. 3e) , there was no well-defined rainfall center in the flood region and rainfall was more scattered. The center of maximum rainfall was shifted eastward to the Great Lakes region, and only about 200 mm rainfall was simulated in the region compared with more than 400 mm peak of observed rainfall. Table 2 lists the maximum rainfall, location error of rainfall center (the location with maximum rainfall), and threat score (TS) of rainfall over 200 mm. The threat score is defined as

$$TS = \frac{A_C}{A_F + A_O - A_C}, \tag{1}$$

where A_C and A_O are, respectively, areas of correctly forecast and observed rainfall over 200 mm, and A_F is the total forecast area. A perfect forecast would give $TS = A_C/A_F = 1$. This table shows that, as reinitialization frequency increases, the location and distribution become better forecast. However, the maximum rainfall increases excessively as reinitialization frequency increases due to the spinup/adjustment (Yap 1995). The downstream drift (position error) of the rainfall area was probably due to the accumulation of positive wind bias in the model (see discussion in next subsection). On the other hand, with more frequent restart the model captured the spatial distribution of rainfall better because the wind fields, which determine the system location and are overpredicted in the model, were set to the observations.

Table 2 Rainfall simulation errors in different experiments

Variable	1x30D	3x10D	6x5D	30x1D	3x13D	Perfect
Max. rainfall (mm)	328	344	381	475	353	331
Position error (km)	900	600	500	350	900	0
TS score (%)	11	12	26	29	11	100

In the 3x13D where the first 3 d of simulation for the second and third 13-d periods were discarded, the rainfall distribution was very similar to that of 1x30D (Fig. 3f). The rainfall distribution, which is one of the most sensitive variables, is essentially the same for the 30-d continuous run and three separate 10-d runs. This strongly supports the feasibility or even the necessity of breaking long climate integrations into collections of short runs.

The rainfall over Montana was probably more dominated by stratiform precipitation over larger scales compared with the intense convective rainfall over the flood regions. All simulations reproduced reasonably well the observed rainfall areas over Montana although the amounts were slightly smaller than the observed. This implies that rainfall totals on larger scales were less sensitive to the initialization frequency than those over smaller scales, presumably because the stratiform rainfall is controlled mainly by synoptic phenomena which are less sensitive to model details than mesoscale convection. On the other hand, none of these experiments captured the observed rainfall along the Texas-Louisiana coast (possibly due to being too close to the boundaries).

4.3 Temporal Variation of Rainfall

The observed domain-accumulated rainfall increased roughly at 2 mm d^{-1} (Fig. 4a). All four experiments (1-4) simulated essentially the same magnitude of rainfall, all being about 15-20% smaller than the observed amounts. During the first half of the 30-d period, the simulated domain-averaged rainfall was about 1.3 mm d^{-1}, 80% of the observed values, but for the second half of the 30-d period, the simulated rainfall was similar to the measurements. At the end of 30 d, the simulated rainfall was around 45 mm, slightly lower than the observation. The underprediction of rainfall is typical of model simulation of heavy rainfall events because sub-

grid scale processes responsible for producing heavy rainfall events are not well resolved by the model. The similar amounts of domain-total rainfall simulated by all the experiments indicate that different updating frequencies alter rainfall distribution within the domain but not the total amount. This implies that total precipitation is mainly governed by large-scale inflow through the boundaries.

The partitioning of total rainfall into convective and non-convective forms helps us understand model dynamics. The partitioning of rainfall was quite different among different experiments although the total amounts of rainfall were almost identical (Fig. 4b). For the 30x1D simulation, about 65 % of rainfall was in convective form whereas the values were 44, 40, and 32 % for the 6x5D, 3x10D and 1x30D experiments, respectively. The larger convective portion of rainfall in the 30x1D simulation indicates that as integration period increases, rainfall processes shifted from convective to the nonconvective form. Since the observed rainfall was indeed mostly convective during this time of the year, the long-term integration in 3x10D and 1x30D biases precipitation toward the nonconvective form. This distortion may be partly explained by the possibility that convection was suppressed by the accumulated numerical smoothing in the model. Also, the ratios in different experiments were rather steady, implying persistence of the difference. It should be noted that the ratio may not be meaningful for the first few days when rainfall was small.

The domain-averaged rainfall may mask features from the individual synoptic systems, so rainfall accumulation over the flood region was analyzed to emphasize heavy rainfall events. The flood region defined here covers 1000x1000 km^2 centered near the observed rainfall center in northeastern Kansas (see Fig. 3a).

The flood-region average rainfall amounts predicted by experiments (1-4) were similar to each other and to the observations, but were smaller than the measured values for the entire period except for the 30x1D which gave significantly larger rainfall than all other simulations as well as the observation (Fig. 4c). This difference steadily grew with time, implying that the difference was continuously generated. On the other hand, the differences among the 6x5D, 3x10D, and 1x30D were smaller and did not increase with time. This may be partly explained

by the fact that a period of 5 or more days is beyond the model spinup/overshooting time. The difference between updated and non-updated model runs occurs mainly within the first couple of days, beyond which the atmospheric state is basically determined by the boundary conditions. The 6x5D and 3x10D simulations are close, implying the spinup problem was much shorter than 5 days. The 30x1D experiment over-simulated accumulated rainfall due to the unrealistically heavy rainfall that occurred during the last five days. On the other hand, the other experiments had rainfall similar to the actual values during this 5-d period.

Diurnal variation of rainfall gives a clue to its underlying cause. We analyzed 6-h rainfall totals over the flood region to examine diurnal distributions. The observed rainfall shows a well defined diurnal cycle that was superimposed on the synoptic waves (Fig. 5a). Heavy rainfall occurred during afternoon and evening (1800-0600 UTC) (Table 3). The 30x1D simulation produced a stronger daily cycle but it shifted the diurnal peak toward late morning (1200-1800 UTC). This shift was due to the model spinup effect that minimized rainfall during 0000-0600 UTC. (Integrations in the 30x1D start at 0000 UTC.) The 3x10D and 1x30D simulated diurnal cycles well although the peaks tended to shift to early morning (0600-1200 UTC) slightly.

Table 3 Six-hourly rainfall (mm) averaged over the 30-d period (times in UTC)

Expt.	00-06	06-12	12-18	18-00
Obs.	1.63	0.94	0.91	1.57
30x1D	0.24	1.48	2.12	2.19
3x10D	1.18	1.11	0.96	1.00
1x30D	1.19	1.13	0.89	0.92

The 30x1D experiment, with its integration period presumably well within the spinup time, produced much more rainfall than the others. The generally accepted view is that the vertical circulation and precipitation should be weak during the spinup period. Rainfall in this experiment was larger by contrast. Possible explanations are either that the model spinup time in this case was much shorter than 1 d and the related overshooting was dominant or that the longer integrations distorted the precipitation processes.

From our previous experience (Pan et al. 1995) with MM4, from which the current model RegCM2 was evolved, rainfall develops rather quickly, within 3-9 h. Once precipitation starts, it intensifies rapidly and then tapers off as the integration proceeds. The model initially tends to adjust all the inconsistencies, such as unphysical convergence, among different variables to achieve a balanced state and may produce spurious rainfall in the process (Horel et al. 1994, Yap 1995). These experiments suggest that the adjustment effects on rainfall are larger than the spinup effects. This adjustment or overshooting was most evident in the last 5-d of the simulation period when atmospheric conditions were conducive to convection. It is responsible for the excessive rainfall seen in Fig. 4c.

The time series of daily rainfall for 3x10D, 1x30D and 3x13D shown in Fig. 5b reveal differences between the 3x10D and 1x30D experiments, especially during the first 3 d of restart. This result corroborates the results of the spatial distribution of the simulated rainfall (Fig. 3e), supporting the validity of dividing a 30-d run into 3 10-d runs, particularly if the overlapping technique is used.

Frequent reinitialization keeps rainfall in the correct location (Fig. 3) but produces excessive amounts (Fig. 4) due to the initial adjustment of imbalanced fields. This adjustment mostly affects the rainfall magnitude but not rainfall location. On the other hand, less frequent reinitialization eliminates the spinup/adjustment problem, but allows rainfall locations to shift downwind because of enhanced simulated winds. An intermediate frequency of initialization seems desirable, with the time-overlapping method applied in 3x13D being an effective means of eliminating excessive rainfall and downstream shift.

In 1x20D, the integration started at day 10. Its 20-d accumulated rainfall (Fig. 6a) was generally similar to that of the last 20-d in 1x30D (Fig. 6b). Note Fig. 6a contains the overshooting in the first couple of days. Figures 6a and 6b would have been more closer to each other if the overlapping technique had been used in experiment 1x20D. This suggests that rainfall of later days was not sensitive to the starting point of the integration. This similarity is reasonable since the initial condition would die off after 2-3 days when there were no major rainfall events during the first 10-d period.

4.4 Upper-Air Fields

Figure 7 shows the wind speed at the 7^{th} model level (σ=0.51) averaged over the interior domain which excludes the boundary forcing zones. In RegCM2 the vertical coordinate is

$$\sigma = \frac{p - p_t}{p - p_s} \tag{2}$$

where p is pressure at a particular model level, p_t is the pressure at model top (=80 hPa), and p_s is the surface pressure. This 7^{th} level is at about 500 hPa near the center of the model domain. All three experiments (1x30D, 3x10D, and 6x5D) simulated similar temporal trends that resemble very well the observations (Fig. 7a). The wind simulation at the 11^{th} level (σ=0.895, about at 900 hPa) is not as good as that at σ=0.51 although simulated winds followed the observed trends well (Fig. 7b). The insensitivity of domain-averaged wind is explained by the fact that the average properties over the whole domain are largely constrained by boundary conditions. The initialization does not significantly change the fluxes at the boundaries which are mostly determined by observations. The model overpredicted noticeably wind speeds, especially at lower levels over the western mountain areas. The restart helped reduce the errors temporarily in the first 2-3 days. The predicted troughs were deeper over the Great Plains and winds were more westerly over the Midwest and Great Lakes region, as compared with the observation (Fig. 8). These overpredicted winds were responsible for the downstream shifting of the rainfall area in the 3x10D and 1x30D experiments seen in Fig. 3.

The small variation of domain averages with different reinitialization frequency does not necessarily imply the insensitivity at a particular location or over subregions. The latter is more dependent on the internal model physics and dynamics whereas the former is more dependent on boundary conditions. We checked the time series of wind speed (and temperature and mixing ratio) simulated by the different experiments at a grid near the observed rainfall center at the 7^{th} model level. Like the domain average, they all followed trends similar to the observations although with some individual differences (not shown).

The errors in the interior domain-averaged temperature simulated at the 7^{th} level were very small, ranging from 0.2 to 0.4 K (Fig. 9a). A negative maximum of $\sim$-1 K occurred during the period of the heavy rainfall that was underpredicted, presumably associated with

convective heating. All three experiments produced essentially the same results except for 2-3 d immediately after restart.

All three runs exhibited negative bias in water vapor mixing ratio at the 11^{th} level (Fig. 9b). The shocks (the deviation from the non-restart run) resulting from the restart were larger and lasted slightly longer in the mixing ratio compared to the temperature and winds at the same level (not shown). It took about 4 days for the effects of the restart to fade out. It is seen that the restart helped reduce the prediction errors, and especially for the atmospheric moisture for which model error was large.

Energy spectra are important characteristics of the atmosphere and correct representation of their distribution is essential for regional climate simulations. As an example, we decomposed the wind fields by a two-dimensional Fourier transform:

$$f(x,y) = \Sigma_{m=0}^{\infty}\Sigma_{n=0}^{\infty} D_{m,n} \times exp\left[i\left(\frac{2\pi m}{S}x + \frac{2\pi n}{T}y\right)\right] \tag{3}$$

where

$$D_{m,n} = \frac{4}{ST}\int_{-S/2}^{S/2}\int_{-T/2}^{T/2} f(x,y) \times exp\left[-i\left(\frac{2\pi m}{S}x + \frac{2\pi n}{T}y\right)\right] \tag{4}$$

where $f(x,y)$ represents an arbitrary two dimensional variable, $D_{m,n}$ is the corresponding Fourier coefficient, S and T are the domain lengths in the E-W and N-S directions, and m and n are the wave numbers in the E-W and N-S directions, respectively. As an example, Fig. 10 shows the time-averaged wave amplitude ($D_{m,n}$) of u-component winds at the 7^{th} level. Observations indicate that energy was sharply concentrated at the longer wave lengths (smaller wave number) in both E-W and N-S directions. The 1x30D simulation gave a much wider spectrum than the observed, indicating the presence of more small-scale motions. Thus, the model indeed generated mesoscale features when forced by the large-scale fields at the boundaries. A similar wind spectrum to the 1x30D run was obtained for the 3x10D simulation.

Renshaw and Fort (1983) suggested that decomposition by one-dimensional Fourier transformation provides a clearer view of spectral behavior. The simulated one-dimensional spectrum has more power over shorter waves (Fig. 11), with the 1x30D results having had slightly more power than those for 3x10D for short wave length in the E-W direction.

5 Effects of Reinitializing Soil Moisture

Long-term forcing due to soil moisture was examined by reinitializing atmospheric variables but keeping soil moisture uninterrupted. Figure 12 shows the results from 3x10DM where the atmosphere was updated but the soil moisture was not interrupted (same as that in the 1x30D run). The 1x30DM accumulated rainfall is closer to that for 3x10D than for 1x30D and the maximum rainfall center coincided with that in 3x10D (Fig. 3d). The similarity of 1x30DM to 3x10D results indicates that updating atmospheric forcing had larger impacts than updating surface forcing. However, the difference in total soil water content was less than 2 mm between the experiments with and without soil-moisture reinitialization (Fig. 13). So, the soil moisture did not change much between the updated and non-updated cases. Also, it seems that in BATS, soil moisture tends to be close to saturation most of the time during this period (F. Giorgi, personal communication). Previous studies have found that the atmospheric response to soil moisture is most sensitive when soil is relatively dry (*e.g.*, Clark and Arritt 1995).

Figure 14 shows the 30-d accumulated rainfall for 1x30DS and 1x30DD. The two experiments produced similar patterns of rainfall that also closely resemble the results for the 1x30D experiment. Drying the soil produced less rainfall compared with 1x30DS over most areas except for isolated spots in Kansas and Oklahoma. The negative correlation between rainfall and soil moisture possibly was due to strengthened low level jets over the dry surface (Paegle et al. 1996, Pan et al. 1996). The small difference in rainfall between these two experiments suggests the secondary importance of soil moisture memory and provides additional evidence that dividing a long simulation into a collection of shorter runs may not be substantially degraded by loss of soil moisture persistence.

6 Summary and Discussion

Long-period simulations of regional climate have the advantage of keeping the long-term forcing uninterrupted. The disadvantage of such long-time integration, however, is that the model atmosphere in the domain interior can drift from the forcing observations during the course of integrations. An optimal reinitialization frequency for the entire domain will re-

tain sufficient long-term forcing but improve the accuracy of the simulated fields. Long-term complete domain reinitialization offers the possibility of dividing long-term simulation into a collection of independent simulations that could be run on a cluster of workstations to speed up the simulation and reduce cost.

Nine experiments reported in this study evaluate the impacts of complete domain reinitialization at various frequencies. The results showed that in continuous integrations without the domain interior updating, meteorological features drifted downstream because of the accumulated positive model bias on wind simulation. On the other hand, when the reinitialization was too frequent, excessive rainfall was produced owing to the spinup/adjustment, although the positioning of rainfall area was improved.

The results showed that *domain-averaged* winds, temperature, mixing ratio and rainfall were not sensitive to reinitialization. The total mass, rainfall, and average winds over the domain were similar during the one-month period whether the model integration was interrupted every 5 d, 10 d, or not at all. These suggest that domain-averaged properties are mainly constrained by boundary conditions fed into the model.

The spatial and temporal distributions of various variables were somewhat sensitive to the frequency of model reinitialization for individual synoptic events. These effects were found to be attributable to atmosphere updating rather than to soil moisture updating, even though the model atmosphere advects out of the model domain within a few days whereas soil moisture influences the model throughout the integration. The secondary importance of surface forcing (long memory variable) provides the opportunity to subdivide a long simulation into shorter ones.

Soil moisture is one of the most poorly observed variables and is usually very crudely represented in most models. Climatological or arbitrarily specified values commonly are used for soil moisture content. The errors introduced by the interruption of long-term forcing from soil moisture are probably well within the range of the uncertainty associated with soil moisture specification.

The differences or shocks in simulated fields among the experiments with different initial-

ization frequencies are mainly limited to 2-3 d after the restart. These shocks, which are caused by the imbalance adjustment, can be eliminated by using a short overlap period. The shocks due to the reinitialization can be enhanced by heavy rainfall events when rain falls and gives a cumulative effect through the interaction of soil moisture with the atmosphere. Therefore, reinitialization should avoid such heavy rainfall events. This implies that the individual segments are likely to be of somewhat unequal length.

In summary, it should be and seems feasible to divide a long regional climate simulation into a collection of shorter ones, provided (1) the minimum simulation interval is long enough to minimize the spinup/adjustment problem, (2) the break point does not occur during a period of heavy rainfall, and (3) the overlapping procedure is applied. This study has shown that even a relatively short one-month period can be subdivided without sacrificing accuracy. From the computational and economical point of view, regardless of the drift caused by continuous integration, dividing a multi-year simulation into multiple one-year runs with a few days of overlapping will introduce differences that are negligible compared to the uncertainties associated with other components of the models but reduce cost and time of the simulations considerably.

Acknowledgments

The authors thank Ms. Christine Shields who kindly provided part of initial and boundary conditions and patient consultation on the RegCM2 code. We are thankful to Dr. Filippo Giorgi for his valuable advice. Helpful discussions with Chris Wikle and Moti Segal are also highly appreciated. Part of computer support used in this study was provided by the National Center for Atmospheric Research sponsored by the NSF. Partial financial support was provided by NASA grant NAG 5-2491.

References

Anthes, R. A., 1977: A cumulus parameterization scheme utilizing a one-dimensional cloud model. *Mon. Wea. Rev.*, **105**, 270-286.

Betts, A. K., J. H. Ball, A. C. M. Beljaars, M. J. Miller, and P. Viterbo, 1994: Coupling between land and surface boundary layer parameterizations and rainfall on local and regional scales: Lessons from the wet summer of 1993. *Preprints, Fifth Symp. on Global Change*, Amer. Meteor. Soc., 65 pp.

Briegleb, B. P., 1992: Delta-Eddington approximation for solar radiation in the NCAR Community Climate model. *J. Geophys. Res.*, **97**, 7603-7612.

Clark, C. A., and R. W. Arritt, 1995: Numerical simulations of the effect of soil moisture and vegetation cover on the development of deep convection. *J. Appl. Meteor.*, **34**, 2029-2045.

Dickinson, R. E, R. M. Errico, F. Giorgi, and G. T. Bates, 1989: A regional climate model for the western United States. *Climate Change*, **15**, 383-422.

Dickinson, R. E., A. Henderson-Sellers, and P. J. Kennedy, 1992: Biosphere-atmosphere transfer scheme (BATS) version 1e as coupled to NCAR community climate model. *NCAR Technical Note, 387+STR*, 72pp.

Gerald, D. B., and J. E. Janowiak, 1995: Atmospheric circulation associated with the Midwest flood of 1993. *Bull. Amer. Meteor. Soc.*, **76**, 681-685.

Giorgi, F., 1990: On the simulation of regional climate using a limited area model nested in a general circulation model. *J. Climate*, **3**, 941-963.

Giorgi, F., M. R. Marinucci, G. T. Bates, and G. De Canio, 1993a: Development of a second-generation regional climate model (RegCM2). Part I: Boundary-layer and radiative transfer. *Mon. Wea. Rev.*, **121**, 2794-2813.

Giorgi, F., M. R. Marinucci, G. T. Bates, and G. De Canio, 1993b: Development of a second-generation regional climate model (RegCM2). Part II: Convective processes and assimilation of boundary conditions. *Mon. Wea. Rev.*, **121**, 2814-2832.

Giorgi, F., L. Mearns, C. Shields, and L. Mayer, 1996: A regional model study of the importance of local versus remote controls of the 1988 drought and the 1993 flood over the central United States. *J. Climate*, **9**, 1150-1162.

Grell, G. A, 1993: Prognostic evaluation of assumptions used by cumulus parameterizations. *Mon. Wea. Rev.*, **121**, 764-787.

Horel J. D, J. B. Pechamann, A. N. Hahmann, and J. E. Geisler, 1994: Simulation of the Amazon basin circulation with a regional model. *J. Climate*, **7**, 56-71.

Kida, H., T. Koide, H. Sasaki, and M. Chiba, 1991: A new approach for coupling a limited area model to a GCM for regional climate simulations. *J. Meteor. Soc. Japan*, **69**, 723-728.

Kuo, S. L., 1974: Further studies of the parameterization of the effect of cumulus convection on large-scale flow. *J. Atmos. Sci.*, **31**, 1232-1240.

Machenhauer, M., 1995: The regionization project: A synthesis of the final report. EEC Environment Program Contract No. EV5V-CT92-0126.

Mo, K. C., J. N. Paegle, and J. Paegle, 1995: Physical mechanisms of the 1993 floods. *J. Atmos. Sci.*, **52**, 879-895.

Paegle, J., K. C. Mo, and J. N. Paegle, 1996: Dependence of simulated precipitation on surface evaporation during the 1993 United States summer floods. *Mon. Wea. Rev.* **124**, 345-361.

Pan, Z., M. Segal, R. Turner, and E. Takle, 1995: Model simulation of impacts of transient surface wetness on summer rainfall in the United States Midwest during drought and flood years. *Mon. Wea. Rev.*, **123**, 1575-1581.

Pan, Z., E. Takle, M. Segal, and R. Turner 1996: Influences of model parameterization schemes on the response of rainfall to soil moisture in the Central U.S. *Mon. Wea. Rev.*, **124**, 1786-1802.

Renshaw, E. and E. D. Ford, 1983: The interpretation of process from pattern using two-dimensional spectral analysis: methods and problems of interpretation. *Appl. Statist.*, **32**, 51-63.

Rodenhuis, D. R., D. Miskus, G. D. Bell, and K. C. Mo, 1994: Meteorological flood - origin, description, and causes of the Great Flood of 1993. *Preprints, Symposium on the Great Flood of 1993*, Nashville, TN, Amer. Meteor. Soc., 65pp.

Sellers, P. J., J. A. Berry, G. J. Collatz, C. B. Field, and F. G. Hall, 1992: Canopy reflectance, photosynthesis, and transpiration. III. A reanalysis using improved leaf models and a new canopy integration scheme. *Remote Sens. Env.*, **42**, 187-216.

Yap, K.-S., 1995: Impact of a Newtonian assimilation and physical initialization on the initialization and prediction by a tropical mesoscale model, *Mon. Wea. Rev.*, **123**, 833-861.

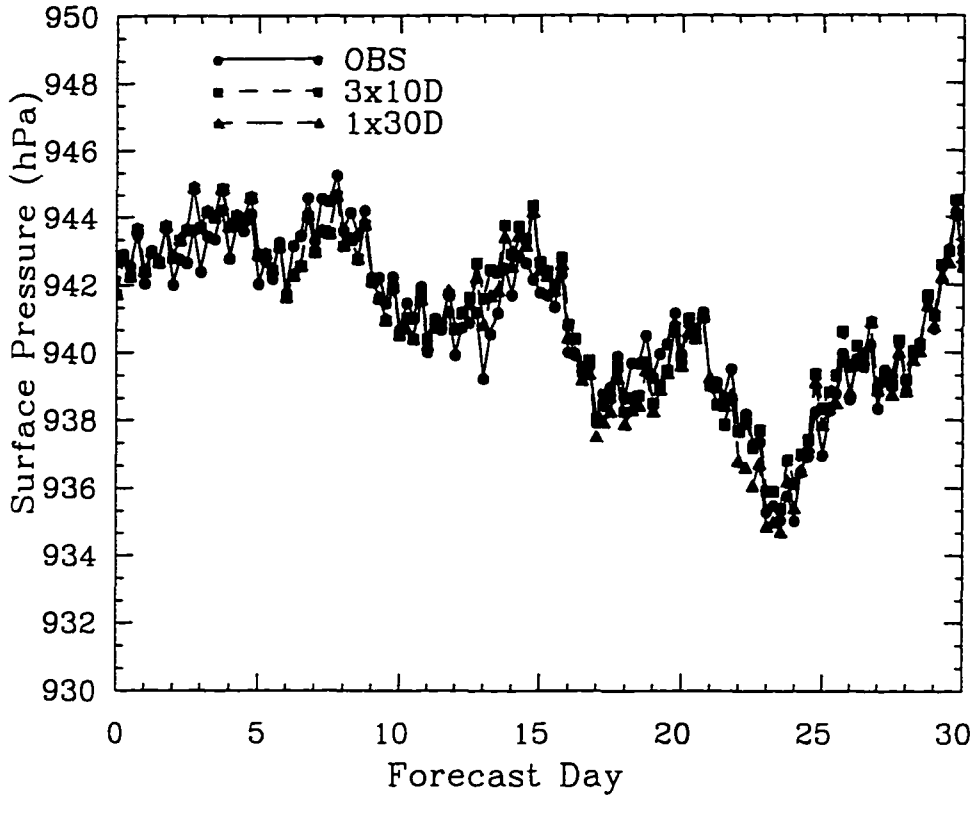

Figure 1 Time series of domain-averaged surface pressure for the 3x10D and 1x30D experiments as compared with observation.

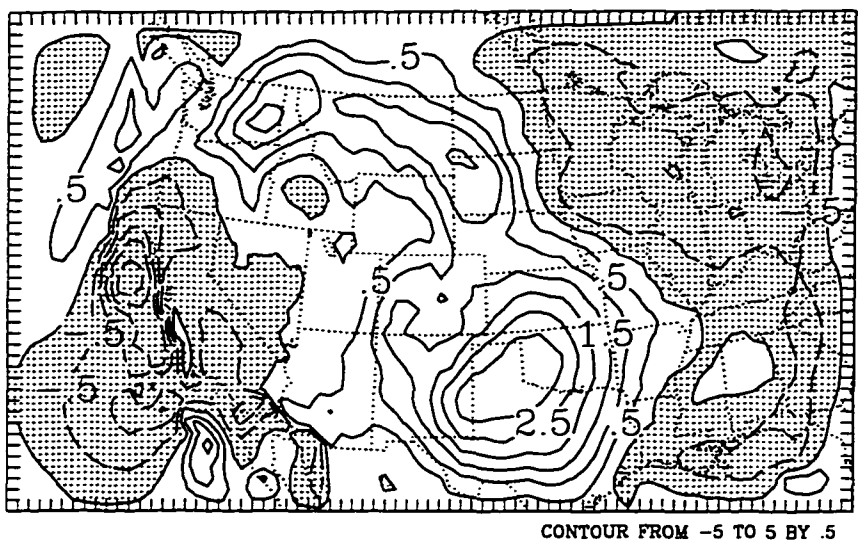

Figure 2 Spatial distribution of the difference (hPa) in 30-d average surface pressure between the simulation (1x30D) and the observation. Areas of negative values are shaded.

(a)

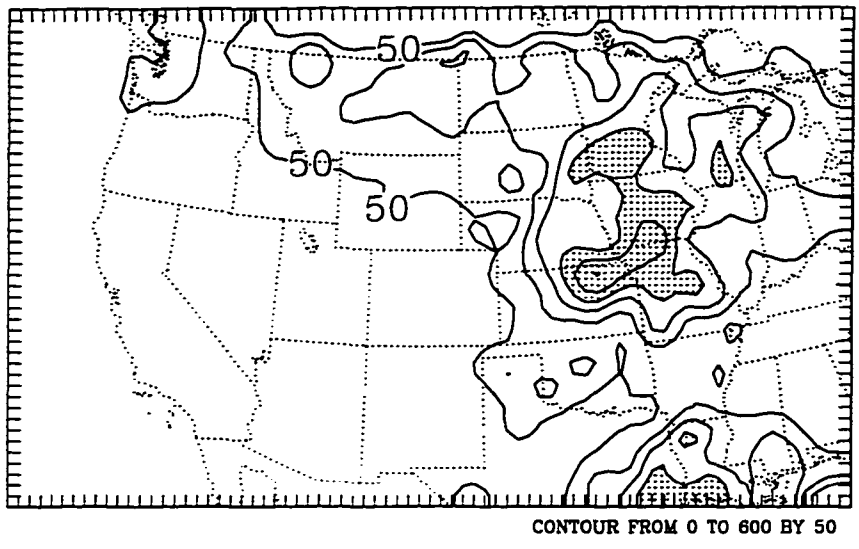

(b)

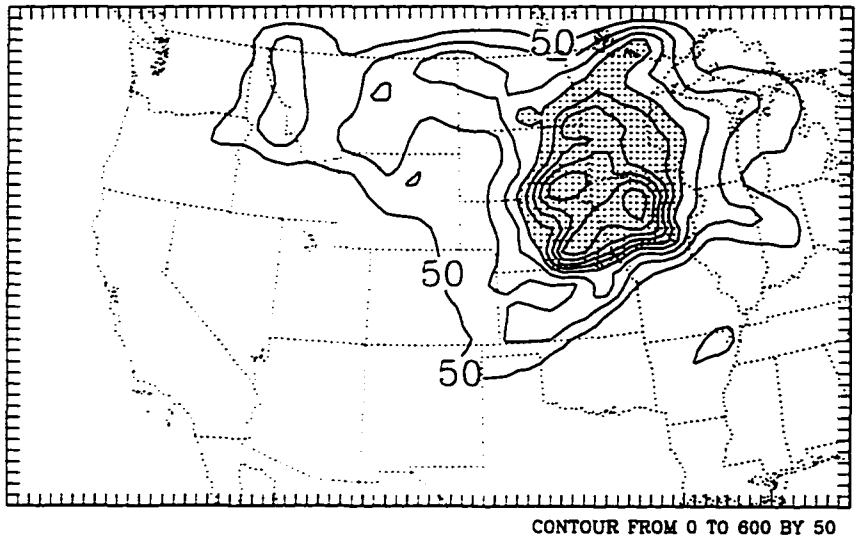

Figure 3 Spatial distribution of observed and simulated 30-d total rainfall (mm). (a) Observed. (b) 30x1D. Areas above 200 mm are shaded.

(c)

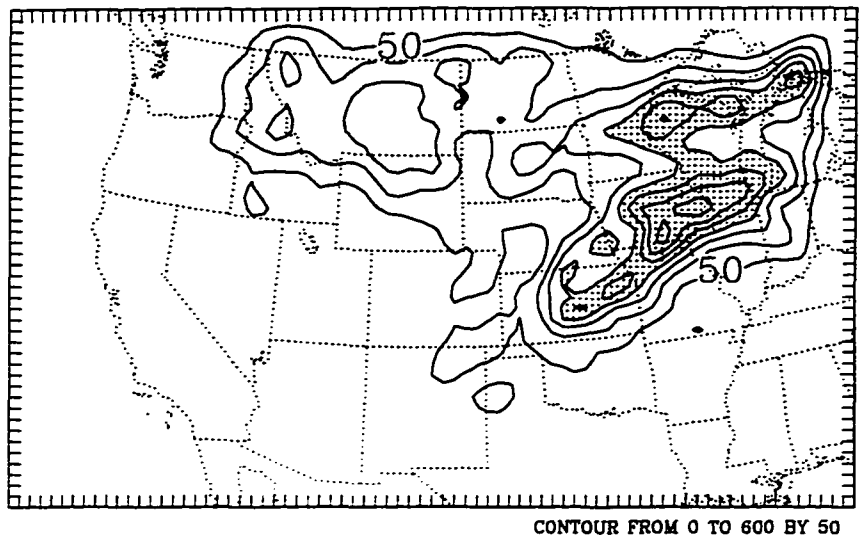

(d)

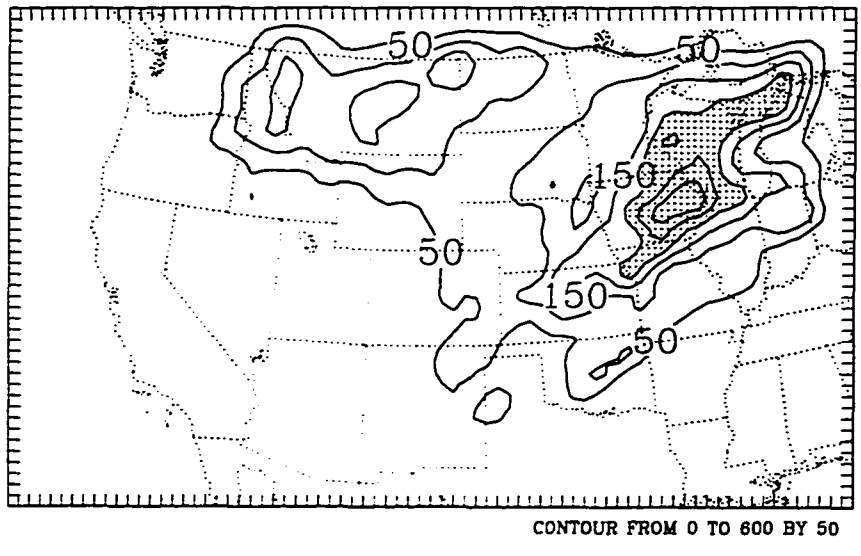

Figure 3 (continued) (c) 6x5D. (d) 3x10D.

(e)

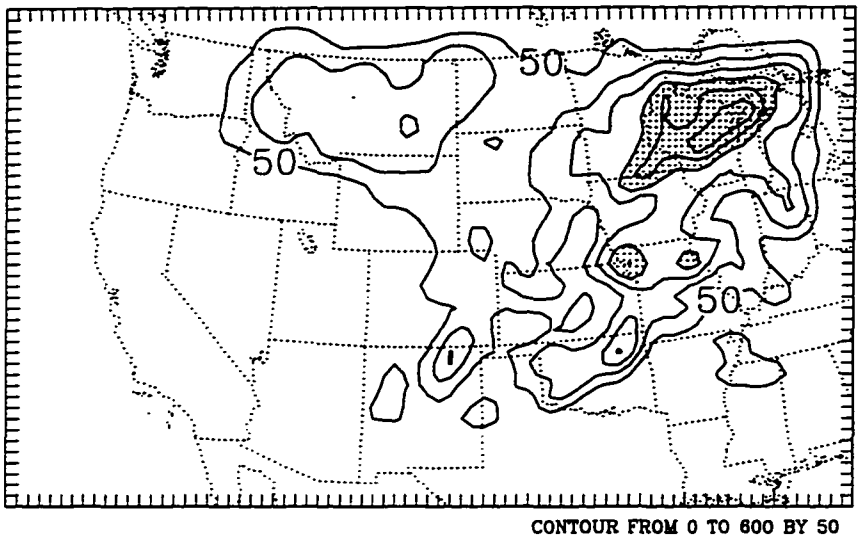

(f)

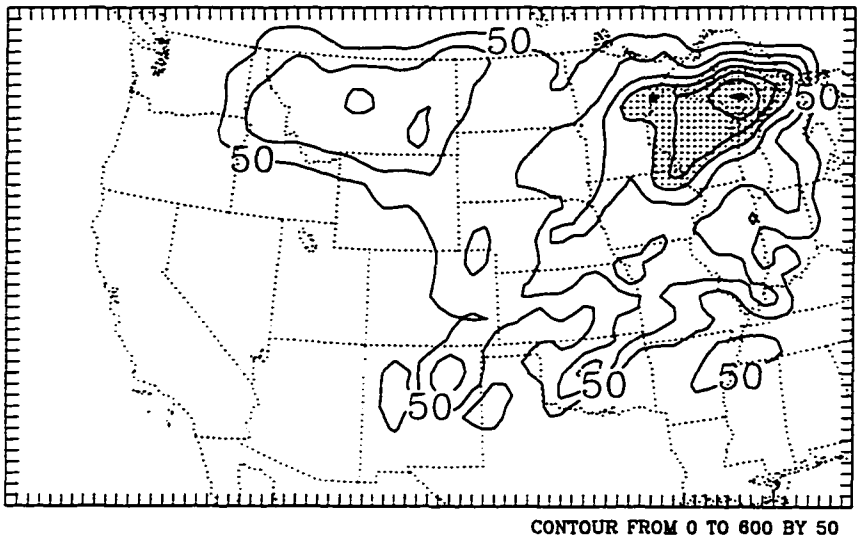

Figure 3 (continued) (e) 1x30D. (f) 3x13D.

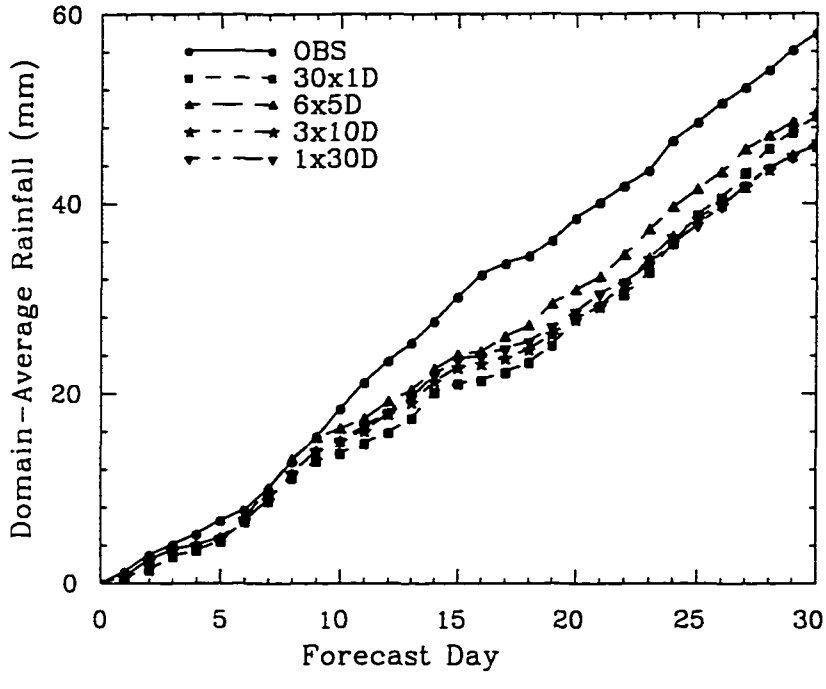

Figure 4 (a) Accumulated rainfall as compared with observations for different experiments averaged over the whole domain.

(b)

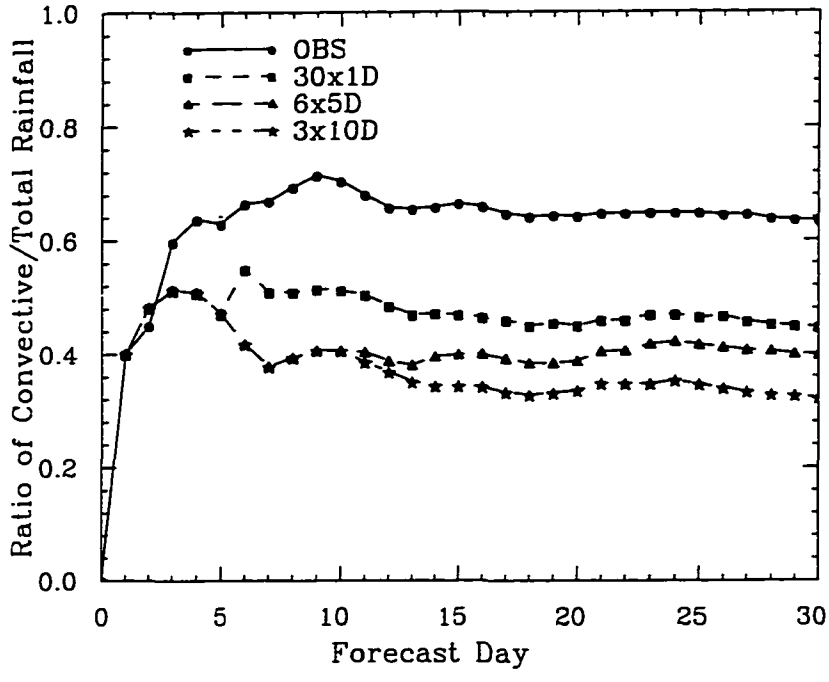

(c)

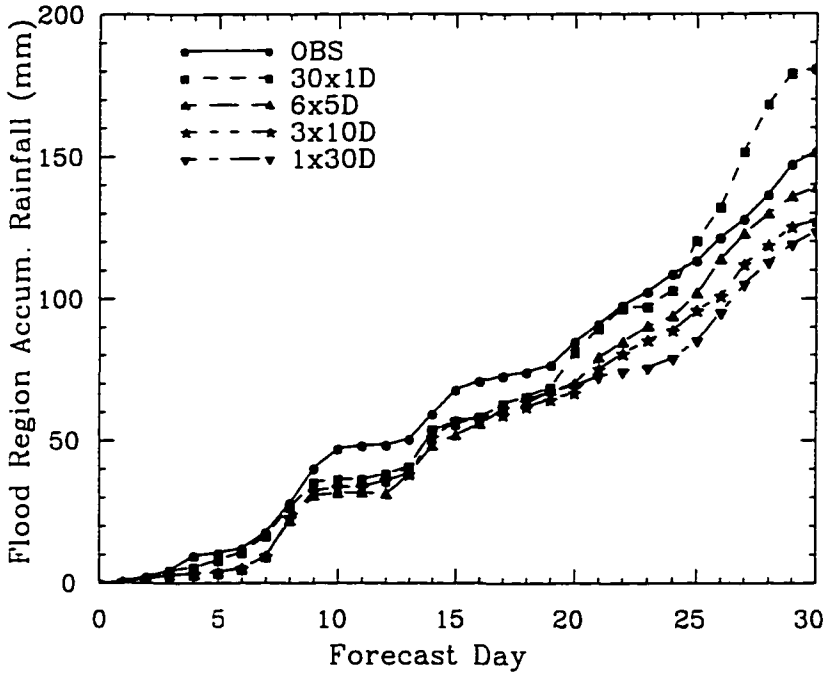

Figure 4 (continued) (b) Ratio of convective rainfall to total rainfall over the whole domain. (c) Accumulated average rainfall over the flood-area.

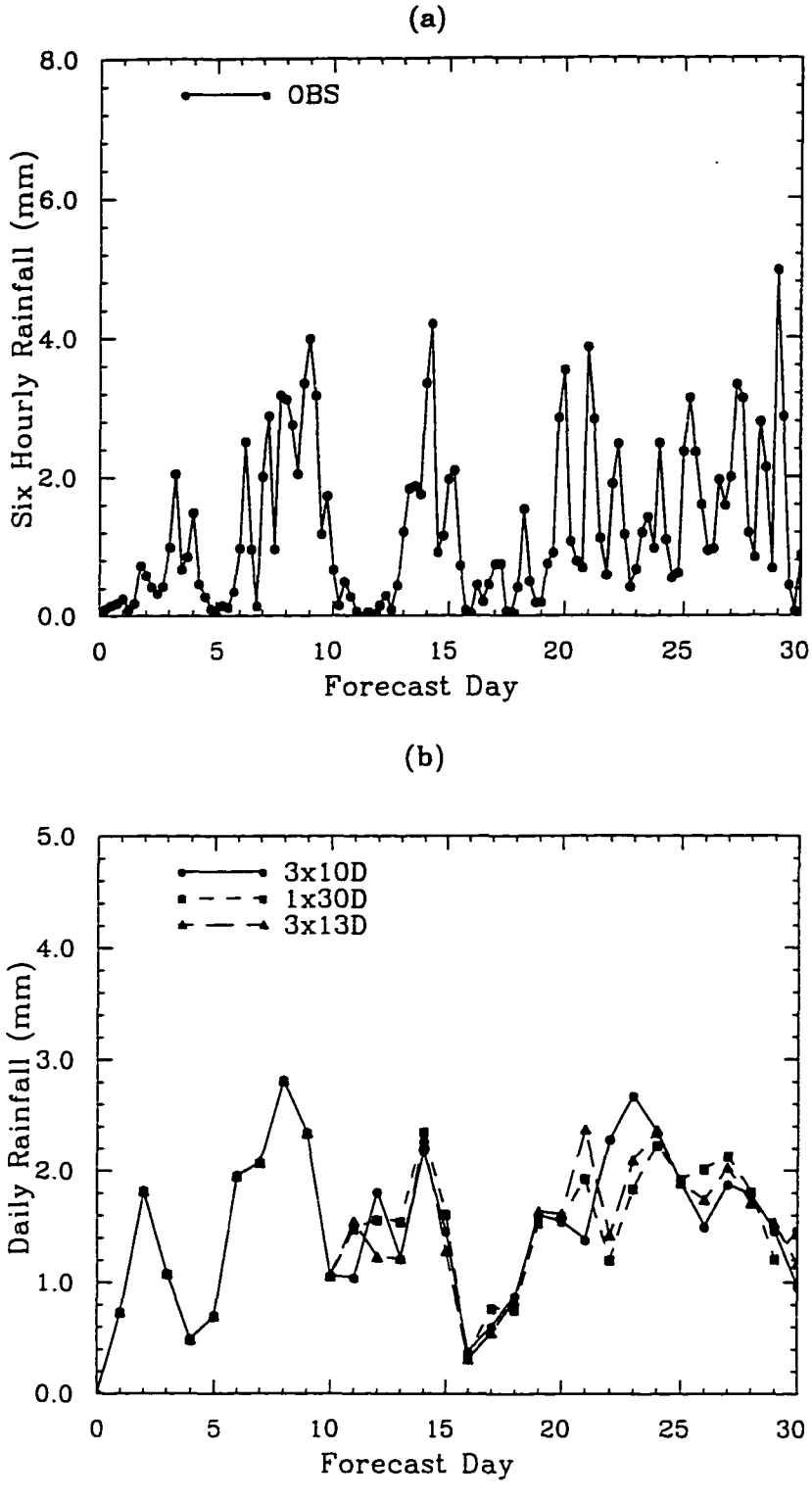

Figure 5 (a) Observed time series of domain-averaged 6-h rainfall, (b) Simulated time series of domain-averaged daily rainfall.

(a)

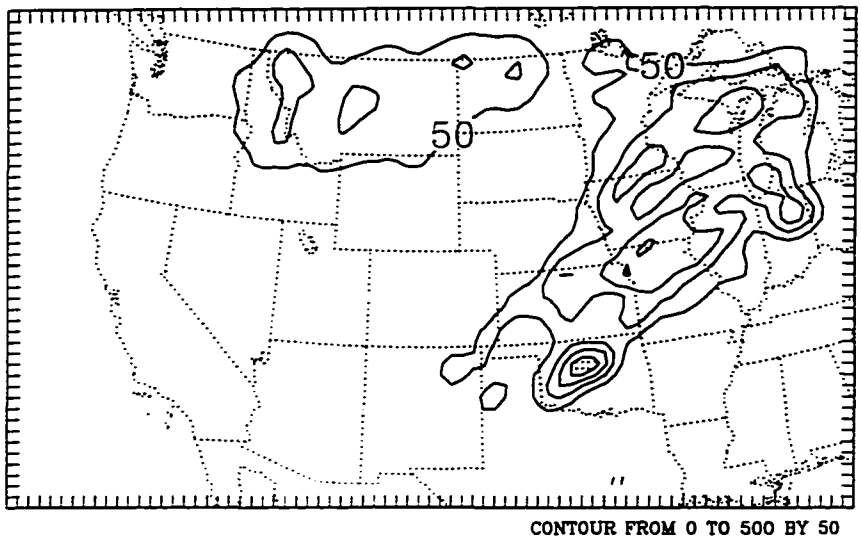

(b)

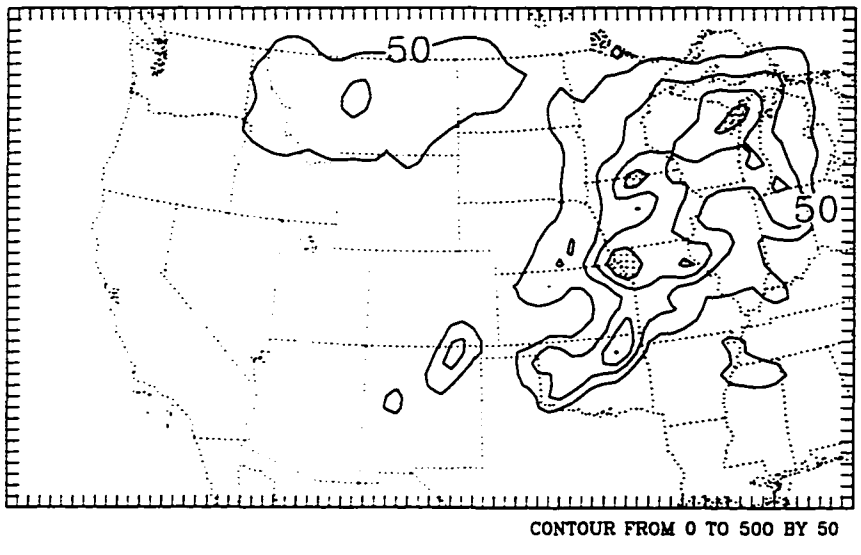

Figure 6 Spatial distribution of accumulated rainfall (mm). (a) 1x20D, (b) last 20-d of 1x30D. Areas above 200 mm are shaded.

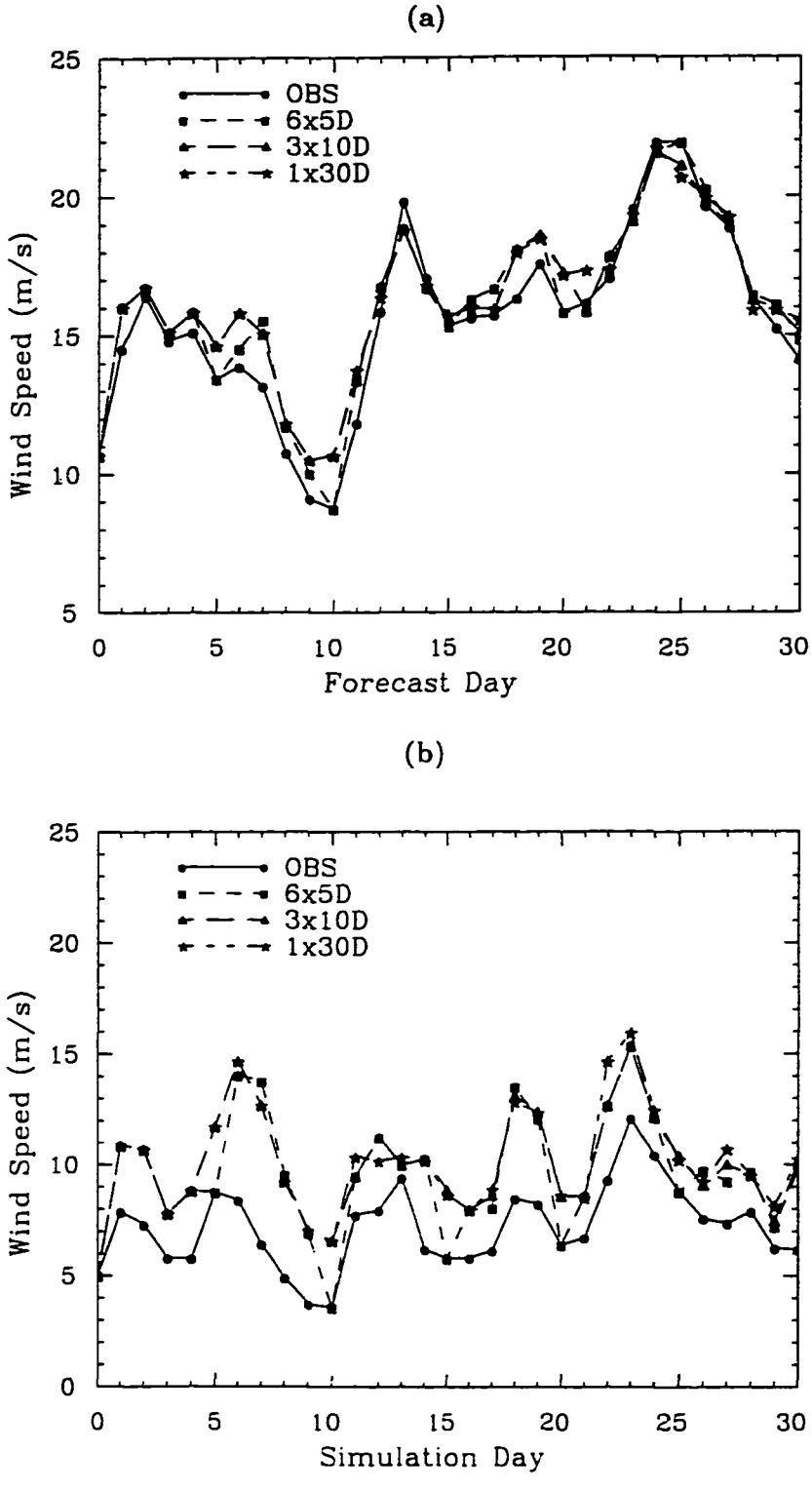

Figure 7 Temporal variations of simulated and observed wind speeds averaged over the interior domain. (a) At σ=0.510, (b) At σ=0.895.

(a)

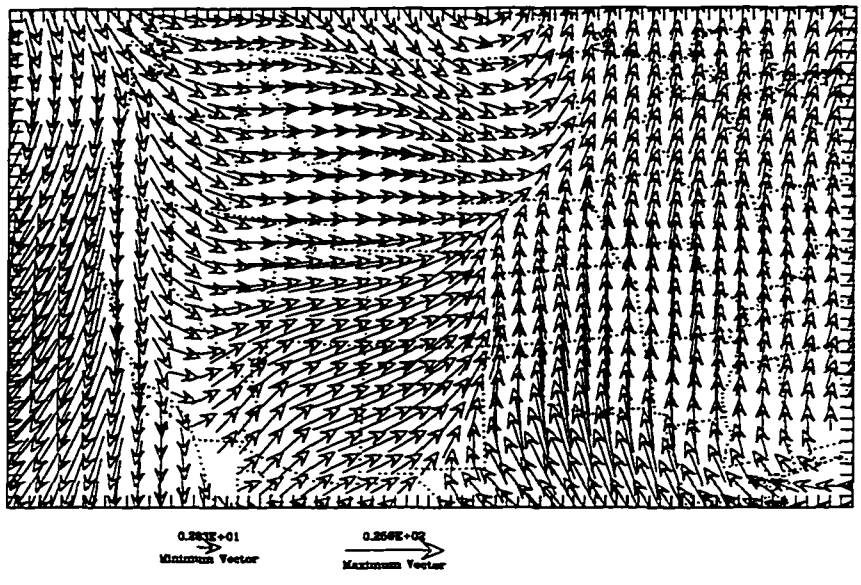

(b)

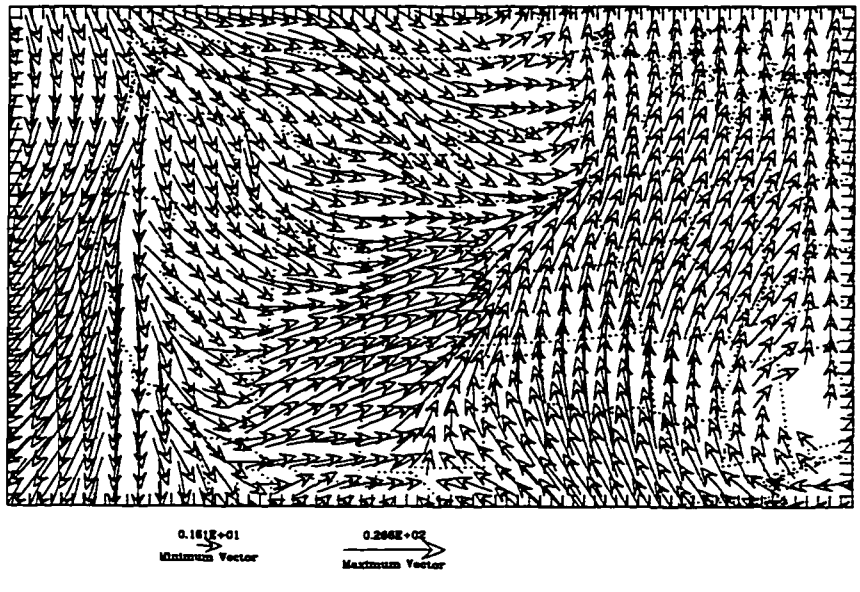

Figure 8 Spatial distribution of observed (a) and simulated (b) wind vector (1x30D) at σ=0.895 averaged over the 30-d period.

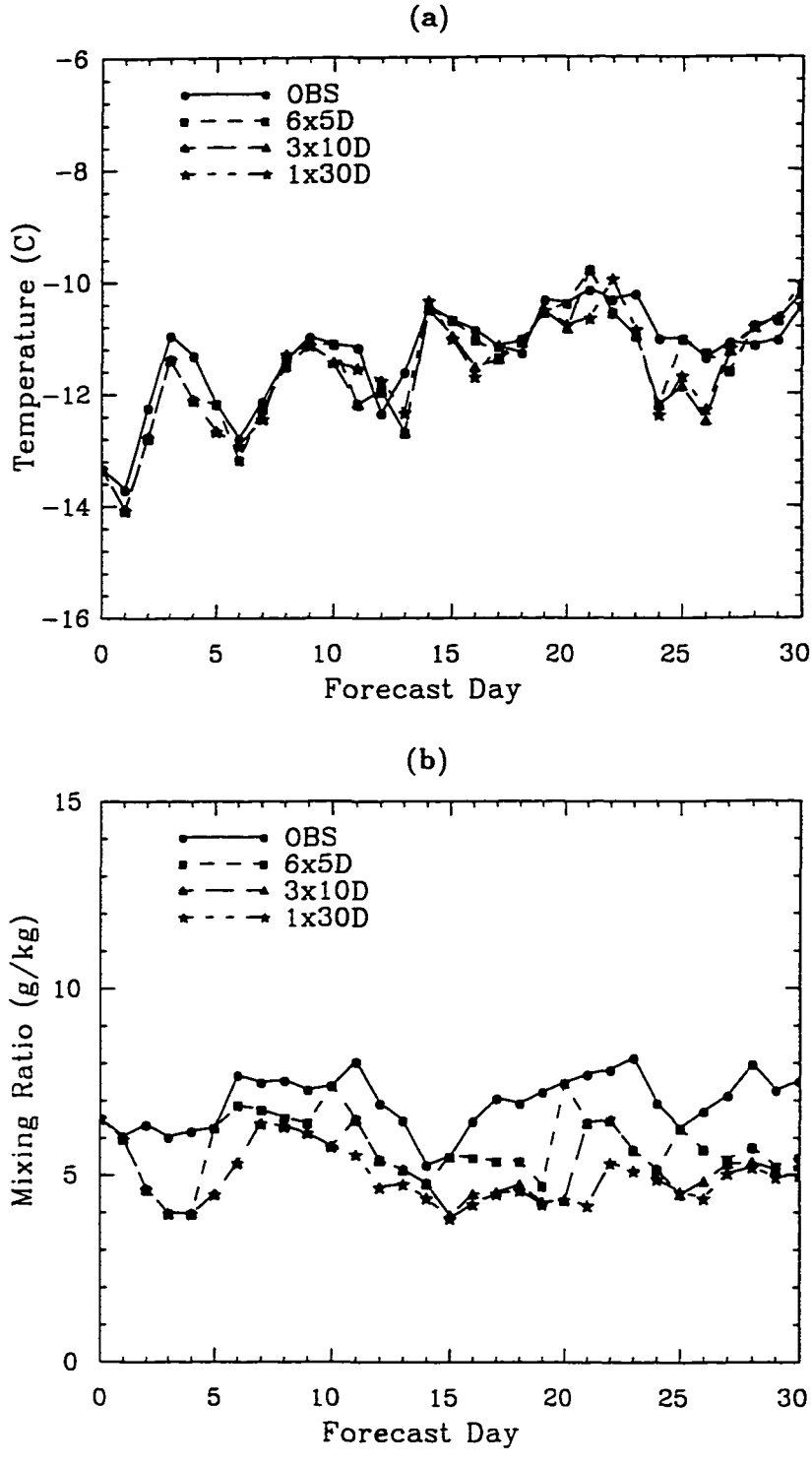

Figure 9 Temporal variations of simulated and observed interior domain-average temperature and mixing ratio. (a) Temperature at σ=0.510, (b) Mixing ratio at σ=0.895.

(a)

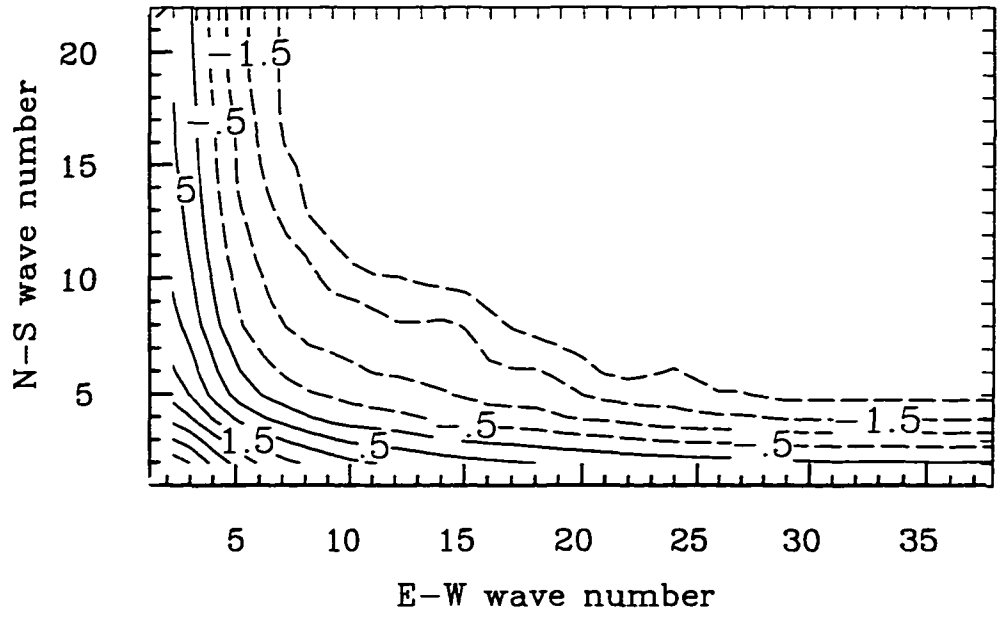

Figure 10 The 30-d average wave amplitudes ($ln\, D_{m,n}$) as functions of wave numbers (m,n) in E-W and N-S directions of u-component wind at σ=0.51. Contour interval=0.5 m s^{-1}. (a) Observed.

(b)

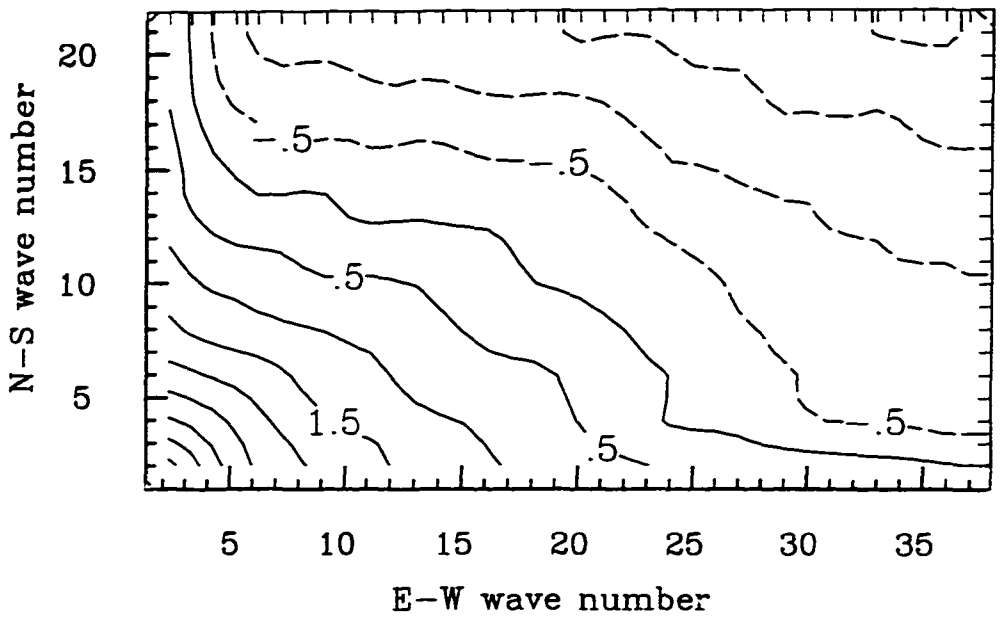

(c)

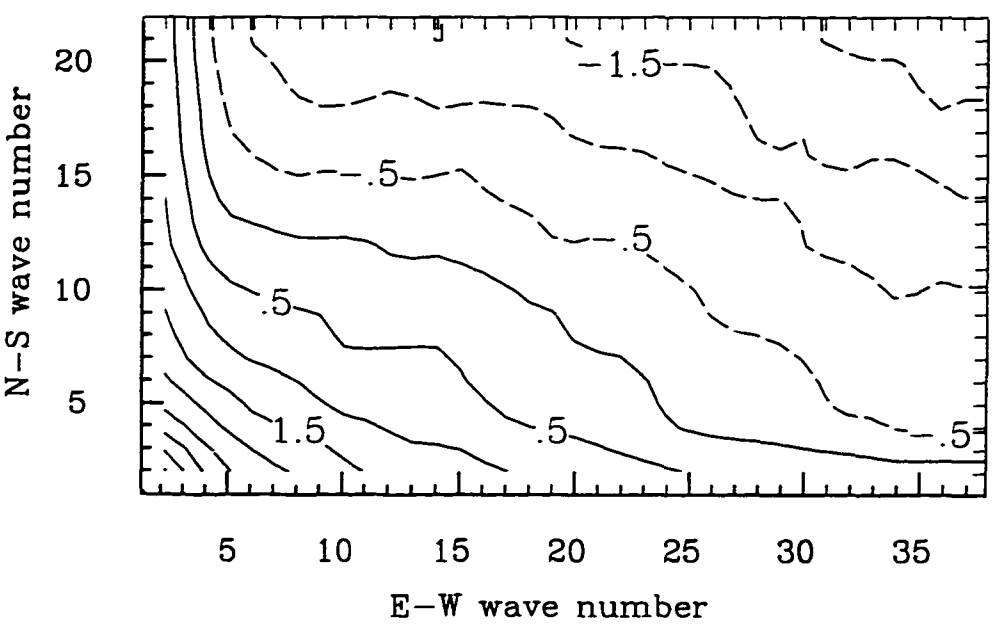

Figure 10 (continued) (b) 3x10D, (c) 1x30D.

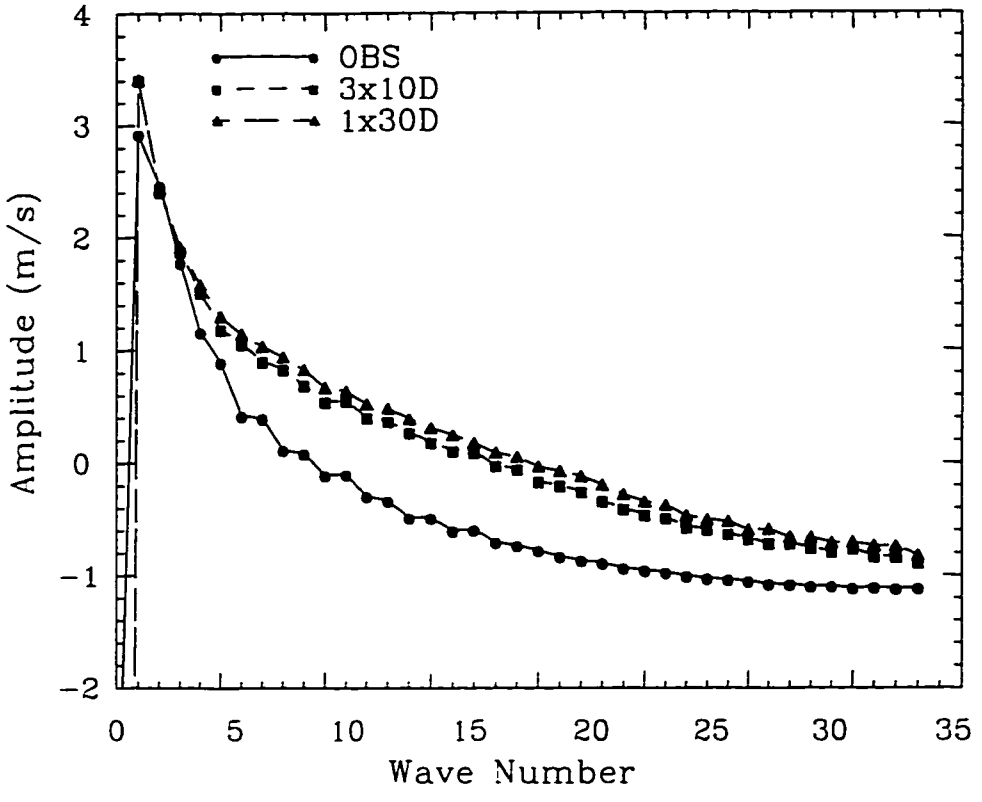

Figure 11 The 30-d average wave amplitudes ($ln\,A$) of one-dimensional Fourier decomposition of u-component wind speed at σ=0.51.

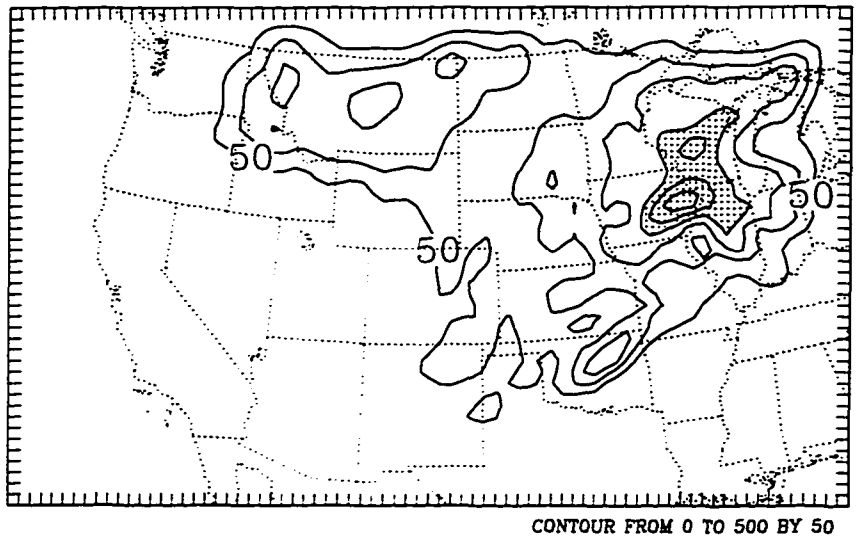

Figure 12 Spatial distribution of 30-d accumulated rainfall (mm) for 3x10DM. Areas above 200 mm are shaded.

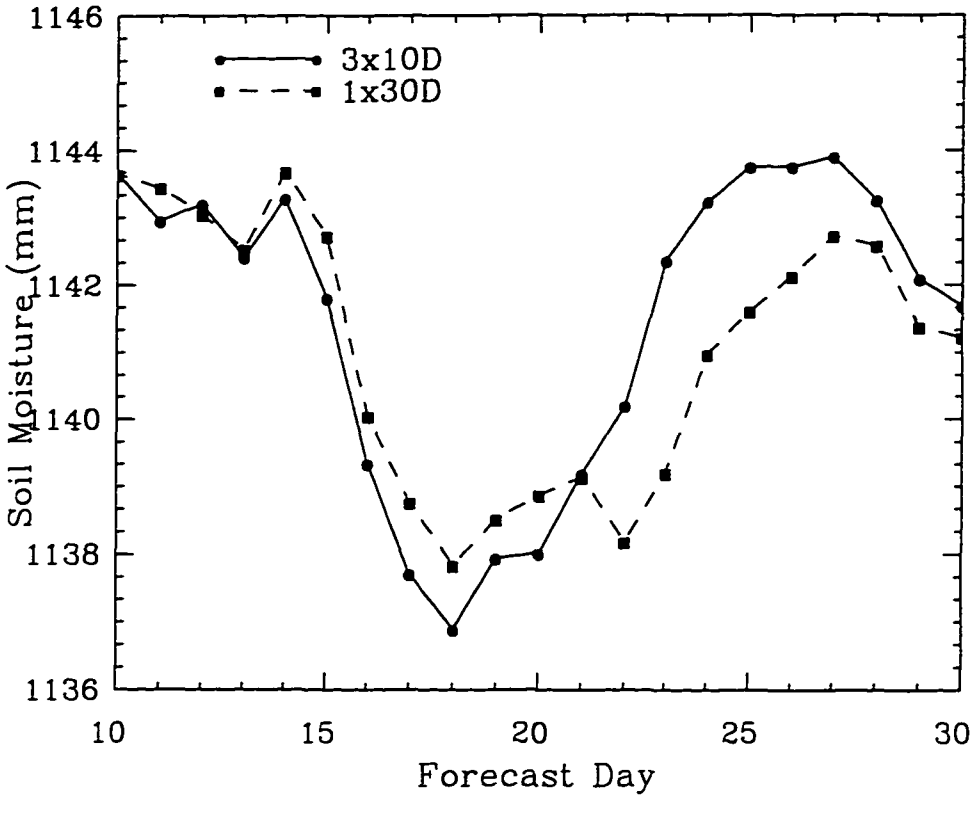

Figure 13 Temporal variation of domain-averaged soil moisture (mm) in 1x30D and 3x10DM.

(a)

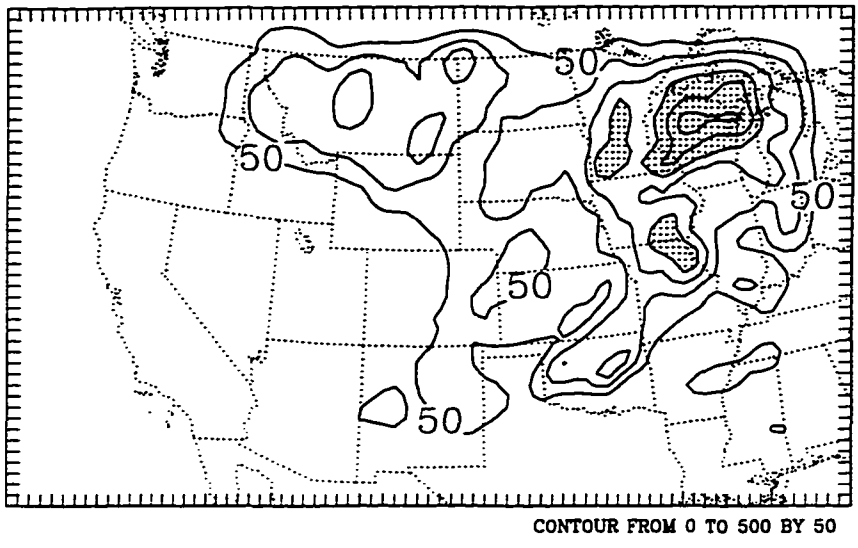

(b)

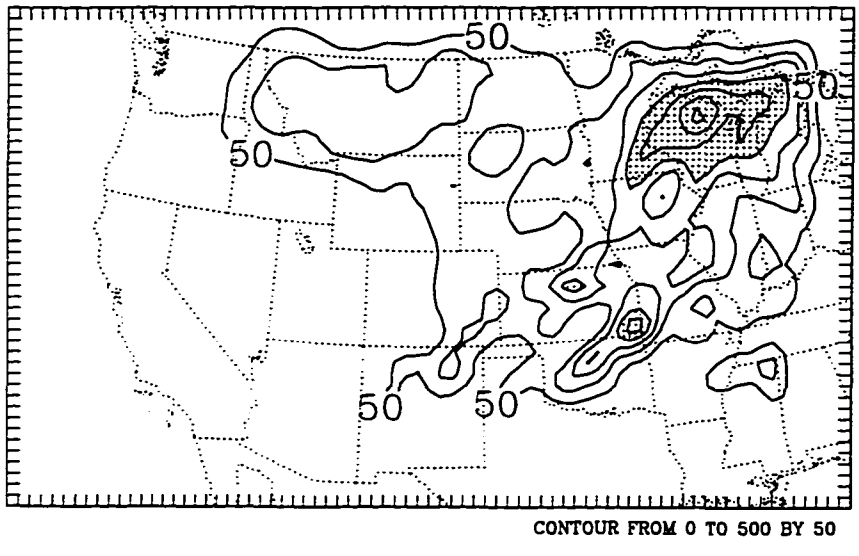

Figure 14 Spatial distribution of simulated 30-d total rainfall (mm). (a) 1x30DS, (b) 1x30DD. Areas above 200 mm are shaded.

SIMULATION OF POTENTIAL IMPACTS OF HUMAN HABITATION ON U.S. SUMMER CLIMATE UNDER VARIOUS CLIMATE REGIMES

A paper to be submitted to *Journal of Climate*

Zaitao Pan, Eugene Takle, Moti Segal, Raymond Arritt

Abstract

Impacts of human settlement on regional summer climate over the central and western U.S. were simulated by considering pre-settlement, current, and hypothetical future landuse scenarios under normal, flood, and drought climate. During a normal year, the current landuse showed a 0.8% increase in domain total rainfall over the natural landuse, a result consistent with the observed 1% increase during the last 100 years. The one-month normal year simulation also supports several observed aspects of surface air temperature which include overall temperature decrease in U.S., cooling in the Midwest and Great Lakes region and warming over the western mountain region, and reduced diurnal variation with the current landuse.

The flood year simulation showed a decrease in domain average rainfall with current and future landuse. This slight decrease in domain total rainfall resulted from a smaller increase in the western U.S. and larger decrease in east-central U.S. which is associated with reduced evapotranspiration caused by the weakened southerly flow and cooler surface air. Simulated domain average rainfall in the drought year showed little sensitivity to different landuse scenarios since the increased evapotranspiration had less chance to translate into rainfall.

1 Introduction

General circulation model (GCM) simulations have indicated trends of global warming and increase in precipitation in the future as the atmospheric levels of greenhouse gases rise continuously, and historical data indeed support these simulated trends (Foland et al. 1991). Many factors are believed to have contributed to these global trends. The anthropogenic greenhouse gases are believed as the primary contributor to global warming and the associated precipitation increase. Numerous studies have been devoted to this effect (*e.g.*. Hansen et al. 1981, Manabe and Wetherald 1980). Landuse modifications by human activities, such as deforestation, urbanization, and agricultural practice, have been also long believed to influence climate (*e.g.*, Charney et al. 1977, Dickinson and Henderson-Sellers 1988, Sagen et al. 1979). These landuse modifications not only alter the energy balance at the surface but also affect the atmospheric CO_2 level.

Although global long-term trends in temperature and precipitation are positive, the magnitudes and even signs of the trends differ regionally and seasonally (Karl et al. 1994, Vinnikov et al. 1993). For example, the annual mean surface air temperature over the U.S. has not shown a clear increase in the past decades despite the global warming (Plantico et al. 1990). Most parts of the central U.S. have in fact experienced slight cooling and drying over the last few decades.

The early European settlement of the U.S. reduced some native forests and grass lands during the 19th century, and then massive immigration and associated agricultural practices changed landuse extensively. In the late 1700's, before major European immigration, the landscape of the North America was mostly composed of forests, grass prairie and swamps. The present landscape is mainly composed of agricultural and grass lands. This is especially true over the Midwest and the Great Plains, the heavily cultivated areas.

Few studies have evaluated climate impacts of landuse using regional climate models over the U.S. although some studies have projected global impacts onto local scales by the so-called downscaling technique. To author's knowledge, the only study was performed by Copeland et al. (1996) that simulated landuse impacts over the continental U.S. in a *normal* year using

a regional model. Other studies (*e.g.*, Giorgi et al. 1995) evaluated the effects of only one parameter of landuse (soil moisture).

Because of the high nonlinearity of the climate system, responses of regional climate to landuse modification under extreme conditions, such as drought and flood, may differ from those under normal conditions. During a normal year with normal rainfall and temperature, crops and other vegetation grow and transpire at normal rates. During hydrological anomalies, however, vegetation may function abnormally. For example in middle latitudes, during normal years most crops transpire more than forests whereas during drought years some crops may transpire less than forests because of their shorter roots (Campbell 1991). Similarly, bare soil may evaporate more than crops during flood periods (as in the 1993 Midwest flood).

The atmospheric responses to surface processes are hydrologically dependent. In a drought year when the atmosphere is relatively dry and warm, thermal forcing is probably adequate so precipitation is sensitive to surface evapotranspiration. More evaporation may enhance the possibility of precipitation (*e.g.*, Mintz 1884, Segal et al. 1995). On the other hand, in a flood year when the atmosphere is moist, increased evaporation may *suppress* rainfall processes because of weakened surface sensible heating (*e.g.*, Paegle et al. 1996, Giorgi et al. 1996). In summary both vegetation and atmospheric responses are hydrologically dependent and this dependency will ultimately affect the impacts of landuse changes on regional climate.

The purposes of this study are (i) to simulate regional climate impacts of the landuse changes caused by human habitation over central and western U.S. under *normal* climate conditions, (ii) to contrast the impacts under normal conditions with those under extreme conditions, (iii) to evaluate regional impacts of human settlement on the severity of flood and drought.

2 Selections of Datasets and Model Schemes

2.1 Data Cases

The most famous and record-breaking drought and flood in recent years are the 1988 Midwest and Great Plains drought and 1993 Great Flood in the upper Mississippi basin.

Thus, they are selected as the extreme dry and wet cases, respectively. The 1988 drought was most pronounced in May and June. Although considerable rain fell in July, the hydrological drought continued throughout the summer because of the extreme drying during previous months (Trenberth and Guillemot 1996). The summer of 1993 was the wettest in recent history over most parts of the upper Mississippi basin. A one-month period covering the peak intensity of the extremes for both the drought and flood year, 0000 UTC 11 June to 0000 UTC 11 July (Gerald and Janowiak 1995), was selected for this study.

The flow patterns over this period in 1988 summer were dominated by a strong anticyclone over the western U.S. The jet stream and associated storm tracks were shifted well north of their climatological position. On the other hand, the jet was displaced well to the south in 1993 so that much moisture was involved in the storm track. The year of 1991 was near normal in terms of rainfall over most parts of the U.S., so the period of 0000 UTC 11 June 1991 to 0000 UTC 11 July 1991 is chosen to represent a normal year.

Three landuse types are constructed: pre-settlement natural, current, future projected landuse. The natural landuse types were deduced from Küchler (1964) by remapping the vegetation classification, which has 116 categories, onto the biosphere-atmosphere transfer scheme (BATS) classification of 18 categories listed in Table 1. The current landuse is derived from Matthews (1983) and Wilson (1984) as described in Dickinson et al. (1992). The main difference between the current and natural landuse types is over the Great Lakes region and Midwest where the natural forest and native-grass prairie were changed to cropland. Another region under significant changes is the southwestern U.S. where the deciduous shrub and needleleaf forest were changed to evergreen shrubs and farmland (Fig. 1).

The trend in landuse shows a rapid expansion of agriculture in the last 200 years, and cropland occupies about one fourth of current simulation domain. To examine the extreme effects of this trend, we approximate future landuse with uniform cropland except over the water and desert. The crops cover about 85% of surface with 15 % bare soil within each grid box during summer (Table 1). This highly hypothetical future landuse allows us to examine the extreme regional impacts of human activities.

Table 1 Characteristics of landuse types (Dickinson et al. 1992)

variable	1	2	3	4	5	6	7	8	9	10	11	12	13	14	15	16	17	18
Max. fract. veg. cover	0.85	0.80	0.80	0.80	0.80	0.90	0.80	0.00	0.60	0.80	0.10	0.00	0.80	0.00	0.00	0.80	0.80	0.80
Veg. cover difference	0.6	0.1	0.1	0.3	0.3	0.5	0.3	0.0	0.2	0.6	0.1	0.0	0.4	0.0	0.0	0.2	0.3	0.2
Roughness (m)	0.06	0.02	1.00	1.00	0.08	2.00	0.10	0.05	0.04	0.06	0.10	0.01	0.03	.002	.002	0.10	0.10	0.80
Depth of rooting zone	0.1	1.0	1.5	1.5	2.0	1.5	1.0	1.0	1.0	1.0	1.0	1.0	1.0	1.0	1.0	1.0	1.0	2.0
Fract. of upper soil layer	0.1	0.1	0.1	0.1	0.1	0.1	0.1	0.1	0.1	0.1	0.1	0.1	0.1	0.1	0.1	0.1	0.1	0.1
Fract. of water extrac. by root	0.30	0.80	0.67	0.67	0.50	0.80	0.80	0.90	0.90	0.3	0.80	0.50	0.50	0.50	0.50	0.50	0.50	0.50
Veg. albedo ($\lambda < 0.7\mu m$)	0.10	0.10	0.05	0.05	0.08	0.04	0.08	0.20	0.10	0.08	0.17	0.80	0.06	0.07	0.07	0.05	0.08	0.06
Veg. albedo ($\lambda > 0.7\mu m$)	0.30	0.30	0.23	0.23	0.28	0.20	0.30	0.40	0.30	0.28	0.34	0.60	0.18	0.20	0.20	0.23	0.28	0.24
Min. stomatal resist. (sm^{-1})	120	200	200	200	200	200	200	200	200	200	200	200	200	200	200	200	200	200
Max. LAI	6	2	6	6	6	6	6	0	6	6	6	0	6	0	0	6	6	6
Min. LAI	0.5	0.5	5.0	1.0	1.0	5.0	0.5	0.0	0.5	0.5	0.5	0.0	0.5	0.0	0.0	5.0	1.0	3.0
Stem area index	0.5	4.0	2.0	2.0	2.0	2.0	2.0	0.5	0.5	2.0	2.0	2.0	2.0	2.0	2.0	2.0	2.0	2.0
Inv. squ. root leaf size	10	5	5	5	5	5	5	5	5	5	5	5	5	5	5	5	5	5
Light sensit. factor	0.02	0.02	0.06	0.06	0.06	0.06	0.02	0.02	0.02	0.02	0.02	0.02	0.02	0.02	0.02	0.02	0.02	0.06

Legend:

1-Crop/mixed farming, 2-Short grass, 3-Evergreen needleleaf tree, 4-Deciduous needleleaf tree, 5-Deciduous broadleaf tree, 6-Evergreen broadleaf tree, 7-Tall grass, 8-Desert, 9-Tundra, 10-Irrigated crop, 11-Semi-desert, 12-Ice cap/glacier, 13-Bog or marsh, 14-Inland water, 15-Ocean, 16-Evergreen shrub, 17-Deciduous shrub, 18-Mixed woodland,

In all three landuse types, the semi-desert and lake/ocean areas remain the same. This is valid since within the time scale of one hundred years the Great Lakes are not likely to change in areal extent. The semi-desert over Nevada and New Mexico experienced little change on large scales although some local changes (unresolvable by our model) do occur in landuse.

The most important landuse parameters for this study are probably albedo for wavelength $> 0.7\mu m$ (α), minimum stomatal resistance, and surface roughness (z_0). The woodland that has been replaced most has about 20% smaller albedo than the grass and crop lands (Table 1). Crops have least minimum stomatal resistance (120 s m^{-1}) as compared with all other vegetation types (200 s m^{-1}). The woodland has larger roughness (z_0=0.8 m) than crops (z_0=0.06 m) and short grass (z_0=0.02 m). The woodland and cropland have larger leaf area index (6) whereas short grass land has only a value of 2. The readers are referred to the BATS description for detailed explanations of various variables (Dickinson et al. 1992).

Table 2 lists domain-averaged values of albedo, soil moisture availability (m) defined as the ratio of actual to potential evaporation, fractional vegetation coverage (f_v), leaf area index (LAI), and roughness length in meters. The overall albedo is decreased by about 2% in the present landuse, and the albedo of the hypothetical uniform cropland is increased by 12% over the present. Albedo has increased over the Great Lakes region, along the Arkansas/Mississippi border, and in parts of the west coast where crops (α=0.3) replaced woodland (α=0.24) and deciduous shrub (α=0.28) (Fig. 2a). Albedo decreased over the western mountain region where the deciduous shrub was replaced by evergreen shrub (α=0.24), and over Mississippi and neighboring states where natural woodland was replaced by needleleaf trees (α=0.23). Over the Midwest albedo remained the same since grass and crops have same α value.

Roughness, which is a function of vegetation height, decreased from 0.281 m for the natural condition to 0.224 m and 0.05 m for the current and future landuse respectively (Table 2). This sharp decrease in roughness is attributable to the expansion of cropland for which z_0=0.06 m as compared to 0.8 m of woodland and 0.1 m of tall grass (Fig. 2b). The m values are 0.365, 0.379, and 0.420 for the pre-settlement, current, and future landuse. The increase in m is contributed by cropland that has a m value of 0.3 as compared with 0.15 for grass prairie (Fig.

Table 2 Domain-average landuse parameters

	α	m	f_v	LAI	z_0
Natural	0.262	0.365	0.625	4.313	0.281
Current	0.257	0.379	0.635	4.313	0.224
Future	0.283	0.420	0.663	4.880	0.051

2c). The m value of cropland is higher than other vegetation types.

Both vegetation coverage (Fig. 2d) and LAI (figure not shown) of present-day increase slightly because of the increase in cropland coverage that has high v_f value (0.85). The hypothetical future landuse has about a 5% increase in vegetation coverage and 10% in LAI (Table 2). In summary, the hypothetical future land surface will be brighter (in the near-IR), greener, wetter and smoother than the pre-settlement, and the current landuse is between, being closer to the pre-settlement.

2.2 Model and Parameterization Schemes

The regional climate model RegCM2 that was developed at NCAR based on the Penn State/NCAR MM4 is used for this study (Giorgi et al. 1993a, 1993b). The RegCM2 incorporates the CCM2 radiation package (Briegleb 1992) and BATS version 1e (Dickinson et al. 1992) surface package. The model domain covers 46x77 grids with Δx=50 km centered at (40.5 N, 106.5W). The model is configured in this study with 14 layers in the vertical, located at σ=0.995, 0.980, 0.950, 0.895, 0.815, 0.720, 0.615, 0.510, 0.405, 0.300, 0.210, 0.135, 0.070, and 0.020. The model top is located at 80 hPa. The simulation domain was so chosen that the western boundary where the incoming flows enter is far from high mountains which can give rise to large interpolation errors.

The initial and boundary conditions (tendencies) were interpolated from ECMWF T42 analyses. The boundary conditions were updated every 6 h, which were linearly interpolated in time from 12-hourly analyses. Within the buffer zone near the boundaries, the model-predicted variables were nudged to the observations. Experiments are carried out for each of the three years and landuse scenarios, resulting in 3x3 experiments.

Two of the most important parameterization schemes relevant to this study are the surface-process and cumulus convection parameterization schemes. The first scheme treats microclimate processes interacting among soil, vegetation and the atmosphere while the second parameterizes subgrid convective processes. With given computer resources we weigh the first process more than the second because we primarily deal with land surface processes. The state-of-art BATS version 1e is chosen for the surface process while the relatively simple Kuo scheme is chosen for cumulus convection in this study (Anthes 1977, Kuo 1974). The choice of a relative simple cumulus parameterization scheme can be justified based on the following: (i) Our primary interest is in temporal and spatial average properties, rather than in timing and locating of individual rainfall events. Possible biases in timing and positioning caused by the less accurate scheme should be smoothed out on the average and thus do not affect the final result severely. ii) Our previous study (Pan et al. 1996) showed that the Kuo scheme is more sensitive to surface wetness than the Grell scheme (Grell 1993). This enhanced sensitivity highlights the roles of surface processes that are affected by changes in landuse. iii) The previous similar study (Copeland et al. 1996) was performed by using the Kuo scheme and its adoption here facilitates the comparison with the previous results.

3 Results of Simulations for 1991 Normal Year

3.1 Model Validation

Model skill in accurately reproducing the real atmosphere is essential for any simulations. Surface pressure is gross measures of total air mass within the model domain. The observed surface pressure exhibits several passages of synoptic waves (Fig. 3). The simulated domain-average surface pressure follows the observed trend quite well, although the simulated pressure is somewhat lower than the observation around day 10. The under-simulation, which is often observed with the MM4 based on which the RegCM2 is framed, is within 1 hPa most of the time and the maximum error is less than 1.5 hPa (Fig. 3). (All figures in this section are from 1991 simulation and model validations are from the simulation with current landuse unless given otherwise.) The monthly mean surface pressure at 0000 UTC shows a small positive

bias over the western mountain region and a somewhat larger negative bias in the east-central U.S. (Fig. 4). The errors are larger along the west coast because of complex terrain. The overall error magnitudes are small, within 1 hPa over most parts of the domain except for those negative centers where error reaches 2-3 hPa.

We choose a mid-troposphere level (σ=0.51, roughly at 500 hPa) to validate the model skill since this is one of the most important levels that steer the movement of the atmospheric systems. Observed wind speed averaged over the whole domain at 0000 UTC changed quite rapidly in time, with high values of 15 m s^{-1} and low values of 10 m s^{-1} (Fig. 5a). The simulated wind followed the observed trend very well, especially after day 13 when the simulated winds were almost exact as wind speeds increased. The reason for the high accuracy when wind speeds increased at day 13 and a few days after that may be because the boundary constraint became stronger and model errors had less time to develop when wind speeds were high. This is perhaps one of the reasons why regional simulations during winter when winds are strong are usually significantly better than during summer. It is noteworthy that the simulated wind had a 1-2 d time lag during the later stage of the simulation when wind had distinct peaks. This is the manifestation of limited-area boundary forcing.

The observed temperature at σ=0.51 was low during the first half and high during the second half of the simulation period. The simulated temperature followed this trend reasonably well although a small cold bias existed most of the time. The largest error was about 1.5 K and average error was less than 0.5 K (Fig. 5b).

The large temporal and spatial variabilities of rainfall makes it one of the most difficult variables to simulate. Precipitation also is the end product of various atmospheric processes including thermal, dynamical, and micro-physical precesses, and errors in any of these processes will be reflected in rainfall. These are the main reasons why precipitation simulations are usually poorest in almost all modeling studies. During the 30-d period in 1991 the observed rainfall exhibited a large amount along the U.S.-Canada border and in the LA-MS-AL region at the southeast corner of the domain (Fig. 6a). The simulation reproduced the heavy rainfall along the U.S.-Canada border and part of Iowa. The model failed to produce the heavy rainfall

that occurred in the LA-MS-AL region, which was partly due to its proximity to the model boundaries and partly to the small scale of these convective rainfall events, which are often associated with local seabreezes that are not resolved by the model. The model considerably overpredicted rainfall in Oklahoma and New Mexico probably because of the so-called grid-point storms caused by model artifacts (Fig. 6b). It is possible also that the excessive rainfall was advected from the LA-MS-AL region where the model should have produced heavy rainfall.

The domain-averaged rainfall was simulated surprisingly well although the model misplaced exact locations of rainfall centers. The simulated domain total rainfall was lower than the observation starting from beginning of the simulation, which was due partly to the spinup effect (Fig. 7). The model rainfall exceeded observed amounts in the later part of the simulated period, which approximately balanced the deficit of the first half month.

In summary, the simulated surface pressure and 500 hPa wind and temperature resembled observations well, and simulated domain-averaged rainfall was realistic although the model did not reproduce the details of rainfall distribution. This gross validation indicates that the model is skillful in reproducing the real meteorological processes reasonably well.

3.2 Domain-Averaged Surface Fluxes

Surface energy budget is an essential component of climate systems. The domain-averaged evapotranspiration (ET) accumulated quite linearly with time for all three experiments, but with different rates (Fig. 8a). The ET is smallest for natural landuse, which evaporated 42.4 mm of water in the 30-d period (1.42 mm d^{-1}). The present landuse, about one fourth of which is translated into cropland that has lowest stomatal resistance, evaporates 45.6 mm during the period (1.52 mm d^{-1}), a 7.5% increase over the natural land. The uniform cropland evaporates 53.1 mm (1.77 mm d^{-1}), a 14 % increase over present landuse.

The sensible heat flux (H) showed a similar trend but with opposite sign to latent heat flux (*i.e.*, ET) because they are coupled by the energy budget equation. The 30-d accumulated sensible fluxes in terms of ET equivalent unit are 75.3, 73.9 ,67.2 mm for natural, present, and future landuse, respectively. The separation among the three landuse types are larger for ET

than H. This is reasonable since cropland expansion is the primary landuse change, and most prominent feature of crops is their lower stomatal resistance. This means the ET increase over cropland is larger than the decrease in sensible heat flux. The residual energy between the ET increase and H decrease may penetrate into the ground and/or may be lost by long wave radiation. Table 3 shows the accumulated domain-averaged, available energy (sum of sensible and latent heat fluxes), the Bowen ratio, incoming solar radiation, and rainfall at various days.

Table 3 Accumulated available energy(HE), Bowen Ratio(β), incoming radiation(R), and rainfall (P). All units are in mm except for β.

Day	5	10	15	20	25	30
			HE			
Natural	18.4	37.3	57.3	77.0	97.6	117.6
Current	18.9	38.0	58.4	78.2	99.0	119.6
Future	19.8	39.2	59.2	79.2	100.1	120.3
			β			
Natural	1.34	1.60	1.70	1.76	1.74	1.78
Current	1.16	1.41	1.53	1.59	1.58	1.62
Future	0.77	1.00	1.12	1.20	1.22	1.26
			R			
Natural	48.2	99.0	145.2	189.6	237.9	285.3
Current	48.6	99.3	146.1	190.3	238.6	286.6
Future	46.9	96.6	142.0	185.2	232.7	279.1
			P			
Natural	5.2	9.9	20.2	26.8	33.0	40.7
Current	5.4	9.9	19.5	26.2	33.0	41.0
Future	6.0	10.7	21.5	28.7	34.1	42.2

The present land surface absorbs most solar energy (286.6 mm) since it has least albedo (Table 2) and the future vegetation absorbs least energy (279.1 mm) because it has largest albedo. The difference is 7.5 mm over the one-month period. The natural landuse receives slightly less energy (285.3) than the present land surface (Fig. 8c). On the other hand, the hypothetical future land produces most available energy out of the least absorbed solar energy. This is because the energy partition is different among these three scenarios. Crops transpire most because of their least stomatal resistance. This increased ET cools the ground and thus

reduces outgoing long wave radiation, thereby making intensive crop coverage more efficient in producing available energy to the atmosphere.

The rainfall accumulation rate is not as linear as the fluxes, indicating its temporal variability (Fig. 8d). The rainfall did not show significant difference among the three experiments until day 15, and then tended to merge again at the end of the 30-d simulation period. Cropland (labeled by "CRP" in all figures) produced the largest rainfall throughout the simulation period, and the natural (labeled by "NAT") and current ("CUR") landuse gave comparable amounts. The separation among the experiments was largest during days 15-20 when the hypothetical future cropland resulted in about 10% higher rainfall than the current landuse. The merging tendency suggests that the atmosphere-surface system may have a self-adjustment mechanism. The total rainfall amounts at the end of the integration are 40.7, 41.0, and 42.2 mm for the natural, current and future landuse (Table 3). The larger rainfall amount with cropland was likely caused by increased ET from crops.

The simulated rainfall with current landuse increased by about 0.8%, far less than an increase of 5% simulated by a similar study (Copeland et al. 1996). The observed rainfall over the U.S. has increased by only 1% over the last 100 years and in fact it has decreased in the last few decades (Plantico et al. 1990). Thus our figure is more consistent with observations.

The latent heat flux averaged between 1800-2100 UTC (about time period of maximum heat fluxes) over the entire domain shows apparent temporal variations (Fig. 9a). The high ET at the beginning and low ET around days 8-9 correspond to the high and low rainfall rates, respectively (see Fig. 8d). The separation among the three experiments is large but consistent. The maximum difference between natural and future landuse reaches 100 W m^{-2}. The corresponding sensible heat flux has less temporal variation and is nearly constant (at 210 W m^{-2}) except during the first 5 days of the simulation when excessive evapotranspiration occurred (Fig. 9b). The temporal variations of latent and sensible heat fluxes do not balance well, suggesting that the land system on this scale can store some amount of heat energy temporarily. The fluctuation of latent heat flux could be attributable to the high dependency of ET on soil moisture. The incoming solar energy changed considerably with time, presumably

due to clouds (Fig. 9c). The maximum radiation reached the surface during the driest days 7-9, and minimum values were found during the first 5 d and between days 16-19 when more rain fell. The future landuse receives least solar energy because of a more humid atmosphere through larger ET and thus more cloudiness and larger albedo.

3.3 Distribution of Surface Fluxes

The 30-d accumulated ET distribution under current landuse shows a large center with a maximum value of 110 mm along the west coast where warm coastal sea water and moist atmosphere exist (Fig. 10a). A secondary (peak value of 70 mm) but wide spread ET maximum area is over the Midwest and Great Lakes region where extensive agriculture dominates the landuse. The ET values over the western mountain region are less than 30 mm. The distribution of sensible heat flux (Fig. 10b) shows a rather uniform value of about 75 mm except over the Great Lakes and oceans. (Large sensible heat fluxes near the boundaries exist because of less clouds, probably resulting from smoother boundary conditions.)

The difference in ET between the current and natural landuse are positive over most parts of the east-central U.S. where more transpiring crops replaced either grass prairie or woodland, both of which consume less water than crops (Fig. 11a). Negative ET difference was found in the southwest U.S. where evergreen shrub replaced deciduous shrub. The difference in sensible heat flux is similar to ET but with opposite sign (Fig. 11b). The radiation difference field correlates well with the albedo changes (see Fig. 2a) in the western U.S. where decreased albedo induced more radiation absorption in this region of normally low cloud coverage (Fig. 11c). Over the east-central U.S the correlation between albedo and incoming radiation is less clear because of the masks of clouds. For example, over most parts of the Midwest where albedo remains the same, the current land receives less radiation compared to the natural land, presumably due to increased cloudiness. The increase in both albedo and radiation over the Great Lakes region is harder to explain. However, rainfall over this region has decreased noticeably (Fig. 11d), indicating the possibility of less cloudiness and consequently more incoming solar radiation. Unlike surface flux and radiation difference fields which are more

uniform, the rainfall difference field is noisier, and several intensive positive/negative centers exist over the Midwest. This is reasonable since rainfall has the largest spatial variation.

The differences between the future and current landuse in all fields is generally larger than those between the current and natural landuse since landuse difference is larger in the former. The ET increased over the whole western U.S. because of the hypothetic replacement of grassland and woodland by crops (Fig. 12a). Over the Great Lakes region and parts of the Midwest where cropland is dominant already, a decrease in ET is simulated. This could be due to the increase in atmospheric vapor content which decreases the moisture gradient between the surface and the atmosphere. Sensible heat decreases almost everywhere except over the desert where it is assumed that no crops are present and the Great Lakes region (Fig. 12b). Solar radiation decreases over the entire western U.S. since crops have larger albedo (Fig. 12c). The increase in radiation over the Great Lakes and Oklahoma could be attributable to cloudiness as suggested by less rainfall (Fig. 12d). The rainfall difference is still mainly limited to the heavy rainfall areas but with larger extent of positive areas.

The difference fields in rainfall between the current and pre-settlement and between the future and current landuse exhibit several positive and negative centers of large magnitudes although the domain total rainfall differs by less than 3% between each of the two experiments. The difference pattern is associated with rainfall pattern rather than to landuse-change pattern (Fig. 11d). The area/magnitude of positive and negative centers tend to balance out and to couple in space. One possible explanation for the positive-negative dipole structure is probably the conservation of moisture. The changed landuse induces more rainfall, dries the atmospheric column, and reduces the amount of moisture downstream, thereby reducing rainfall. Similarly if the altered landuse decreases rainfall *in situ* it could leave more rainfall downstream. The dipole structure can also be explained by the horizontal displacement of rainfall centers. This negative spatial correlation was found by other modeling studies (*e.g.*, Paegle et al. 1996) and observational studies (*e.g.*, Rasmussen 1967).

3.4 Screen Height Analyses

Variables at screen height (2 m AGL) are interpolated between the surface (at z_0) and lowest model level (σ=0.995, about 40 m AGL) using the logarithmic profile which corresponds to neutral stratification (Dickinson et al. 1992). For most vegetation types z_0 is much less than 2 m except for evergreen broadleaf trees which do not exist in the current simulation domain.

Wind speed averaged over the domain at 2100 UTC exhibits significant difference among the three experiments although they followed similar trends in time. The future winds would be about 0.5 m s^{-1} higher than the the current which is slightly windier than the natural landuse, because crops have smaller roughness height than forest (Fig. 13a). The separation in domain average temperature at 2100 UTC is generally small except for a few days at the beginning of simulation (Fig. 13b). The natural land provides slightly warmer air at this height even though it has slightly higher average albedo. This is because the large increase in ET overwhelmed the small albedo effect. The future landuse gives lowest temperature since it has both larger albedo and ET. Mixing ratio shows constant separation during the entire simulation period (Fig. 13c). The moisture content is well explained by increased ET for the current and future landuse.

The 30-d average wind speed has increased over the Midwest where cropland of small roughness (z_0=0.06 m) has replaced tall grass prairie of z_0=0.1 m and over the southwest U.S where crops and shrub replaced woodland (Fig. 14a). Temperature patterns show a general cooling over the east-central U.S. and warming in the west. The cooling is likely associated with the increased ET under the current landuse, and the warming is related to the increased radiation and sensible heat flux from the ground and to albedo decrease (Fig. 14b). Mixing ratio shows an increase in the central U.S. and decrease in the western U.S. This pattern is directly related to ET distribution (Fig. 14c). The ground temperature of top soil showed similar trends to that at screen height in Fig.13b (not shown).

Future winds would be increased noticeably over the western mountain area, Mississippi valley and Great Lakes forests. The increase can reach 2 m s^{-1}. Temperature and mixing ratio will decrease and increase respectively due to higher ET imposed by uniform cropland (Figs.

15a-c).

Surface temperature is a very important climate variable, probably next to precipitation. The annual mean surface temperature over the contiguous U.S. has actually decreased by 0.06 K over the period of 1948-87. This observed result is consistent with our simulated slight decrease in air temperature at the screen height under the current landuse compared to the natural landuse as seen in Fig. 13b although landuse changes occurred well before 1940's.

The observed summer temperature (JJA) has decreased over the lower Mississippi basin and the Gulf Coast and it has increased over the western mountain region. The general pattern of observed trends, and cooling in the east-central U.S. and warming in the western U.S. resembles well the simulation presented in Fig. 14b.

There are no extensive wind and mixing ratio records to verify our simulation on these variables. However, our domain averaged increase in wind speed and mixing ratio in present landuse is consistent with the Copeland et al. (1996) simulation.

4 Flood and Drought Contrast

4.1 1993 Flood

The domain average rainfall in the 1993 flood year appears to be less sensitive to landuse compared with the normal year, and the natural landuse gives largest rainfall while the current landuse results in least rainfall (Fig. 16a). The domain-averaged flux variations among different experiments are very similar to those for 1991 (Fig. 16b). The following explores why similar surface flux variations between the normal and flood year result in opposite signs in rainfall responses.

Figures 17 and 18 depict ET and rainfall differences between the current and natural landuse and between future and current landuse respectively. Both the current and future landuse show a general decrease in rainfall as compared with the natural landuse over the Midwest and Mississippi basin where the 1993 flood occurred and general increase in the western U.S. The overall pattern matches well with the ET distribution, especially for the difference between the future and current landuse (Fig. 18a,b) where the difference in landuse is larger. ET

increases over the western U.S. and decreases in the Midwest. ET and rainfall centers coincide quite well. This strongly suggests that the decrease in rainfall was associated with reduced ET on the regional scale. Previous studies have found that increased ET (decreased sensible heat flux) is conducive to rainfall (*e.g.*, Segal et al. 1995). However this is true only over the regional scale, not over the entire domain. The rainfall decreases over the flood area, and a relatively slight decrease in rainfall results in large absolute drop in rainfall amount.

In order to examine the causes for the decreased rainfall over the flood area, we plot the screen height temperature (Fig. 19) at the negative center (i=61, j=21 in Fig. 17b). It is seen that current temperature is about 1 K cooler than that with the natural landuse, especially during the earlier days of the simulation. This lower temperature could suppress convection and consequently weaken rainfall amount.

The v-component wind speed at this same grid at σ=0.895 is noticeably weaker with the current landuse (Fig. 20). The weakened wind might reduce ET and moisture transport from the south, and thus reduce rainfall. This reduced rainfall also could be associated with the weakened nocturnal low-level jet (LLJ) because of the reduced planetary boundary layer (PBL) height. The PBL height is closely associated with nocturnal LLJ. Under current and future landuse, ET is increased and thus sensible heat flux is reduced over the Texas area where the nocturnal LLJ occurs most often (Mitchell et al. 1995). The LLJ is one of the important factors for heavy rainfall events during the 1993 flood.

4.2 1988 Drought

The domain-average rainfall in the 1988 drought case exhibits little sensitivity to landuse changes, and differences among the three experiments are within 1 mm except for a few days around day 5 (Fig. 21a). The domain-average flux changes among different landuse types are similar to the normal year (Fig. 21b). The spatial correlation between the ET and rainfall difference fields are not as clear as in 1991 and 1993 (Fig. 22). The lower correlation could be explained as follows. Moisture is a passive constituent, which means that it does not interact with the atmosphere until it condenses, except for a slight effect on radiation. The atmosphere

in 1988 was dry and far from condensation on average. It is less likely that the small increased ET would increase atmospheric moisture to saturation compared with the other two years. Thus, the increased ET had less chance to translate into rainfall.

It is noteworthy that the difference field in rainfall between the current and natural landuse is very localized and the magnitudes of the difference are large although the domain averages are very close between the two experiments. These localized "storms" tend to occur when the the atmosphere is dry since there are less major synoptic systems to organize the localized individual convection (Giorgi et al. 1993b, Pan et al. 1996).

4.3 Synthesis of the Three Years

The current and future landuse showed an overall rainfall increase in the drier western U.S. and decrease in the moist east-central U.S. These general patterns can be conceptually explained by the fact that to increase precipitation, the dry atmosphere in the western U.S. is more in need for moisture while that in the east-central U.S. is more in need for sensible heating.

The response of domain total rainfall to the landuse scenarios depends on the relative magnitudes of the decrease in the east-central U.S. and increase in the western U.S. Rainfall in the 1993 flood was more concentrated in the Mississippi basin, relative to the east as compared with 1991 and 1988 (Figs. 11d, 17b, and 22b) and thus is more subject to decrease with the current and future landuse. On the other hand, rainfall in 1991 extended more westward (Fig. 6b) and thus has higher chance for increase with the current and future landuse.

5 Summary and Discussions

The impacts of human settlement on regional summer climate over the central and western U.S. are examined by considering three vegetation scenarios (pre-settlement natural, current, and hypothetical future cropland) under normal, flood, and drought climate. During the normal year, the current landuse showed a 0.8% increase in domain-average rainfall over the natural landuse, a result in agreement with the observed 1% increase during the last 100

years and consistent with the other similar simulations (although the magnitudes of increase differ considerably). The hypothetical future uniform cropland would result in 3% increase in domain-average rainfall over the current landuse.

In the flood year, the domain-averaged rainfall responded to landuse differently from that in the normal year not only in magnitude but also in sign as summarized at the top of Table 4. Both current and future landuse exhibited a decrease in accumulated rainfall over the wetter Midwest and Mississippi basin and an increase in the drier western U.S. This rainfall decrease/increase pattern correlated to the evapotranspiration (ET) field. The decreased ET and thus rainfall in the Midwest was associated with (i) lower surface temperature caused by larger evapotranspiration from crops that replaced natural grass prairie and (ii) weakened low-level jet due to less sensible heating in the Texas area. The rainfall increase in the western U.S. was attributed to the increased ET.

In the drought year, domain total rainfall exhibited little sensitivity although large localized differences existed among the three landuse scenarios. The reduced sensitivities on average may be due to the fact that the increased ET had less chance to translate into rainfall when the atmosphere was dry and less conducive to precipitation processes.

Domain-average surface fluxes responded to landuse scenarios similarly among the three years: increase in ET (decrease in sensible heat flux) as cropland expands in the current and future landuse, but rainfall responded differently. In fact in 1993, the domain-total rainfall decreased slightly with the current and future landuse. This decreased rainfall with increasing ET over the whole domain appears to be counter-intuitive. The reason is obscured by the domain average. On regional and local scales, rainfall correlates to surface fluxes quite well. The low correlation between ET and rainfall on the domain scale indicates the dominance of dynamic processes while better correlation over the regional scale indicates the dominance of thermodynamic processes on the respective scales.

Our simulation for the 1991 normal year showed a 0.8 % increase in domain average rainfall, as compared to 5% in a similar study (Copeland et al. 1996). Although our result is closer to the observed 1% increase during past 100 years, it is still useful to point out that their

Table 4 Thirty-day accumulated rainfall (P), evapotranspiration (ET), available energy (HE), and incoming radiation (R). All units are in mm.

	1988	**1991**	**1993**
		P	
Natural	41.98	40.68	49.94
Current	41.89	41.02	48.12
Future	41.33	42.22	49.34
		ET	
Natural	44.33	42.35	54.23
Current	46.98	45.64	56.57
Future	54.35	53.10	63.89
		HE	
Natural	122.83	117.64	128.59
Current	124.14	119.57	129.83
Future	124.95	120.25	129.77
		R	
Natural	297.04	285.30	290.62
Current	297.31	286.56	291.54
Future	290.74	279.14	282.99

simulated heavy rainfall increase was along the south and east coasts which are not covered by our simulation domain. Rainfall over the Midwest and Great Lakes region increased least and even slightly decreased in their simulation, which is in agreement with our simulation of 1991.

The domain average and distribution of temperature showed a slight cooling with the current landuse, which resulted from stronger cooling over the Midwest and Great Lakes region where crops replaced grass prairie and natural woodland. This result is in general agreement with observations. Several reasons were proposed to explain why the U.S. has not experienced higher temperature in response to global warming. One popular argument is that the heavily released sulfate and other aerosols blocked the sunshine and counteracted with the effect of greenhouse gases. In our experiments, both the change in greenhouse gases and in sulfate aerosols are excluded. The cooling or warming of our simulations is purely caused by the landuse changes. The gross resemblance between the observed and simulated trend distribution seems to suggest that the observed trends counter to global warming over the U.S. may also

be associated with the landuse changes. The expansion in agriculture over native grass and forests tends to cool the atmosphere.

Acknowledgments

The authors would like to thank Drs. Bill Gutowski, T.-C. Chen, and Al Austin for their careful review of the manuscript and insightful suggestions. Part of computer support used in this study was provided by the National Center for Atmospheric Research sponsored by the NSF. Partial financial support was provided by NASA grant NAG 5-2491.

References

Anthes, R. A., 1977: A cumulus parameterization scheme utilizing a one-dimensional cloud model. *Mon. Wea. Rev.*, **105**, 270-286.

Briegleb, B. P., 1992: Delta-Eddington approximation for solar radiation in the NCAR Community Climate model. *J. Geophys. Res.*, **97**, 7603-7612.

Charney, J. G., W. J. Quirk, S. H. Chow, and J. Kornfield, 1977: A comparative study of the effects of albedo change on drought in semi-arid regions. *Atmos. Sci.*, **34**, 1366-1385.

Campbell, G. S., 1991: Simulation of water uptake by plant roots, in *Modeling Plant and Soil Systems*, Hanks J. and J. T. Ritchie (ed), Agronomy Monograph No. 31, Amer. Soc., 273-320.

Copeland, J., R. A. Pielke and T. Kittel, 1996: Potential impacts of vegetation change: A regional modeling study. J. Geophys. Res., 101, 7409-7418.

Dickinson, R. E., and A. Henderson-Sellers, 1988: Modeling tropical deforestation: a study of GCM land-surface parameterizations. *Qurt. J. Roy. Meteor. Soc.*, **114**, 439-462.

Dickinson, R. E., A. Henderson-Sellers, and P. J. Kennedy, 1992: Biosphere-atmosphere transfer scheme (BATS) version 1e as coupled to NCAR community climate model. *NCAR Technical Note, 387+STR*, 72pp.

Foland, C. K., T. Karl and K. Y. Vinnikov, 1991: Observed climate variations and change, in *Climate Change*, the IPCC scientific assessment, Houghton, J. T., G. J. Jenkins, and J. J. Ephramus (ed), Cambridge University Press, 199-238.

Gerald, D. B., and J. E. Janowiak, 1995: Atmospheric circulation associated with the Midwest flood of 1993. *Bull. Amer. Meteor. Soc.*, **76**, 681-685.

Giorgi, F., M. R. Marinucci, G. T. Bates, and G. De Canio, 1993a: Development of a second-generation regional climate model (RegCM2). Part I: Boundary-layer and radiative transfer. *Mon. Wea. Rev.*, **121**, 2794-2813.

Giorgi, F., M. R. Marinucci, G. T. Bates, and G. De Canio, 1993b: Development of a second-generation regional climate model (RegCM2). Part II: Connective processes and assimilation of boundary conditions. *Mon. Wea. Rev.*, **121**, 2814-2832.

Giorgi, F., L. Mearns, C. Shields, and L. Mayer, 1996: A regional model study of the importance of local versus remote controls of the 1988 drought and the 1993 flood over the central United States. *J. Climate*, **9**, 1150-1162.

Grell, G. A, 1993: Prognostic evaluation of assumptions used by cumulus parameterizations. *Mon. Wea. Rev.*, **121**, 764-787.

Hansen, J. E., D. Johnson, A. Lacis, S. Lebedeff, and P. Lee, 1981: Climate impact of increasing atmospheric carbon dioxide. *Science*, **231**, 957-966.

Karl, T. R, D. R. Easterling, R. W. Knight, and Hughes, 1994: U. S. national and regional temperature anomalies. In: *Trends'93: A compendium of data on global change*, T. A. Boder, D. P. Kaiser, R. J. Sepanski, and F. W. Stoss (ed), 686-736.

ORNL/CDIAC-65. Carbon Dioxide Information Analysis Center, Oak Ridge National Laboratory, Oak Ridge, Tenn., U.S.A.

Kuchler, A. W., 1964: Potential natural vegetation of the contiguous United States. *Amer. Geogr. Soc.*, 116pp.

Kuo, S. L., 1974: Further studies of the parameterization of the effect of cumulus convection on large-scale flow. *J. Atmos. Sci.*, **31**, 1232-1240.

Manabe, S., and R. T. Wetherald, 1980: On the distribution of climate change resulting from an increase in CO_2 content of the atmosphere. *J. Atmos. Sci.*, **37**, 99-118.

Matthews, E., 1983: Global vegetation and land use: New high resolution data bases for climate studies. *J. Climate Appl. Meteor.*, **22**, 474-487.

Mintz, Y., 1984: The sensitivity of numerically simulated climates to land-surface boundary conditions. In: *The Global Climate*, J. T. Houghton (ed), Cambridge University Press, 79-105.

Mitchell, M. J., R. W. Arritt, and K. Labas, 1995: A climatology of warm season Great Plains low-level jet using wind profiler observations. *Wea. Forecasting*, **10**, 576-591.

Paegle J., K. C. Mo, and J. N. Paegle, 1996: Dependence of simulated precipitation on surface evaporation during the 1993 United States summer floods. *Mon. Wea. Rev.* **124**, 345-361.

Pan, Z., E. Takle, M. Segal, and R. Turner 1996: Influences of model parameterization schemes on the response of rainfall to soil moisture in the central U.S. *Mon. Wea. Rev.*, **124**, 1786-1802.

Plantico, M. S., T. R. Karl, G. Kukla, and J. Gavin, 1990: Is recent climate change across the United States related to rising levels of anthropogenic greenhouse gases? *J. Geophys. Res.*, **95**, 16617-16637.

Rasmussen, E. M., 1976: Atmospheric water vapor transport and the water balance of North America: Part I. Characteristics of the water flux field. *Mon. Wea. Rev.*, **95**, 603-426.

Sagen, C., O. B. Toon, and J. B. Pollack, 1991: Anthropogenic albedo changes and the earth's climate, *Science*, **206**, 1363-1368.

Segal, M., R. W. Arritt, C. Clark, R. Rabin, and J. M. Brown, 1995: Scaling evaluation of the effect of surface characteristics on potential for deep convection over uniform terrain. *Mon. Wea. Rev.*, **123**, 383-400.

Trenberth, K. E., and Guillemot, 1996: Physical processes involved in the 1988 drought and 1993 floods in North America. *J. Climate*, **9**, 1288-1298.

Vinnikov, K. Ya., P. Ya. Groisman, and K. M. Lugina, 1990: Empirical data on contemporary global climate changes (temperature and precipitation). *J. Climate*, **3**, 662-677.

Wilson, M. F., 1984: The construction and use of land sufrace information in a general circulation climate model. Ph. D. thesis, University of Liverpool, United Kingdom, 346 pp.

(a)

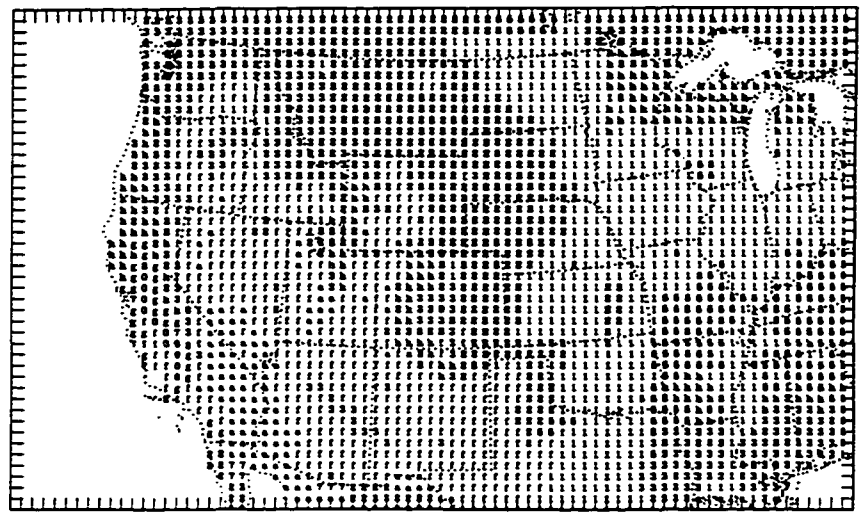

(b)

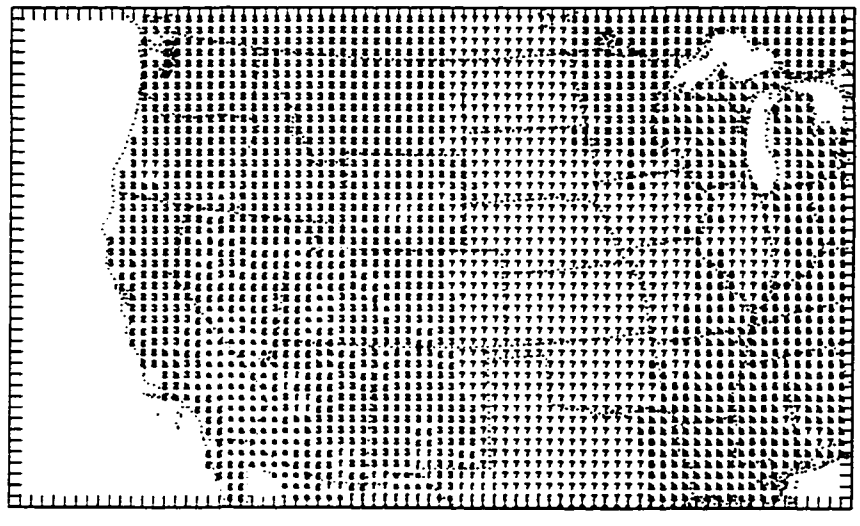

Figure 1 Landuse type. (a) present climatology, (b) potential natural landuse adapted from Küchler (1964). Legends: 1–crop/mixed farming, 2–short grass, 3–evergreen needleleaf tree, 4–deciduous needleleaf tree, 5–deciduous broadleaf tree, 6–evergreen broadleaf tree, 7–tall grass, 8–desert, 9–tundra, 0–irrigated crop, a–semi-desert, b–ice cap/glacier, c–bog or marsh, d–inland water, e–sea, f–evergreen shrub, g–deciduous shrub, h–mixed woodland.

(a)

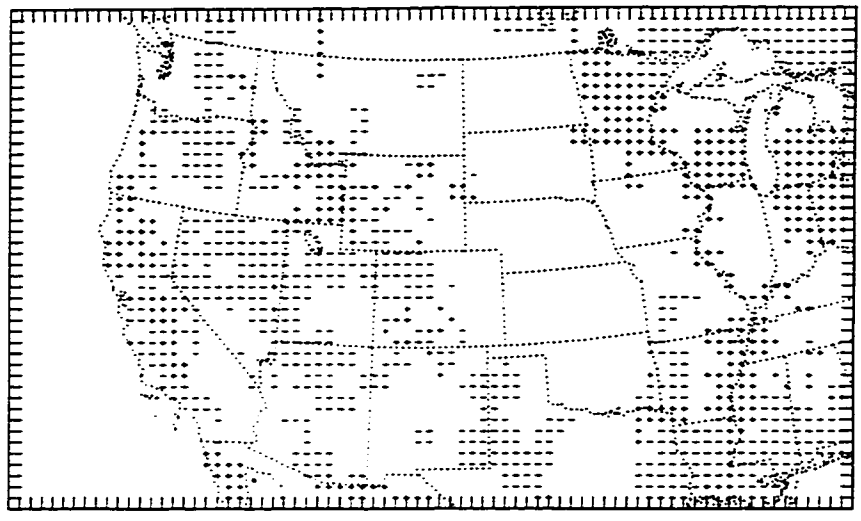

(b)

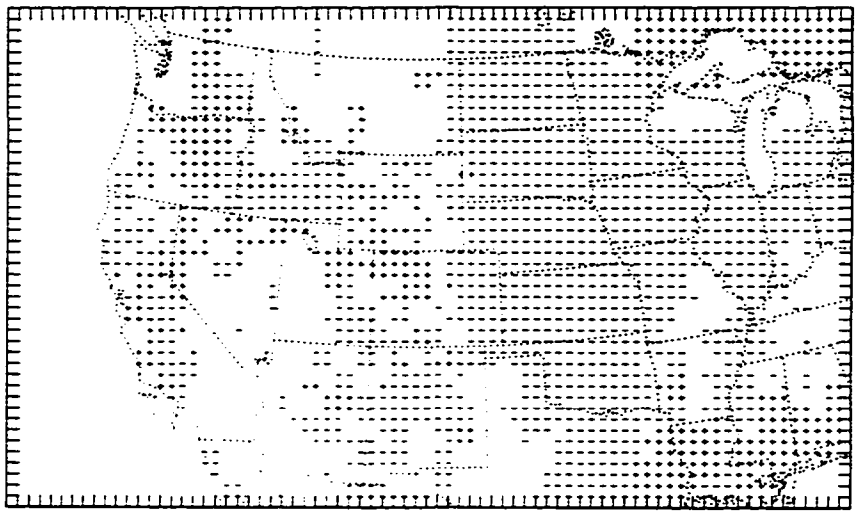

Figure 2 Sign difference fields in various landuse parameters between the current and natural landuse. (a) Albedo, (b) Roughness (m).

(c)

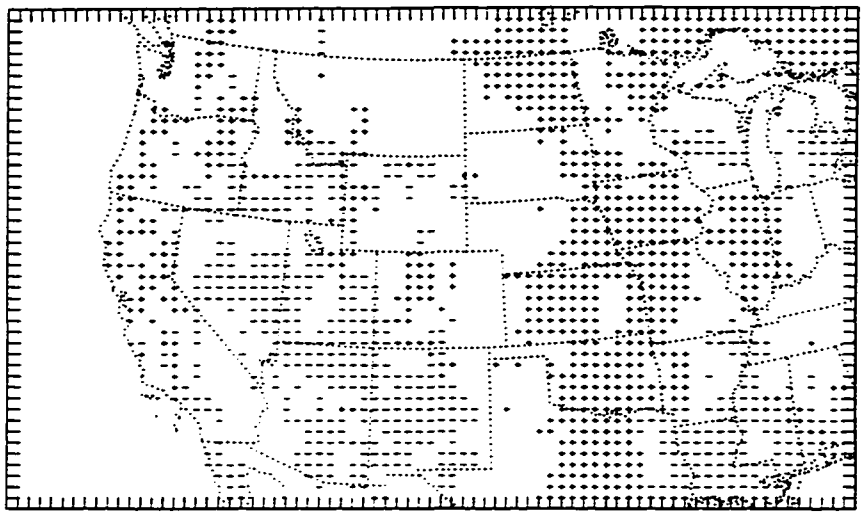

(d)

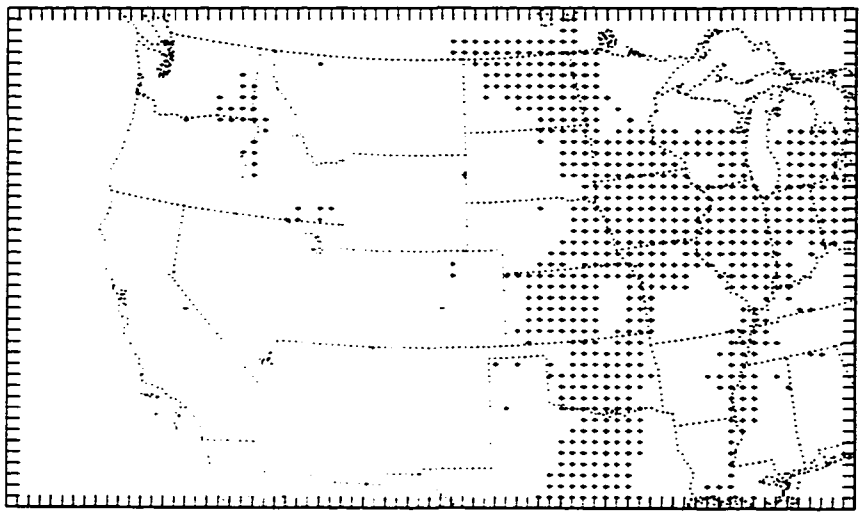

Figure 2 (continued) (c) Moisture availability. (d) Fractional vegetation coverage.

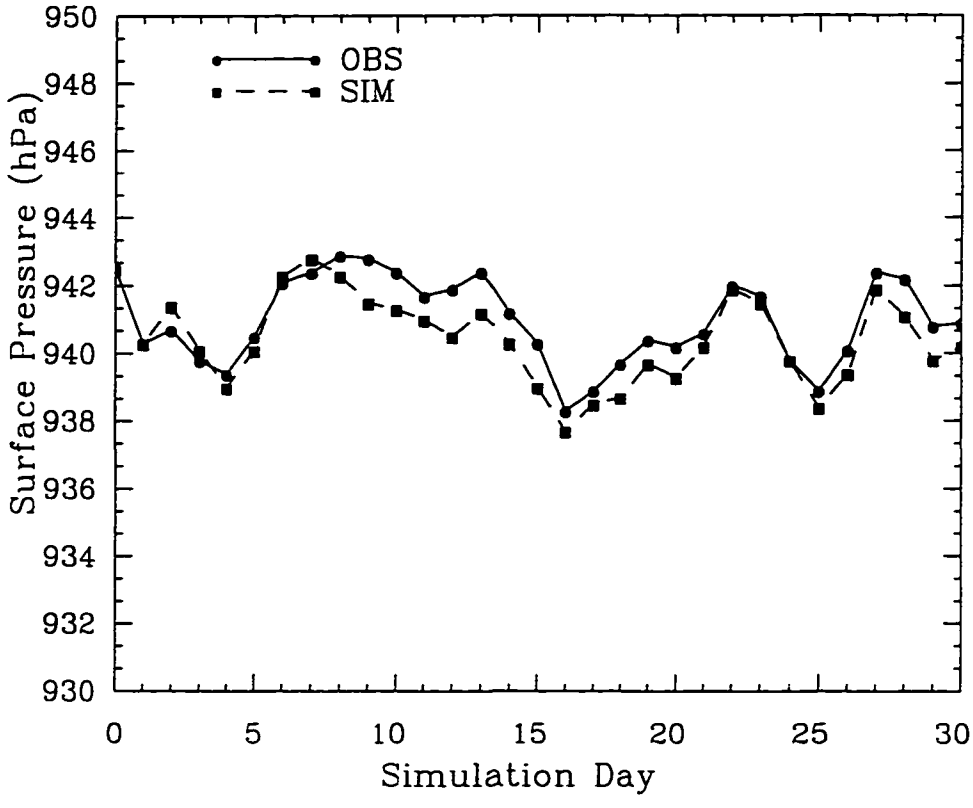

Figure 3 Time series of domain-averaged surface pressure as compared with observation.

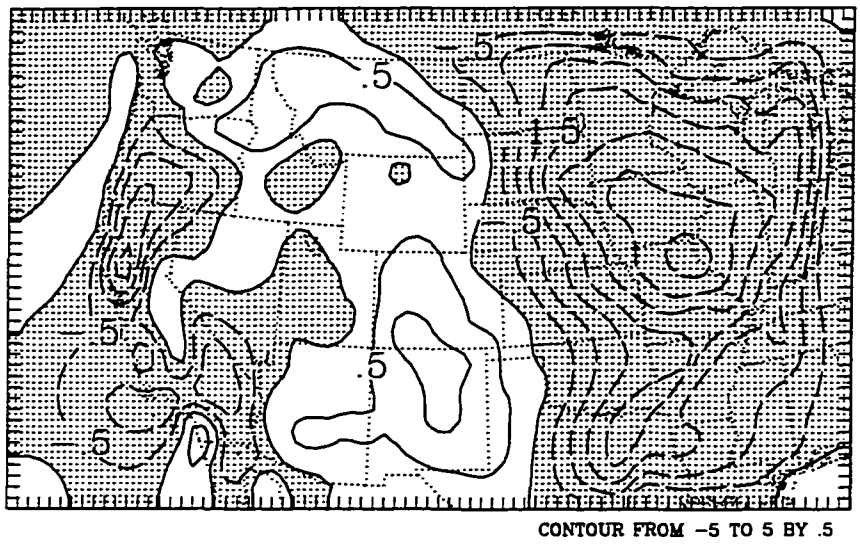

Figure 4 Spatial distribution of the difference (hPa) in 30-d averaged surface pressure between the simulation and observation. Areas of negative values are shaded.

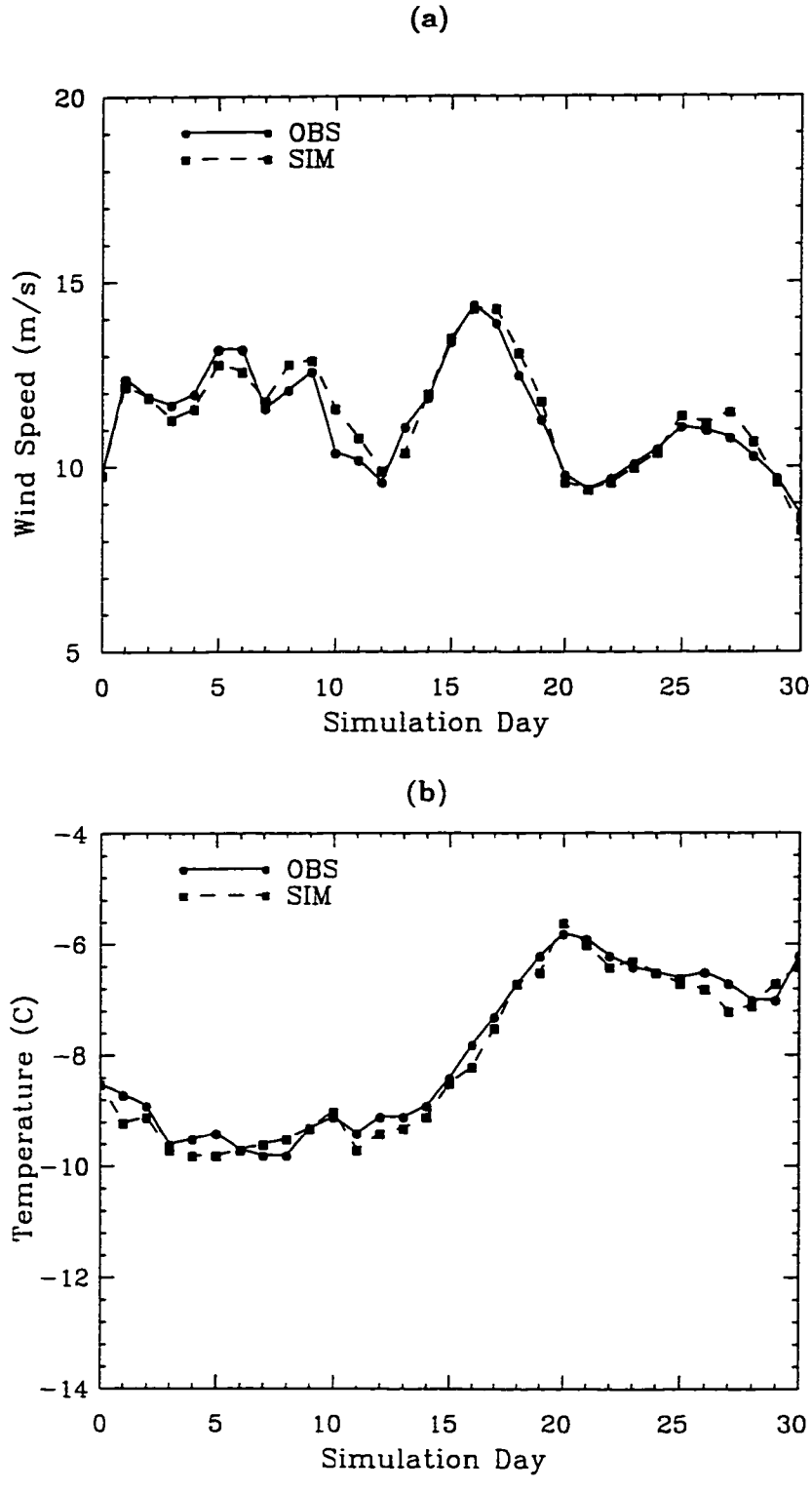

Figure 5 Time series of domain-averaged variables at 7th model level (σ=0.51) as compared with observation. (a) Wind, (b) Temperature.

(a)

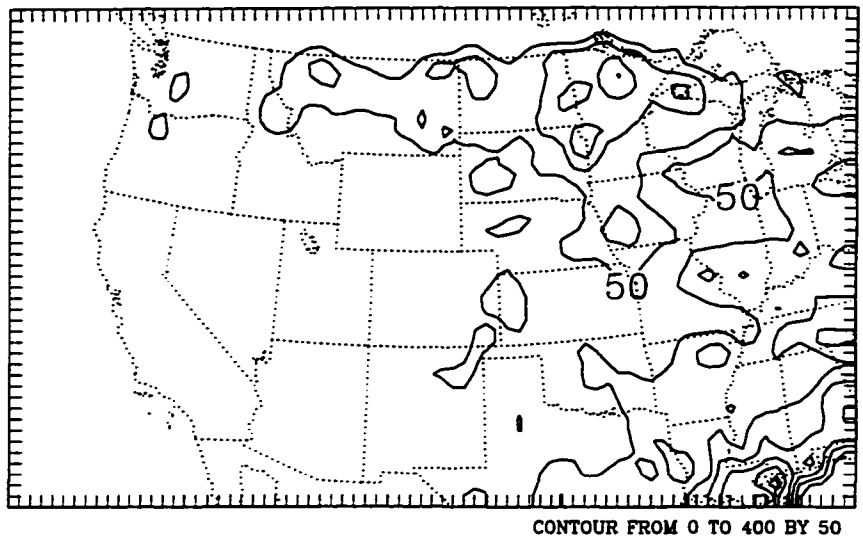

(b)

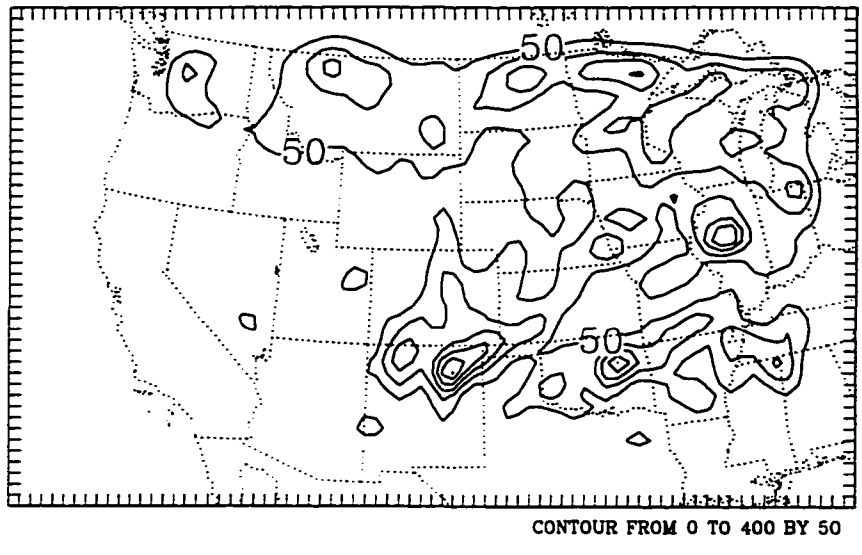

Figure 6 Spatial distribution of observed (a) and simulated (b) 30-d accumulated rainfall (mm).

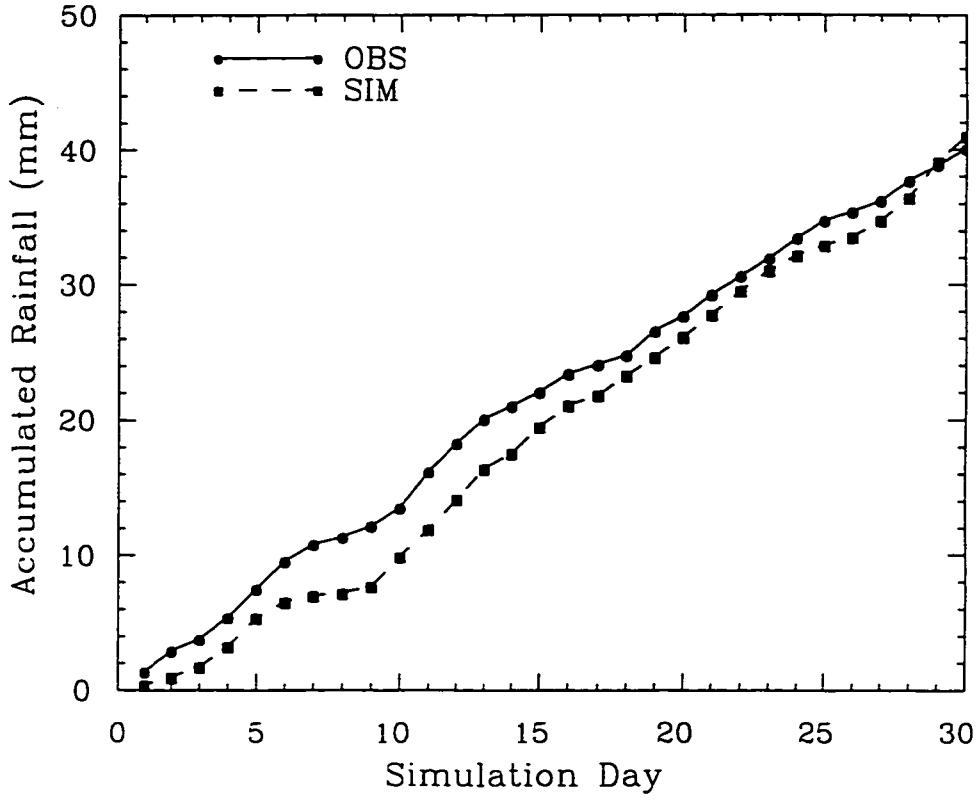

Figure 7 Time series of accumulated domain-averaged rainfall as compared with observation.

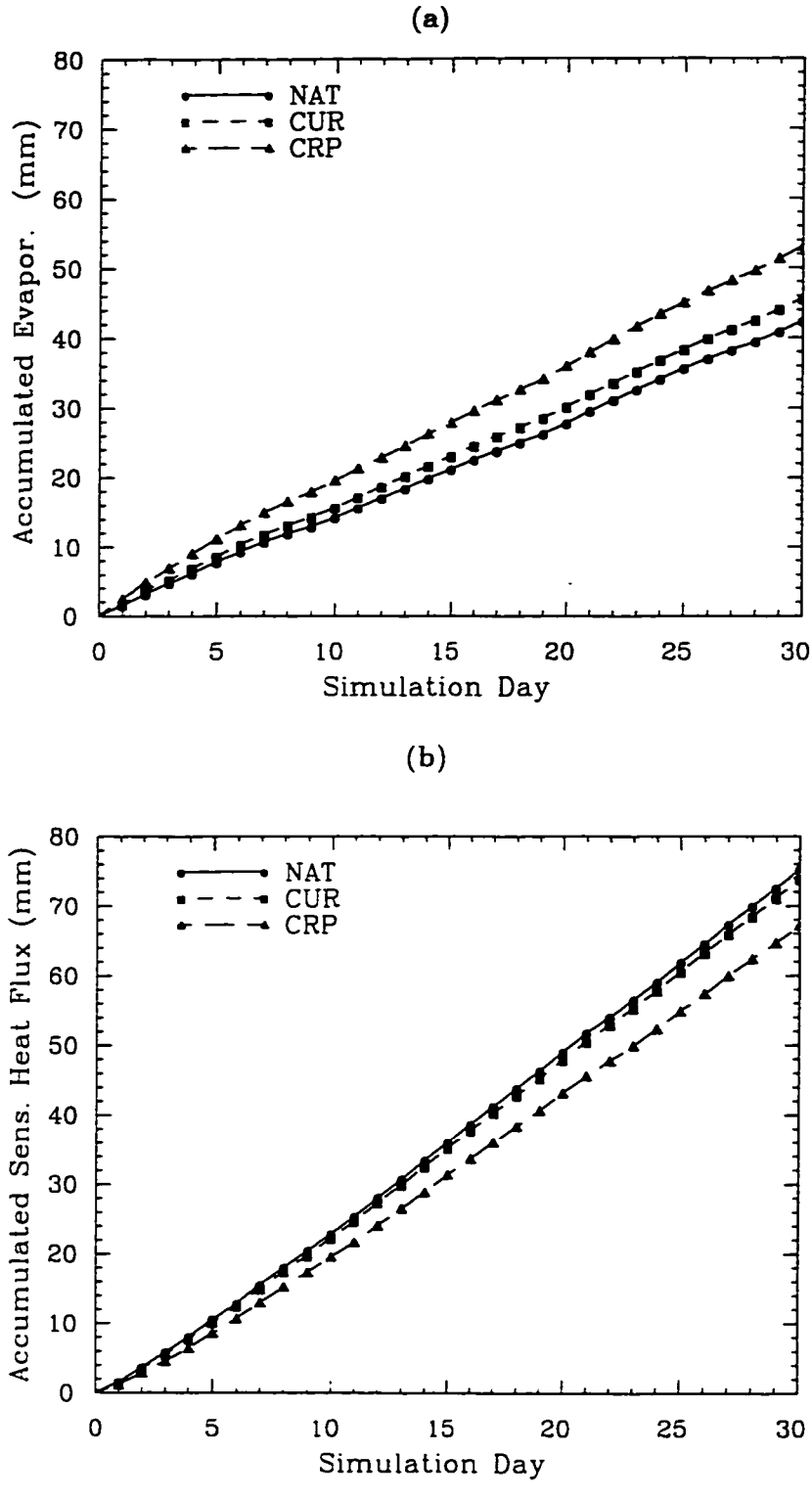

Figure 8 Time series of accumulated domain-averaged surface fluxes. (a) Latent heat flux. (b) Sensible heat flux.

(c)

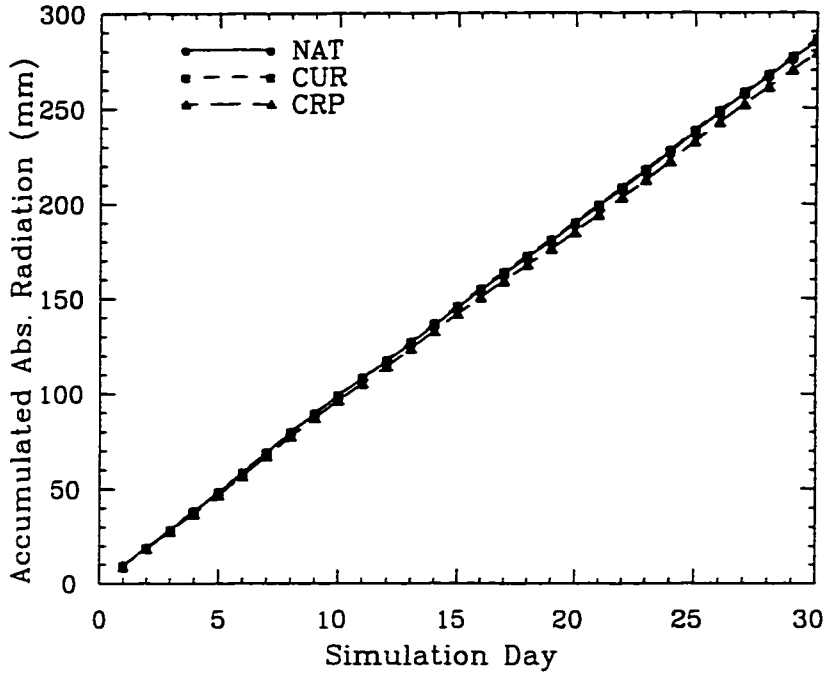

(d)

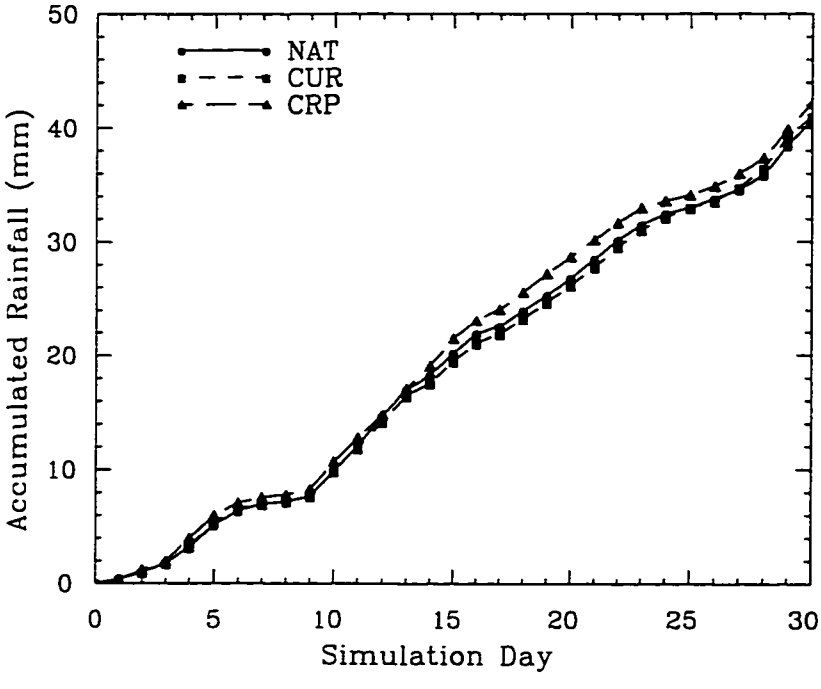

Figure 8 (continued) (c) Incoming solar radiation, (d) Rainfall.

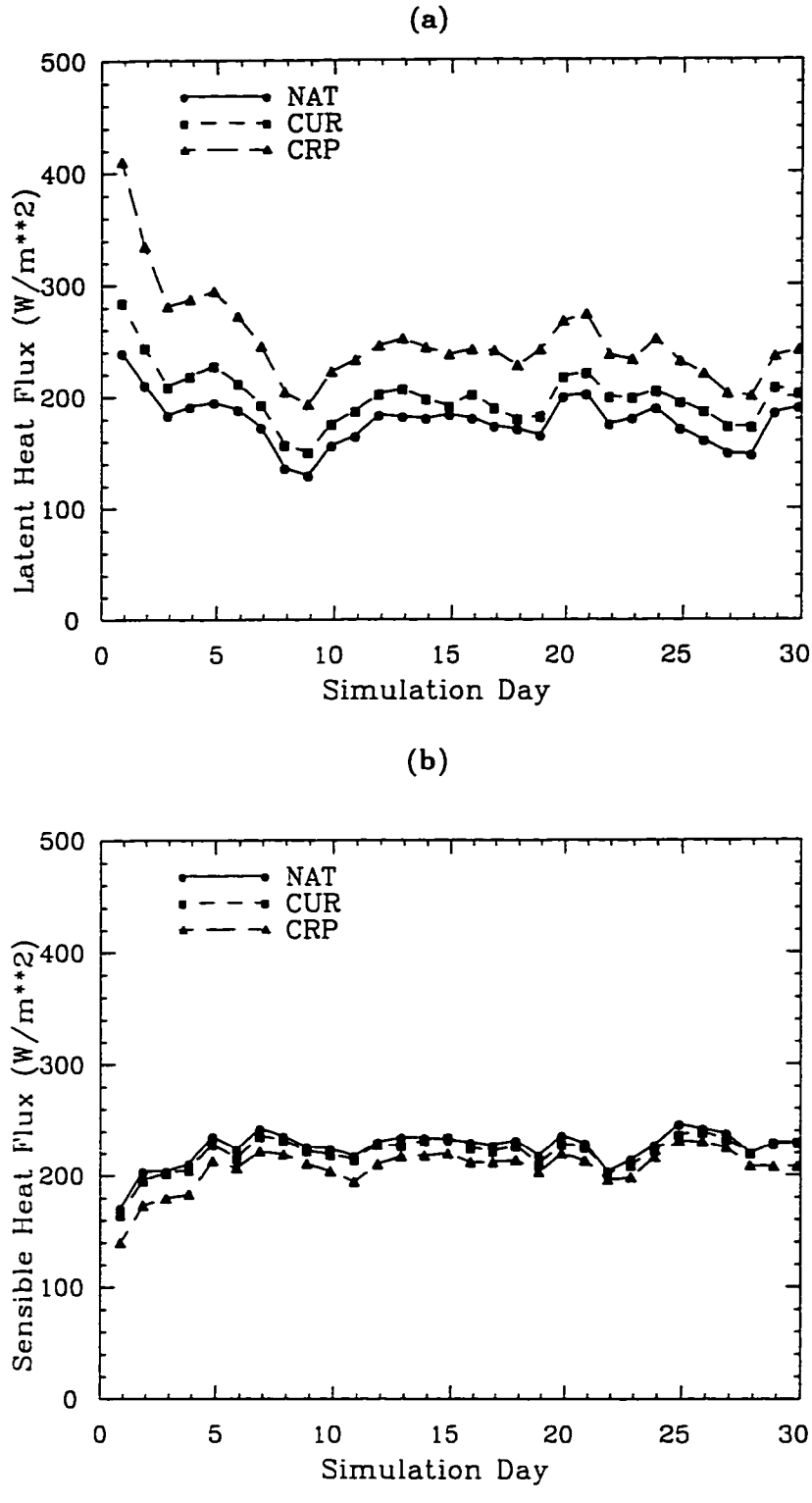

Figure 9 Time series of domain-averaged energy fluxes averaged over 1800-2100 UTC and entire domain. (a) Latent heat flux. (b) Sensible heat flux.

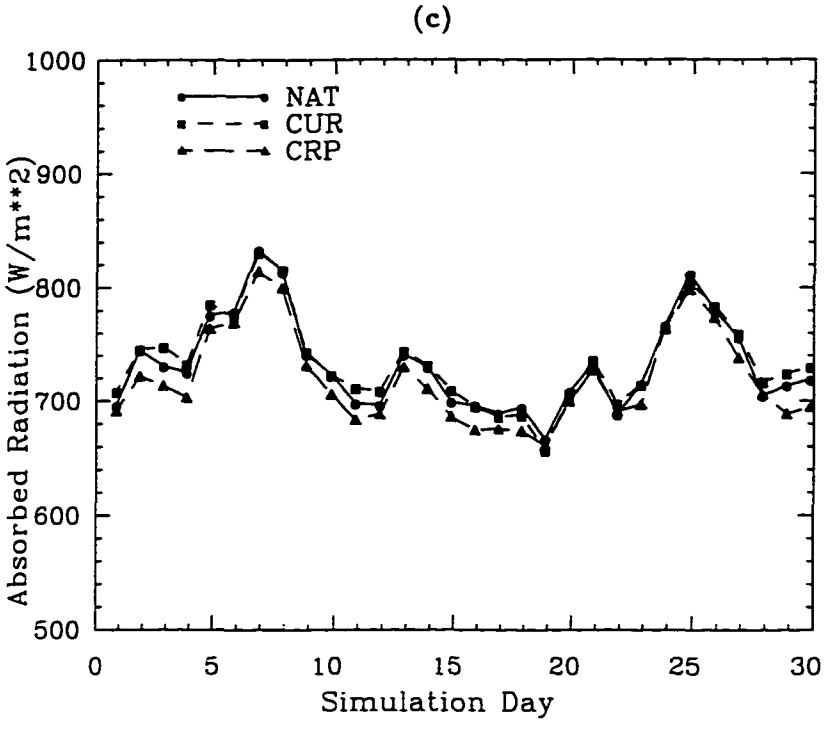

Figure 9 (continued) (c) Incoming solar radiation.

(a)

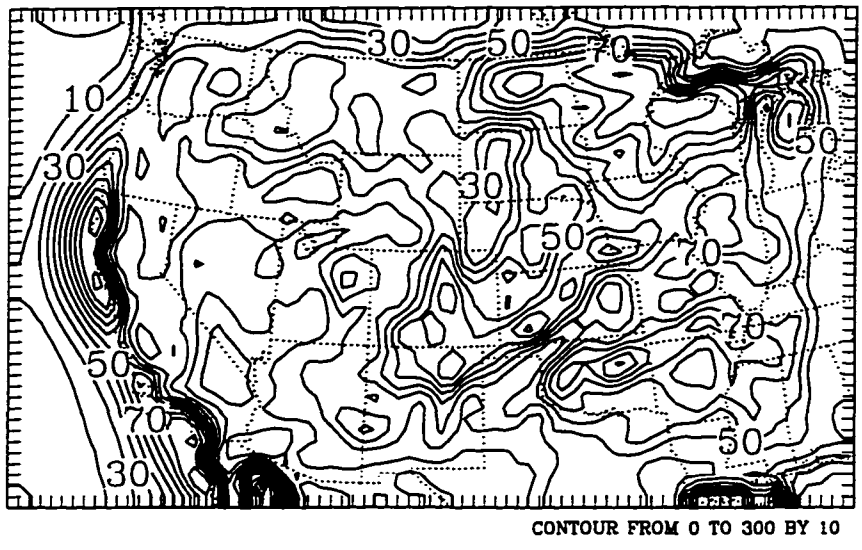

(b)

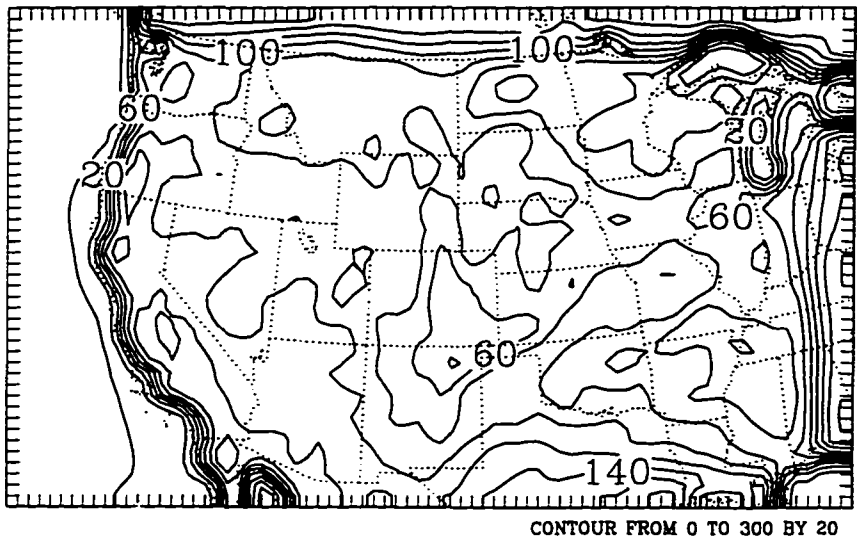

Figure 10 Spatial distribution of 30-d accumulated heat flux (mm). (a) Latent, (b) Sensible.

(a)

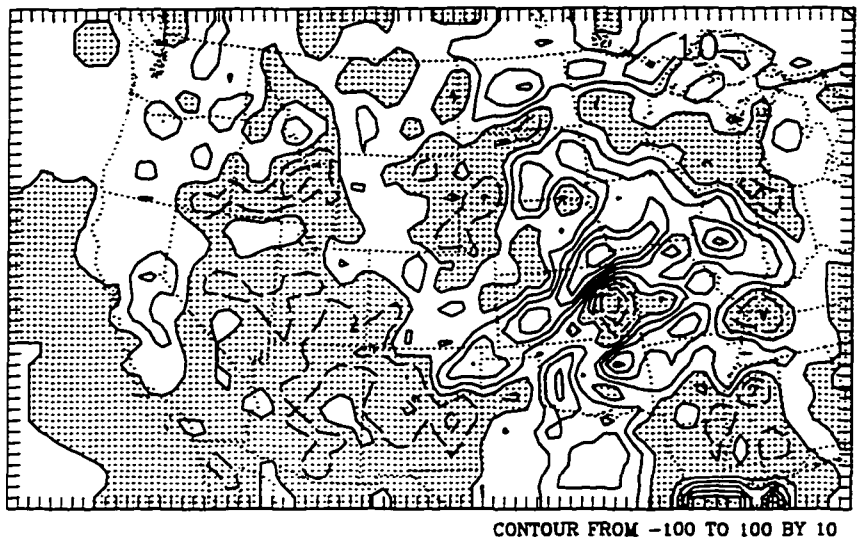

(b)

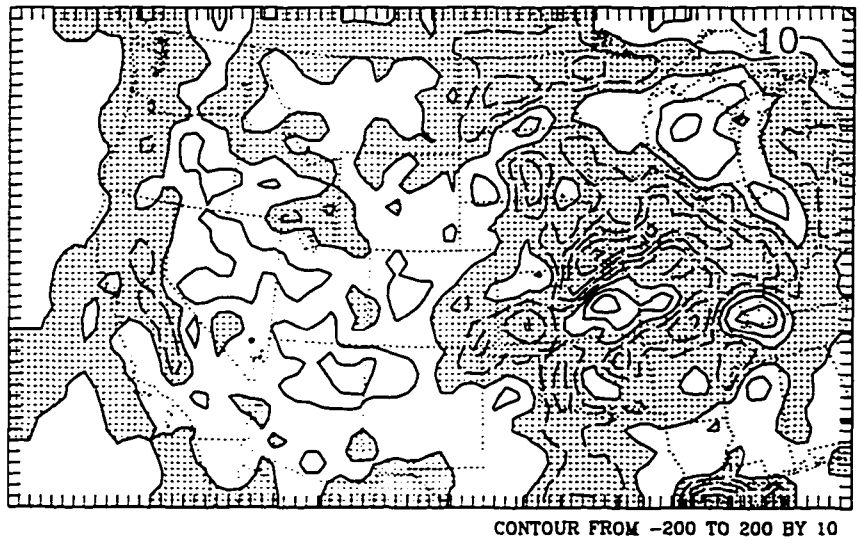

Figure 11 Difference fields (mm) in 30-d accumulated fluxes between the current and natural landuse. Areas of negative values are shaded. (a) Latent. (b) Sensible.

(c)

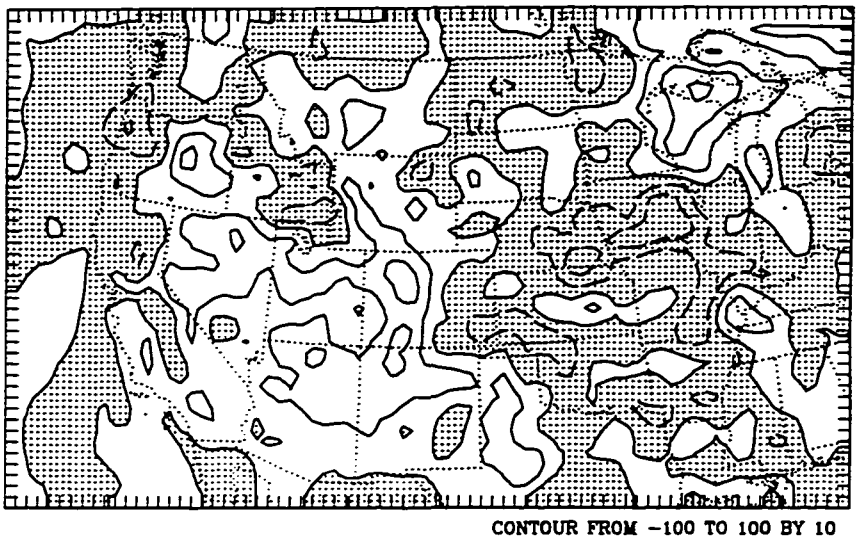

(d)

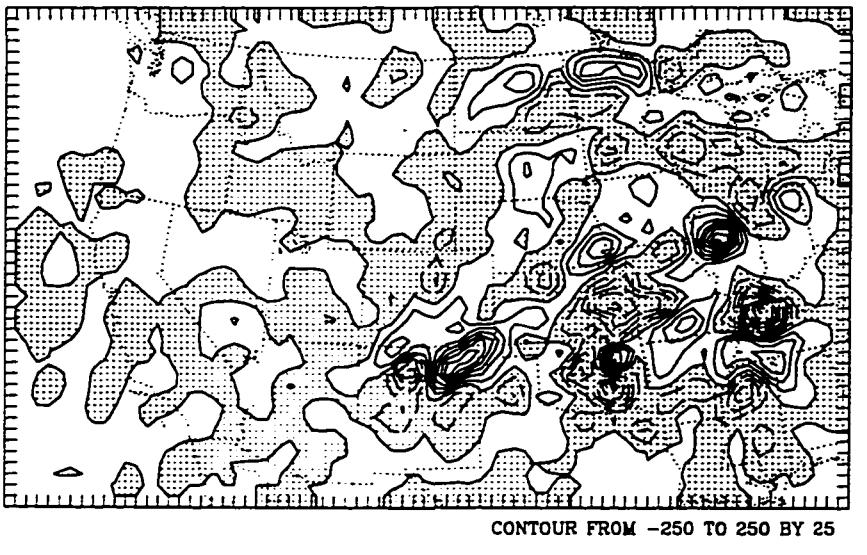

Figure 11 (continued) (c) Incoming solar radiation, (d) Rainfall.

(a)

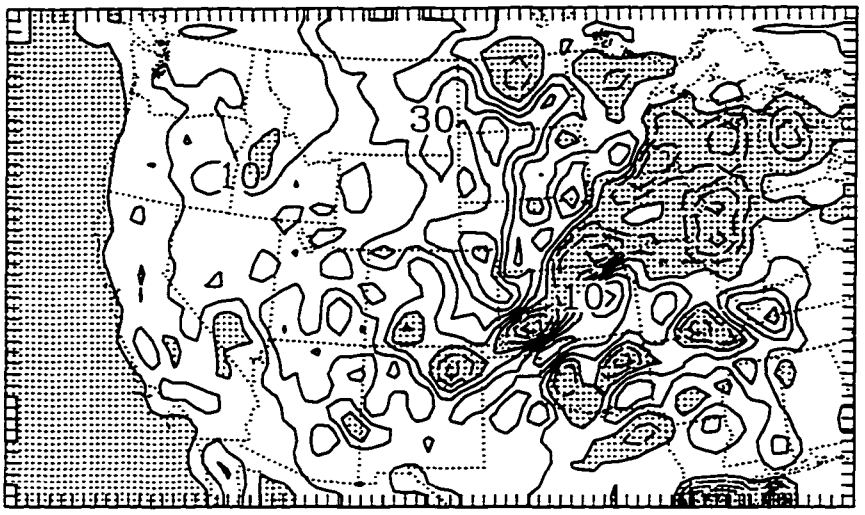

(b)

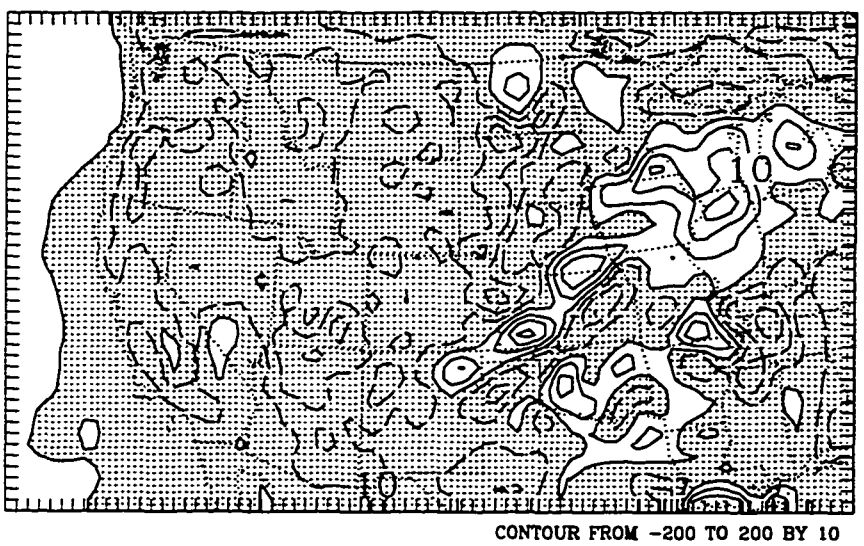

Figure 12 Difference fields (mm) in 30-d accumulated fluxes between the future and current landuse. Areas of negative values are shaded. (a) Latent, (b) Sensible.

(c)

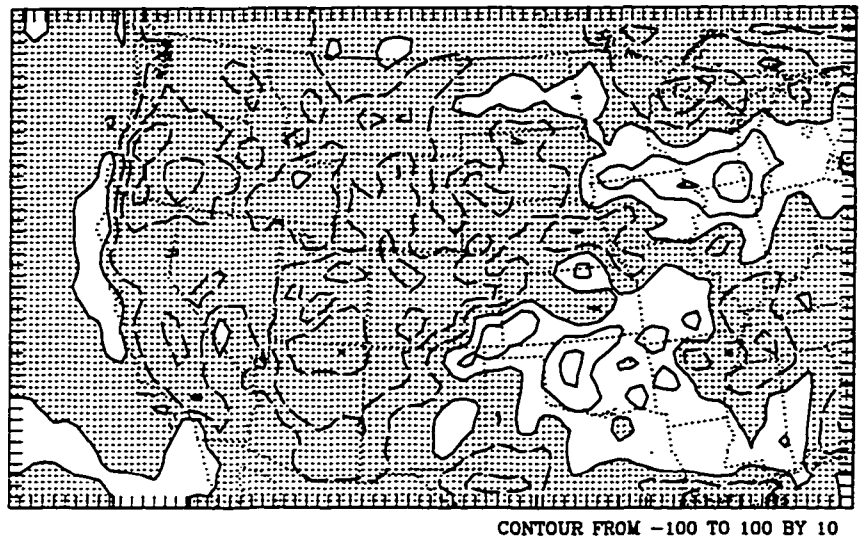

(d)

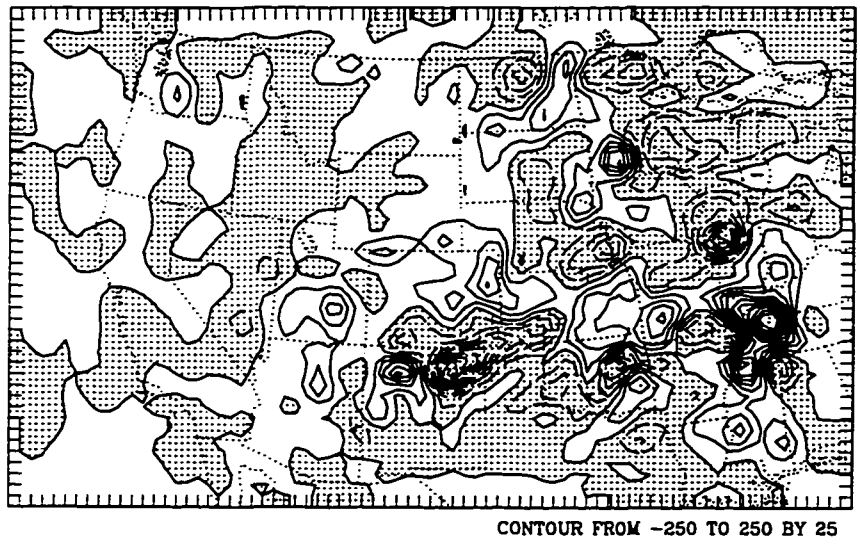

Figure 12 (continued) (c) Incoming solar radiation, (d) Rainfall.

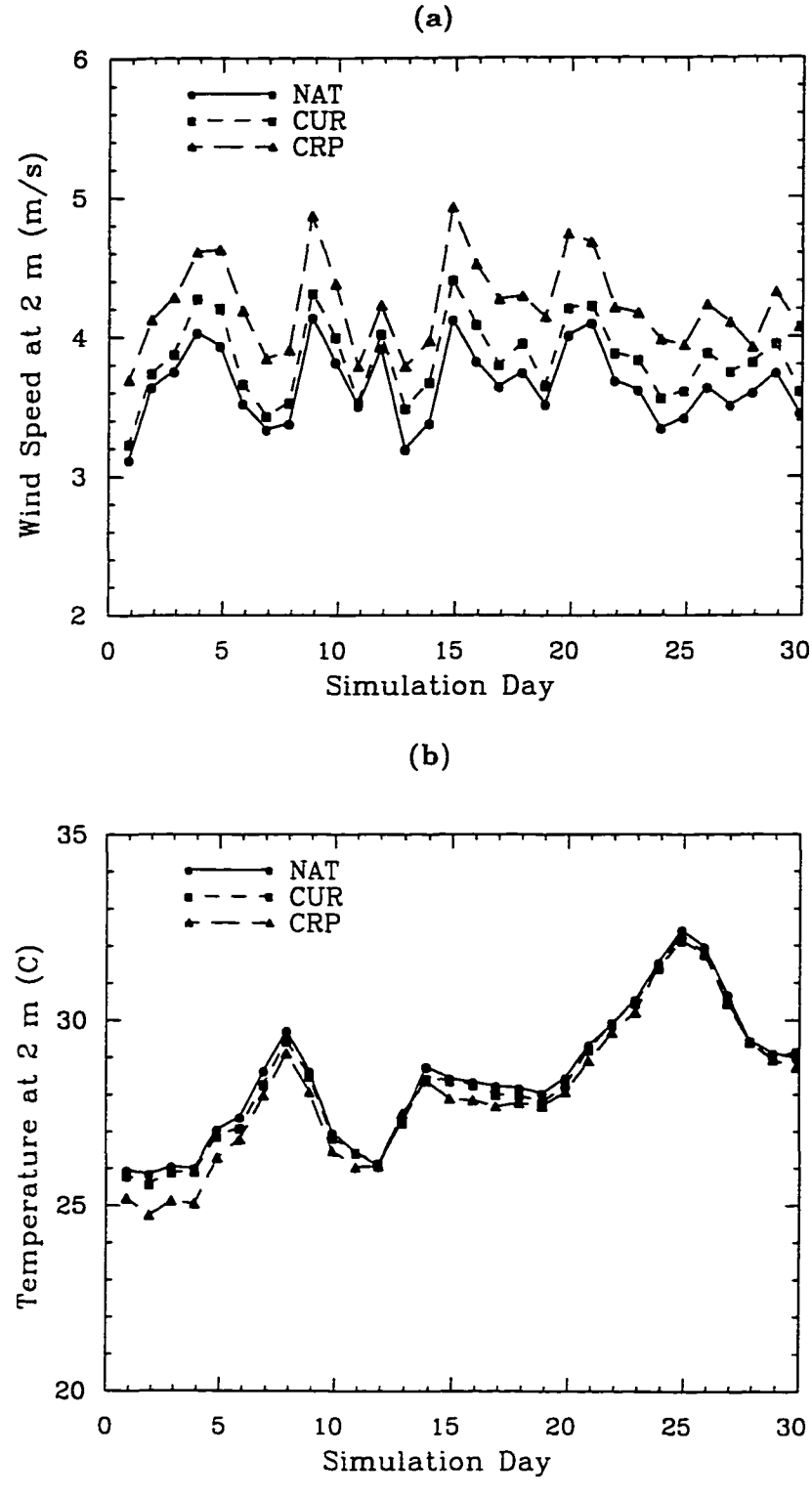

Figure 13 Time series of various domain-averaged variables at screen height (2m). (a) Wind speed, (b) Temperature.

(c)

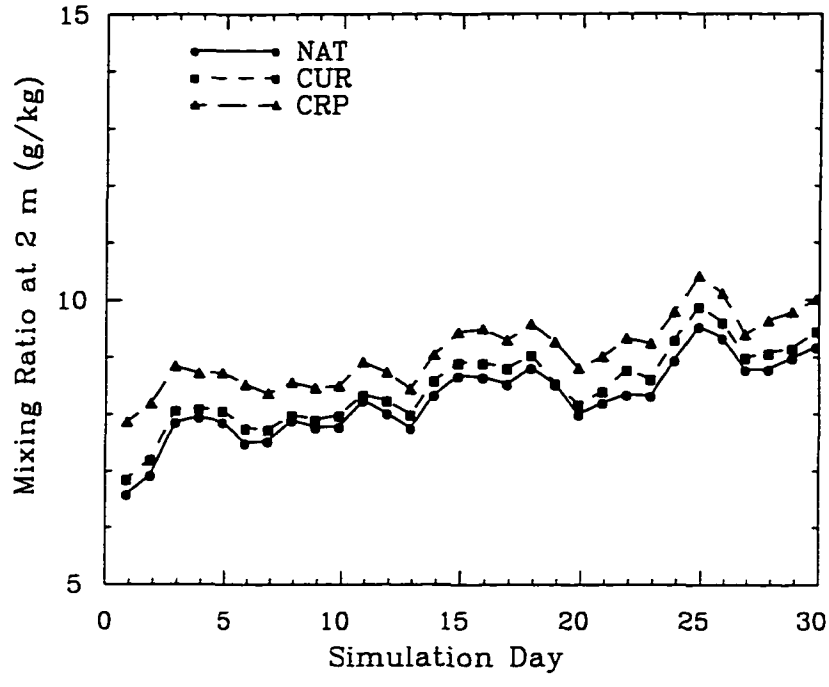

Figure 13 (continued) (c) Mixing ratio.

(a)

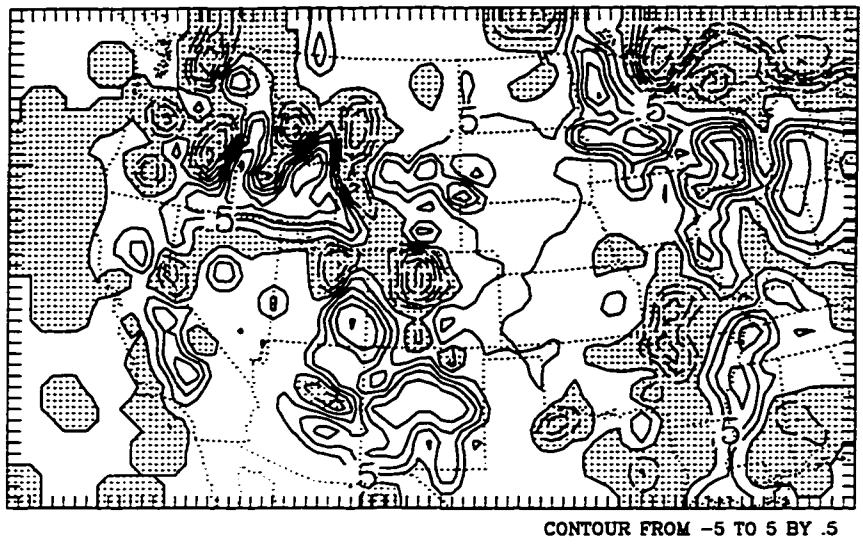

(b)

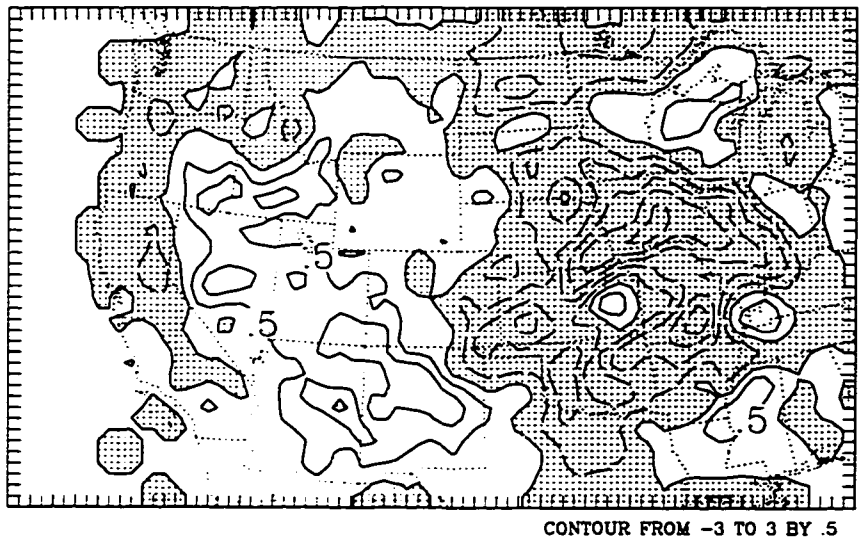

Figure 14 Difference fields in 30-d averaged variables at screen height (2m) between the current and natural landuse. (a) Wind speed (m s^{-1}), (b) Temperature (K). Areas of negative values are shaded.

(c)

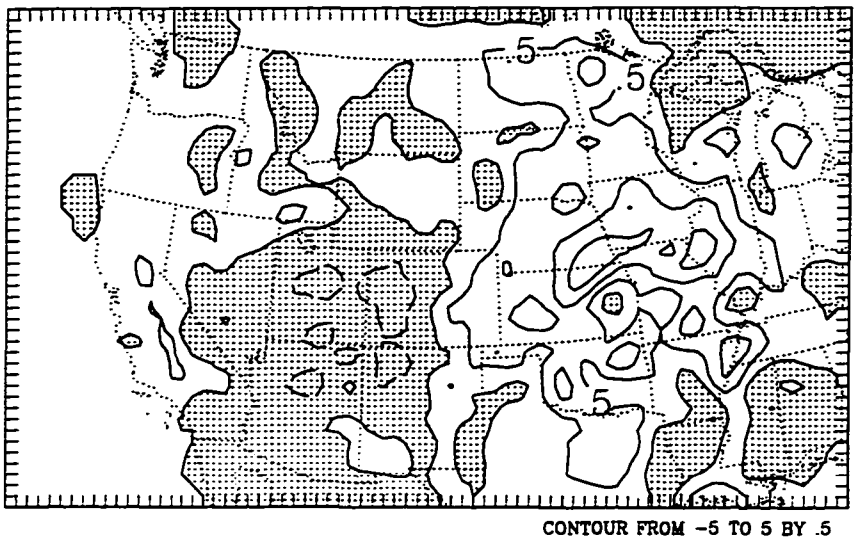

Figure 14 (continue) (c) Mixing ratio (g kg^{-1}).

(a)

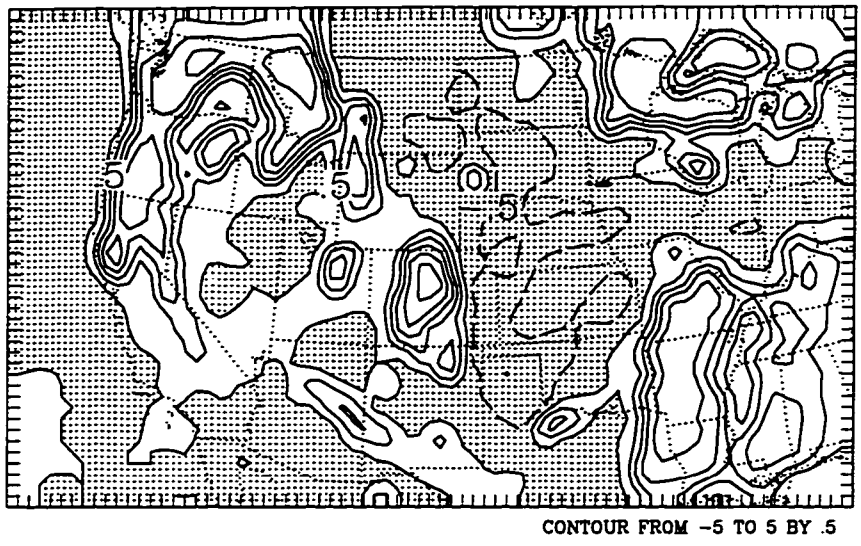

(b)

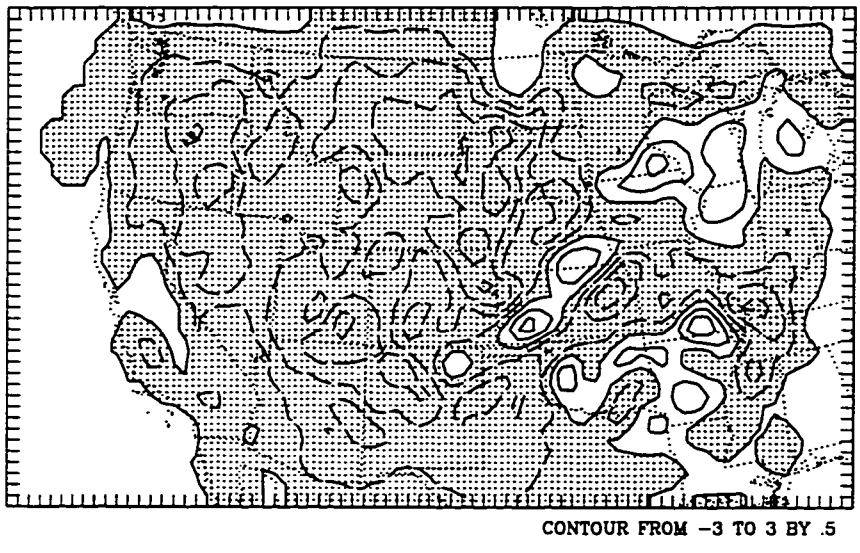

Figure 15 Difference fields in 30-d averaged variables at screen height (2m) between the future and current landuse. (a) Wind speed ($m\ s^{-1}$), (b) Temperature (K). Areas of negative values are shaded.

(c)

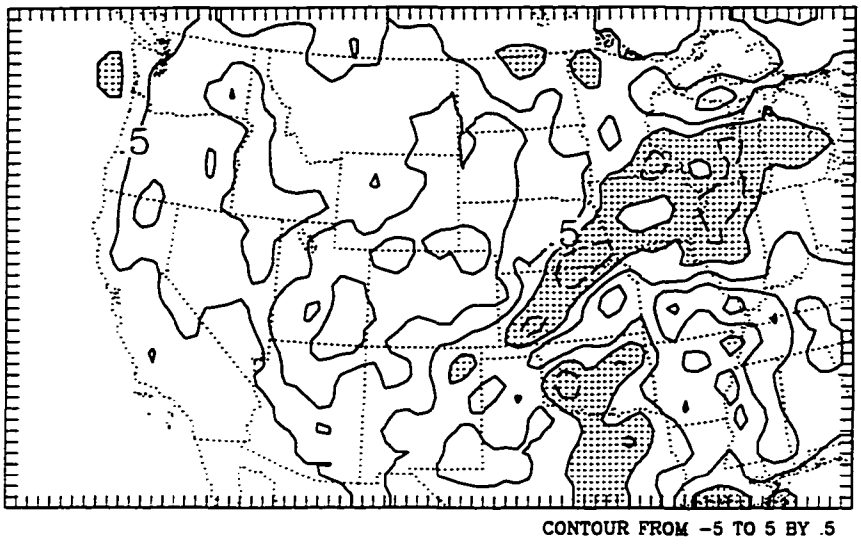

Figure 15 (continue) (c) Mixing ratio (g kg^{-1}).

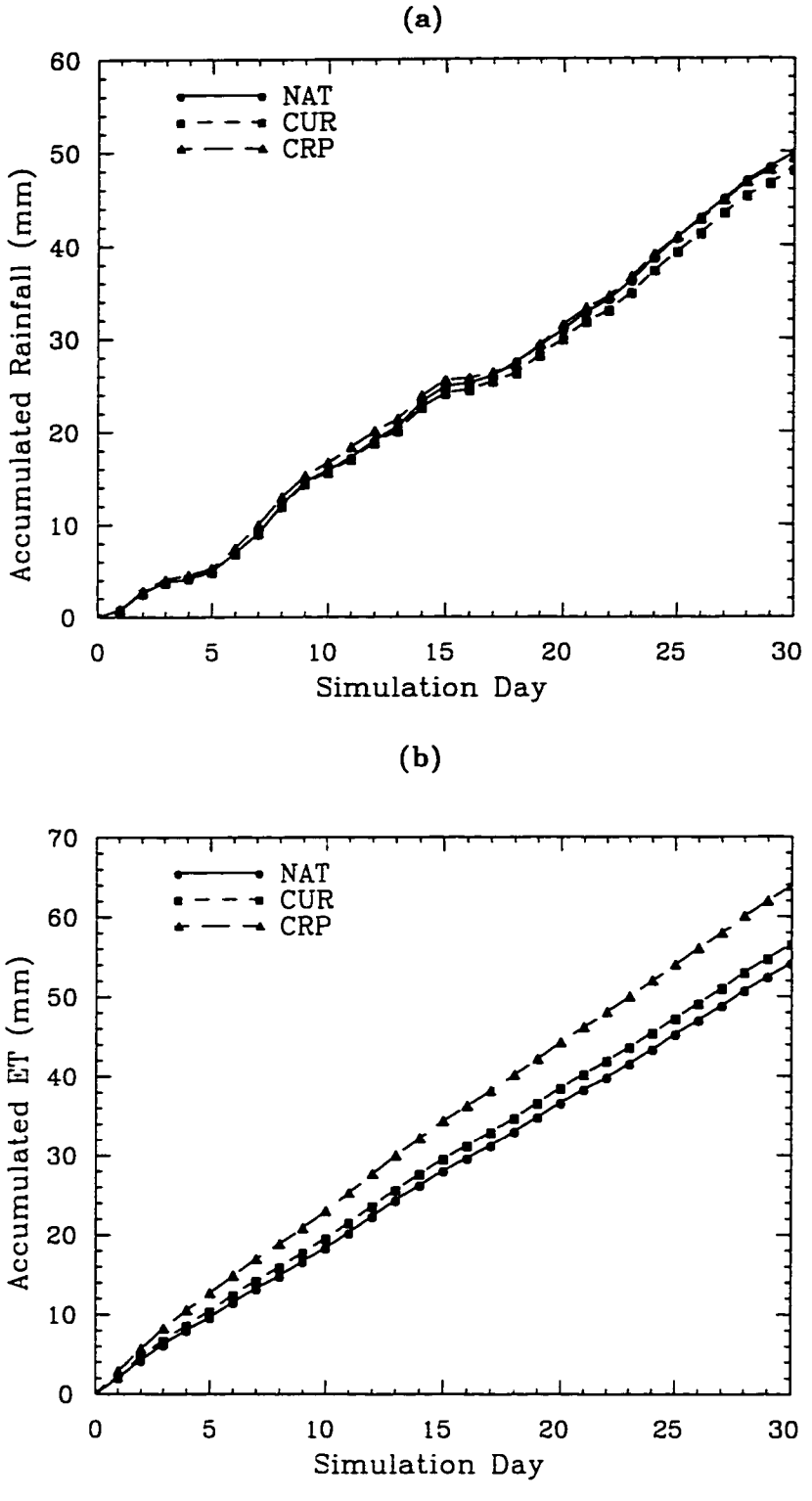

Figure 16 Time series of accumulated domain-averaged rainfall (a) and latent heat flux (b) for 1993.

(a)

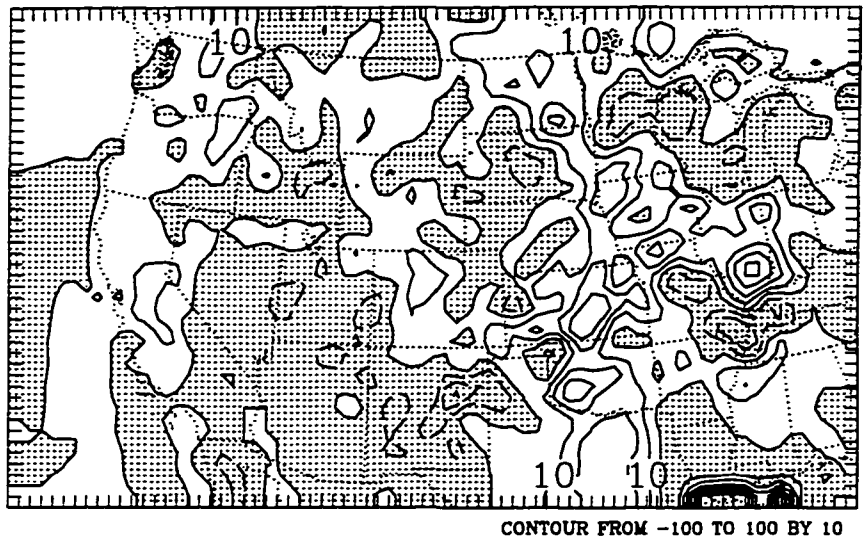

(b)

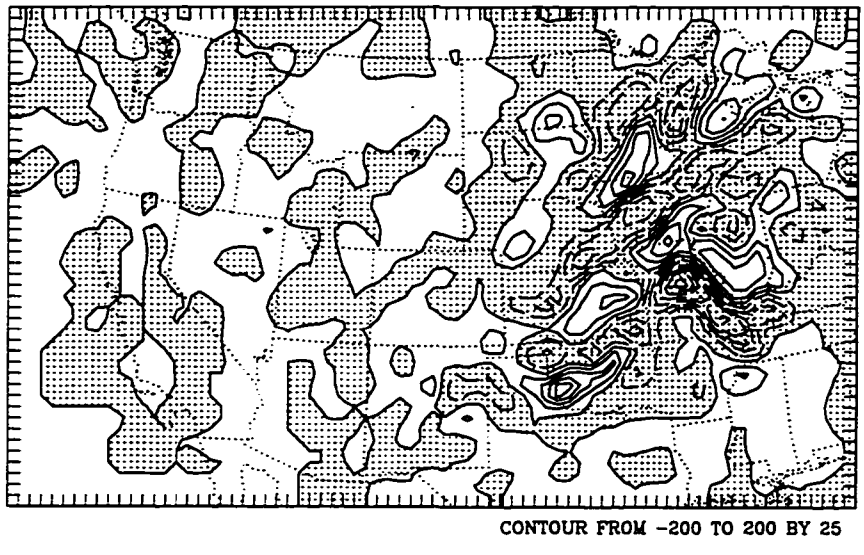

Figure 17 Difference fields (mm) in 30-d accumulated latent heat flux (a) and rainfall (b) between the current and natural landuse in 1993. Areas of negative values are shaded.

(a)

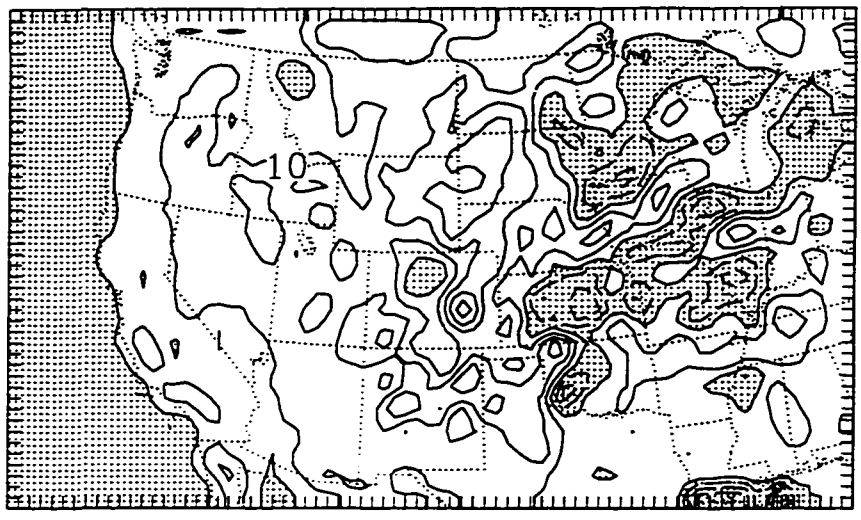

(b)

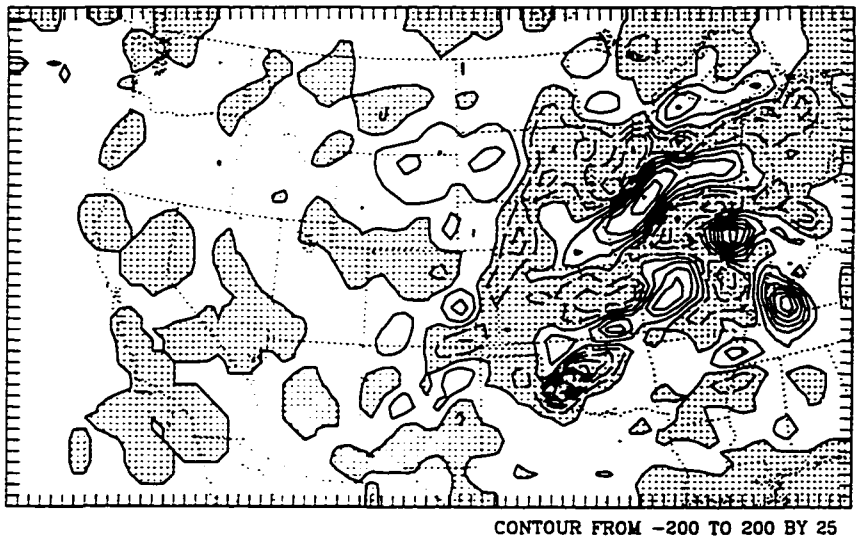

Figure 18 Difference fields (mm) in 30-d accumulated latent heat flux (a) and rainfall (b) between the future and current landuse for 1993. Areas of negative values are shaded.

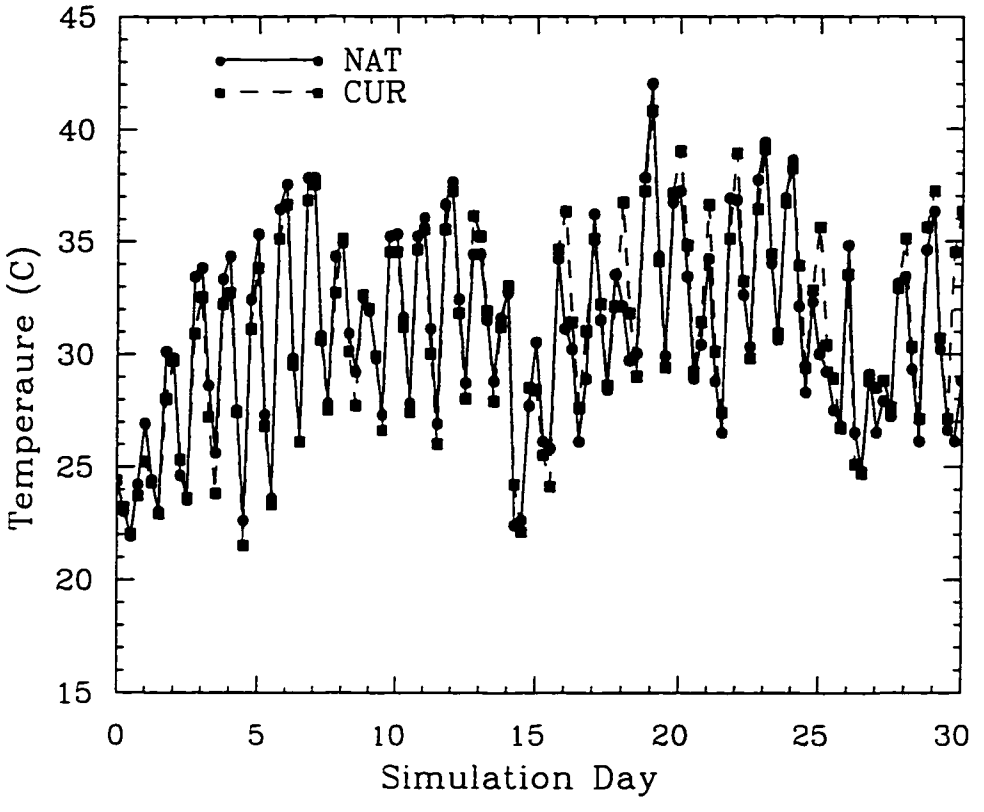

Figure 19 Six-hourly temperature at screen height (2m) at grid (61,21) for 1993.

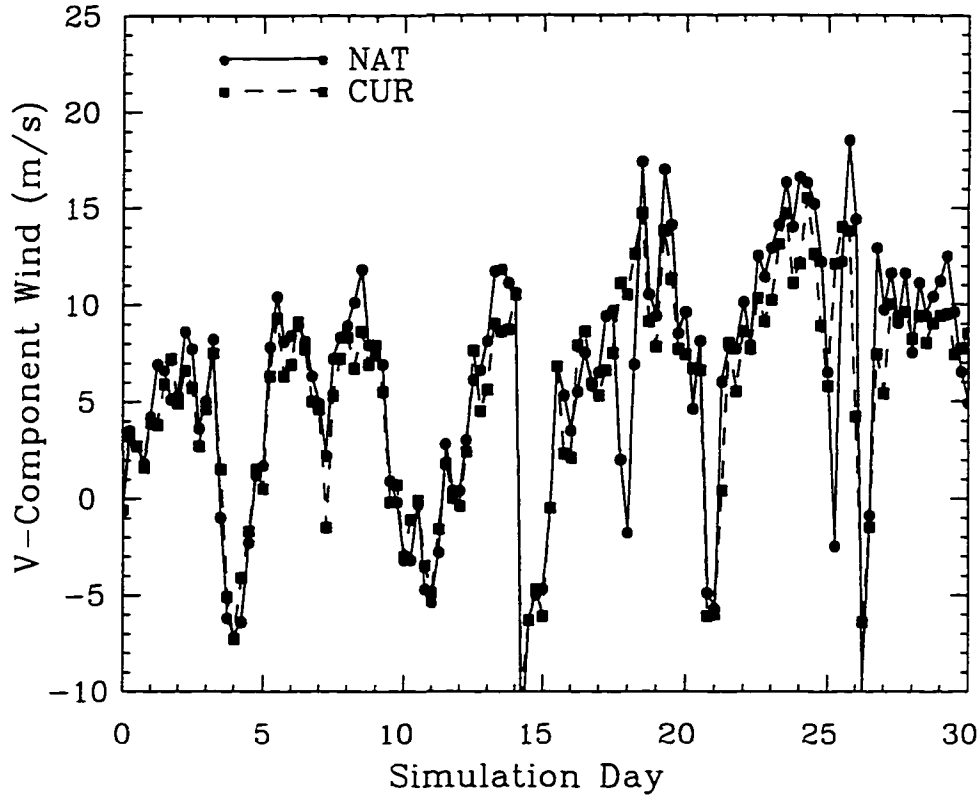

Figure 20 Six-hourly v-component wind at σ=0.895 at grid (61,21) for 1993.

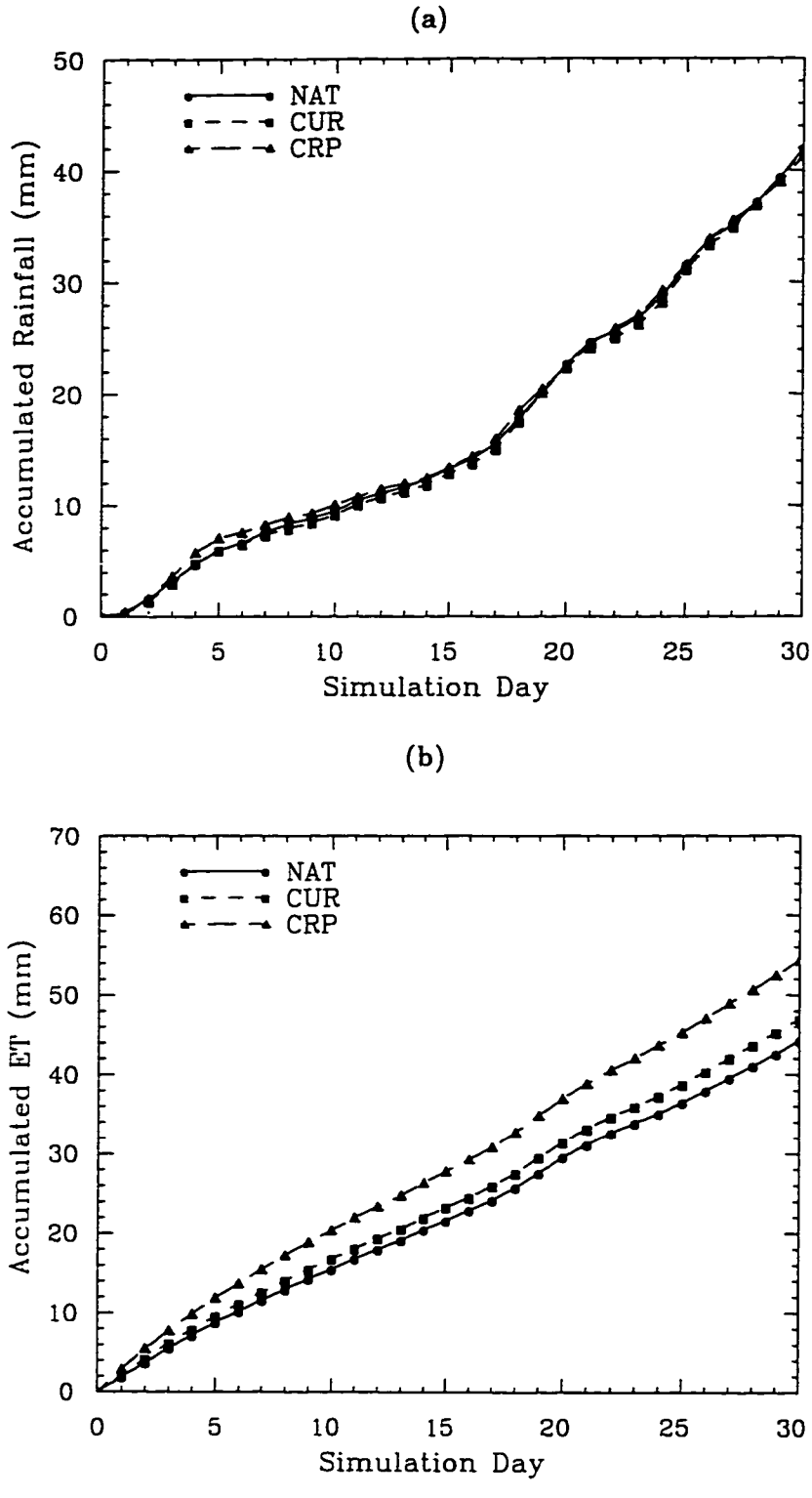

Figure 21 Time series of accumulated domain-averaged rainfall (a) and latent heat flux (b) for 1988.

(a)

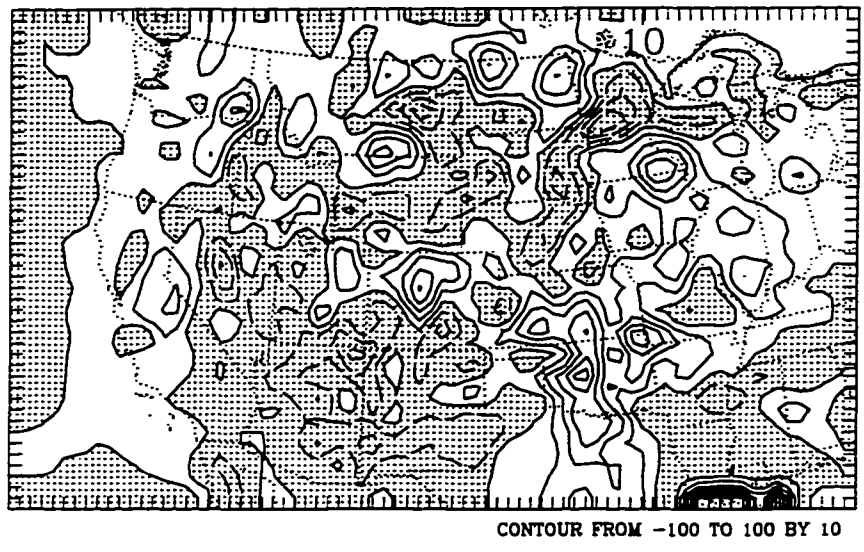

(b)

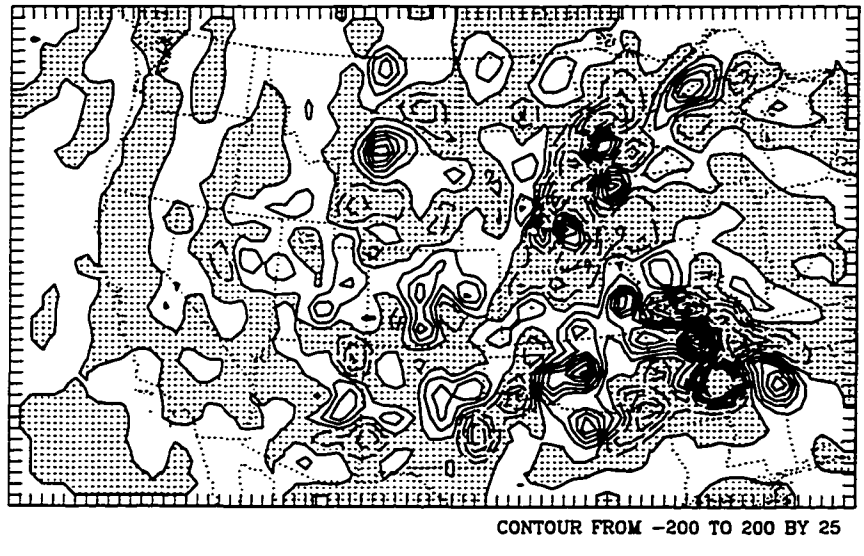

Figure 22 Difference fields (mm) in 30-d accumulated latent heat flux (a) and rainfall (b) between the current and natural landuse in 1988. Areas of negative values are shaded.

GENERAL CONCLUSIONS

1 Summary

Regional climate is determined by both regional (local) and global (remote) forcing. The relative importance of these two types of forcing is one of the central issues in regional climate studies. Remote forcing involves essentially atmospheric dynamics whereas local forcing depends basically on the surface characteristics. The dissertation contains three individual papers which evaluated the relative importance of surface forcing under different atmospheric conditions over the continental U.S.

Surface-moisture fluxes over land are important forcing for the atmosphere over continents. Numerous studies have been carried out to evaluate their impacts using different model schemes. In the first paper of this dissertation, the sensitivities of soil-moisture impacts on summer rainfall in the central U.S. to different cumulus parameterization and surface flux schemes are examined under different atmospheric and soil-moisture conditions. Results showed that a transient increase in soil moisture enhanced total rainfall over the simulation domain. The increase in soil moisture enhanced local rainfall when the lower atmosphere was thermally unstable and relatively dry, but it decreased the rainfall when the atmosphere was humid and lacked sufficient thermal forcing to initiate deep convection.

Regional climate simulations are long-term integrations over an open system where model variables over parts of the model domain are updated periodically. Model reinitialization after a certain length of integration can save wall-clock time and avoid possible drift caused by accumulated model errors. We investigated in the second paper the necessity and feasibility of subdividing long integrations through a number of experiments. It was found that for inte-

grations continued without reinitialization, locations of specific meteorological features drifted downstream because of the positive model bias on wind speeds, implying the necessity of periodically reinitializing the model. The simulated domain-averaged variables, including rainfall, were not sensitive to model reinitialization since they are largely constrained by boundary conditions, suggesting the possibility of dividing long regional climate simulations into a set of shorter segments that could be run in parallel.

In the last paper we evaluated numerically the potential impacts of landuse changes associated with human habitation on U.S. summer climate under various climate conditions. The results suggested that the current landuse, in which cropland occupies about one fourth of the total land area simulated, increased domain-averaged rainfall by less than 1% over the pre-settlement landuse, and the hypothetical future landuse which was simply assumed to be uniform cropland increased total rainfall by 3% under normal conditions. Regionally, with increasing proportion of cropland, the current and future landuse tended to reduce rainfall over most parts of east-central U.S. and to increase rainfall over most parts of the western U.S., especially in the flood year.

The following conclusions may be drawn from the studies presented in the dissertation as to surface forcing versus atmospheric forcing: (i) The mean properties over the continental scale are determined mainly by large-scale atmospheric forcing, and surface forcing seems to have little impact on them. (ii) With given large-scale atmospheric forcing, surface forcing has noticeable roles to redistribute atmospheric variables among different regions by either shifting specific patterns around or modulating them. (iii) The shifting or modulating of weather patters can result in large difference in climate variables, especially in rainfall, on *local* scales.

2 Discussions and Recommendations

Our simulations have found that the quantified soil-moisture impacts on rainfall are somewhat model scheme dependent, and thus caution should be taken in interpreting the simulated soil-moisture impacts. Regional climate simulations are computationally intensive and they are usually performed on supercomputers at high costs or on a workstation for a long time.

We investigated the feasibility of subdividing a long regional climate integration into several segments that can be run on workstations in parallel. We recommend, based on the results in the second paper, that the subdivision is appropriate provided (1) the minimum simulation interval is long enough to minimize the spinup/adjustment problem, (2) the break point does not occur during a period of heavy rainfall, and (3) the overlapping procedure is applied. The landuse changes due to human habitation in North America seem to have noticeable impacts on climate over regional scales. The long-term landuse management should be planned in the future.

Finally, the period of our simulations was relatively short (one-month) limited by computer resources availability. Much longer integrations are needed in the future when computer power allows.

APPENDIX. MODEL GOVERNING EQUATIONS

Regional Climate Model (RegCM2)

The horizontal momentum equations for (u) and (v) component can be written in flux form as (Anthes et al. 1987)

$$\frac{\partial p^* u}{\partial t} = -m^2 \left[\frac{\partial p^* uu/m}{\partial x} + \frac{\partial p^* vu/m}{\partial y}\right] - \frac{\partial p^* u\dot{\sigma}}{\partial \sigma}$$

$$-mp^* \left[\frac{RT_v}{p^* + p_t/\sigma}\frac{\partial p^*}{\partial x} + \frac{\partial \phi}{\partial x}\right] + p_* fv + D_u \qquad (A1)$$

and

$$\frac{\partial p^* v}{\partial t} = -m^2 \left[\frac{\partial p^* uv/m}{\partial x} + \frac{\partial p^* vv/m}{\partial y}\right] - \frac{\partial p^* v\dot{\sigma}}{\partial \sigma}$$

$$-mp^* \left[\frac{RT_v}{p^* + p_t/\sigma}\frac{\partial p^*}{\partial y} + \frac{\partial \phi}{\partial y}\right] - p_* fu + D_u \qquad (A2)$$

where T_v is virtual temperature, ϕ is geopotential height, f is the Coriolis parameter. m is the map scale factor, R is the dry gas constant, and D_u and D_v represent diffusion terms for u and v, respectively.

The vertical coordinate, σ, is defined as

$$\sigma = \frac{p - p_t}{p_s - p_t}$$

and

$$p^* = p_s - p_t$$

here p is pressure, p_s is surface press and p_t is the pressure at the top of the model.

Equations A1 and A2 can be derived from conventional momentum equations and continuity equation (Haltiner 1971).

The continuity equation in hydrostatic system can be written as

$$\frac{\partial p^*}{\partial t} = -m^2 \int_0^1 \left(\frac{\partial p^* u/m}{\partial x} + \frac{\partial p^* v/m}{\partial y} \right) d\sigma \tag{A3}$$

The vertical velocity, $\dot{\sigma} = \frac{d\sigma}{dt}$, is written as

$$\dot{\sigma} = -\frac{1}{p^*} \int_0^\sigma \left[\frac{\partial p^*}{\partial t} + m^2 \left(\frac{\partial p^* u/m}{\partial x} + \frac{\partial p^* v/m}{\partial y} \right) \right] d\sigma' \tag{A4}$$

The thermodynamic equation in flux form is written as

$$\frac{\partial p^* T}{\partial t} = -m^2 \left[\frac{\partial p^* uT/m}{\partial x} + \frac{\partial p^* vT/m}{\partial y} \right] - \frac{\partial p^* T\dot{\sigma}}{\partial \sigma}$$

$$+ \frac{RT_v \omega}{c_p(\sigma + p_t/p^*)} + p^* \frac{\dot{Q}}{c_p} + D_T \tag{A5}$$

$$\omega = p^* \dot{\sigma} + \sigma \frac{dp}{dt}$$

where

$$\frac{dp}{dt} = \frac{\partial p^*}{\partial t} + m \left(u \frac{\partial p^*}{\partial x} + v \frac{\partial p^*}{\partial y} \right) \tag{A6}$$

where T is temperature and c_p is the specific heat at constant pressure for the moist atmosphere.

The hydrostatic equation takes the form of

$$\frac{\partial \phi}{\partial ln(\sigma + p_t/p^*)} = -RT_v \left(1 + \frac{q_c + q_r}{1 + q_v} \right)^{-1} \tag{A7}$$

were q_v, q_c and q_r are the mixing ratio of water vapor, cloud water and rain water respectively. The second term in the parenthesis on the right represents the effects of water load on pressure.

Three other predictive equations for moisture, cloud water, and rain water are

$$\frac{\partial p^* q_v}{\partial t} = -m^2 \left[\frac{\partial p^* u q_v/m}{\partial x} + \frac{\partial p^* v q_v/m}{\partial y} \right] - \frac{\partial p^* q_v \dot{\sigma}}{\partial \sigma}$$

$$+ p^*(P_{RE} - P_{con}) + D_{qv} \tag{A8}$$

$$\frac{\partial p^* q_c}{\partial t} = -m^2 \left[\frac{\partial p^* u q_c/m}{\partial x} + \frac{\partial p^* v q_c/m}{\partial y} \right] - \frac{\partial p^* q_c \dot{\sigma}}{\partial \sigma}$$

$$-p^*(P_{RA} + P_{RC} - P_{con}) + D_{qc} \tag{A9}$$

$$\frac{\partial p^* q_r}{\partial t} = -m^2 \left[\frac{\partial p^* u q_r / m}{\partial x} + \frac{\partial p^* v q_r / m}{\partial y} \right] - \frac{\partial p^* q_r \dot{\sigma}}{\partial \sigma}$$

$$+p^*(P_{RA} + P_{RC} - P_{RE}) + F_H qr \tag{A10}$$

where P_{RA} represents accretion term by which falling raindrops collect cloud droplets,

P_{RC} represents autoconversion by which cloud droplets are collected by raindrops,

P_{RE} is the evaporation of rain water, and

P_{con} is condensation/evaporation of cloud water.

Equations A1-A3, A5, and A8-A10 consist a closed system for dependent variables u, v, p^*, T, q_v, q_c, and q_r.

Penn State/NCAR Mesoscale Model (MM5)

The governing equations for the hydrostatic part are similar to RegCM2 described above and thus not repeated here. The MM5 is so designed that it can make use of existing hydrostatic framework of MM4 and at the same time take care of nonhydrostatic effects (Grell et al. 1993). First, reference states for pressure (p), temperature (T), and density (ρ), are defined as

$$p(x, y, z, t) = p_0(z) + p'(x, y, z, t) \tag{A11}$$

$$t(x, y, z, t) = T_0(z) + T'(x, y, z, t) \tag{A12}$$

$$\rho(x, y, z, t) = \rho_0(z) + \rho'(x, y, z, t) \tag{13}$$

where p' is a predicted variable. The full pressure

$$p = p^* \sigma + p_t + p' \tag{A14}$$

While taking the advantage of nonhydrostatic formulation, the horizontal momentum equations can be expressed as

$$\frac{\partial p^* u}{\partial t} = -m^2 \left[\frac{\partial p^* u u / m}{\partial x} + \frac{\partial p^* v u / m}{\partial y} \right] - \frac{\partial p^* u \dot{\sigma}}{\partial \sigma} + uDIV$$

$$-\frac{mp^*}{\rho}\left[\frac{\partial p'}{\partial x}-\frac{\sigma}{p^*}\frac{\partial p^*}{\partial x}\frac{\partial p'}{\partial \sigma}\right]+p^* fv+D_u \tag{A15}$$

and

$$\frac{\partial p^* v}{\partial t}=-m^2\left[\frac{\partial p^* uv/m}{\partial x}+\frac{\partial p^* vv/m}{\partial y}\right]-\frac{\partial p^* v\dot{\sigma}}{\partial \sigma}+vDIV$$

$$-\frac{mp^*}{\rho}\left[\frac{\partial p'}{\partial y}-\frac{\sigma}{p^*}\frac{\partial p^*}{\partial y}\frac{\partial p'}{\partial \sigma}\right]-p^* fu+D_v \tag{A16}$$

where

$$DIV=m^2\left[\frac{\partial p^* u/m}{\partial x}+\frac{\partial p^* v/m}{\partial y}\right]+\frac{\partial p^*\dot{\sigma}}{\partial \sigma}$$

In a nonhydrostatic system, vertical velocity is a predicted variable.

$$\frac{\partial p^* w}{\partial t}=-m^2\left[\frac{\partial p^* uw/m}{\partial x}+\frac{\partial p^* vw/m}{\partial y}\right]-\frac{\partial p^* w\dot{\sigma}}{\partial \sigma}+wDIV$$

$$+p^* g\frac{\rho_0}{\rho}\left[\frac{1}{p^*}\frac{\partial p'}{\partial \sigma}+\frac{T_v'}{T}-\frac{T_0 p'}{T p_0}\right]-p^* g\left[(q_c+q_r)\right]+D_w \tag{A17}$$

The same is true with pressure which is no longer a diagnostic variable, but is solved from the continuity equation.

$$\frac{\partial p^* p'}{\partial t}=-m^2\left[\frac{\partial p^* up'/m}{\partial x}+\frac{\partial p^* vp'/m}{\partial y}\right]-\frac{\partial p^* p'\dot{\sigma}}{\partial \sigma}+p'DIV$$

$$-m^2 p^*\gamma p\left[\frac{\partial u/m}{\partial x}-\frac{\sigma}{mp^*}\frac{\partial p^*}{\partial x}\frac{\partial u}{\partial \sigma}+\frac{\partial v/m}{\partial y}-\frac{\sigma}{mp^*}\frac{\partial p^*}{\partial y}\frac{\partial v}{\partial \sigma}\right]$$

$$+\rho_0 g\gamma p\frac{\partial w}{\partial \sigma}+p^*\rho_0 gw \tag{A18}$$

$$\frac{\partial p^* T}{\partial t}=-m^2\left[\frac{\partial p^* uT/m}{\partial x}+\frac{\partial p^* vT/m}{\partial y}\right]-\frac{\partial p^* T\dot{\sigma}}{\partial \sigma}+TDIV$$

$$+\frac{1}{\rho c_p}\left[p^*\frac{Dp'}{Dt}-\rho_0 gp^* w-D_{p'}\right]+p^*\frac{\dot{Q}}{c_p}+D_T \tag{A19}$$

Similar to RegCM2, the equations for vapor, cloud water, and rain water mixing ratio are written as

$$\frac{\partial p^* q_v}{\partial t} = -m^2 \left[\frac{\partial p^* u q_v / m}{\partial x} + \frac{\partial p^* v q_v / m}{\partial y} \right] - \frac{\partial p^* q_v \dot{\sigma}}{\partial \sigma}$$

$$+p^* (P_{RE} - P_{con}) + D_{qv} \tag{A20}$$

$$\frac{\partial p^* q_c}{\partial t} = -m^2 \left[\frac{\partial p^* u q_c / m}{\partial x} + \frac{\partial p^* v q_c / m}{\partial y} \right] - \frac{\partial p^* q_c \dot{\sigma}}{\partial \sigma}$$

$$-p^* (P_{RA} + P_{RC} - P_{con}) + D_{qc} \tag{A21}$$

$$\frac{\partial p^* q_r}{\partial t} = -m^2 \left[\frac{\partial p^* u q_r / m}{\partial x} + \frac{\partial p^* v i q_r / m}{\partial y} \right] - \frac{\partial p^* q_r \dot{\sigma}}{\partial \sigma}$$

$$+p^* (P_{RA} + P_{RC} - P_{RE}) + F_H \tag{A22}$$

$$\sigma = \frac{p_0 - p_t}{p_s - p_t}$$

$$\dot{\sigma} = -\frac{\rho_0 g}{p^*} w - \frac{m\sigma}{p^*} \frac{\partial p^*}{\partial x} u - \frac{m\sigma}{p^*} \frac{\partial p^*}{\partial y} v \tag{A23}$$

The predicted variables are u, v, w, p', T, q_v, q_c, and q_r.

References

Anthes, R. A., E.-Y. Hsie, and Y.-H. Kuo, 1987: Description of the Penn State/NCAR Mesoscale Model Version 4 (MM4). *NCAR Tech. Note*, NCAR/TN-282+STR, 66 pp.

Grell, G. A., J. F. Dudhia, and D. Stauffer, 1993: A description of the fifth generation Penn State/NCAR Mesoscale Model (MM5). *NCAR Tech. Note*, NCAR/TN-398+IA, 107pp. [Available from NCAR P.O. Box 3000, Boulder, CO 80307.]

Haltiner, G. J., 1971: Numerical Weather Prediction. *New York, Wiley*, 317pp.

ACKNOWLEDGMENTS

This dissertation would never be completed without the encouragement, help, and support from many professors, students, friends, and my family. Firstly, I am deeply indebted to my advisor Dr. Eugene Takle who provided the financial support for my Ph. D. program and guided my research that leads to the completion of this dissertation. His experienced guidance, which ranges from research direction and insightful scientific views to technical English writing, is crucial to this dissertation and is highly appreciated.

Secondly, I appreciate the valuable time and effort that the committee members put into this study. Their knowledgeable suggestions and critical comments substantially strengthened my dissertation. In particular, I am grateful to Dr. Raymond Arritt who carefully reviewed every part of the dissertation and provided many critical comments. I appreciate Dr. Bill Gutowski's thorough review and many insightful suggestions. Dr. T.-C. Chen's knowledgeable and critical comments from large-scale dynamic point of view are appreciated. I am thankful to Dr. Al Austin for his many thoughtful hydrological ideas and valuable time out of his vacation.

Thirdly, many of my colleagues and fellow students helped me from all aspects. Moti Segal provided many insightful suggestions to my research. Richard Turner helped me a lot with NCAR graphics. Many casual discussions with Chris Wikle improved my statistical knowledge and dissertation writing. Scientific chatting with Robert Horton also contributed to this dissertation. I am thankful to my officemates Susan Kiehne, John Iselin, Chris Anderson, Alkhalil Adoum, and Hao Wang. The help from Zekai Otles, Dennis Todey, Weidong Jiang, Yibin Chen and many others facilitated my study and research. I am thankful to Dr. Douglas Yarger for allowing me to use the computers and Dr. Dick Carlson for providing some disk

space.

Finally, I would not have finished this program without my family's constant support. Especially, I appreciate my wife Jianhua's support and my son Xin's patience. I thank my former colleagues and friends John Brown, Stan Benjamin, and Tom Schlatter for providing encouragement for my study.